Thesis.

LapaJoy: A 3D-printed ergonomic handle design for a steerable laparoscopic instrument with minimised part assembly.

Author:
J.P.E. Alkemade
Delft University of Technology

Date: April 8, 2021
Student: Joost Alkemade
Number: 4213815
Mail address: J.P.E.Alkemade@student.tudelft.nl
Supervisors: Lussenburg, ir. K., Culmone, MSc. C. and Breedveld, Prof.dr.ir. P.

Delft University of Technology
Faculty of 3mE
Mekelweg 2
2628 CD Delft
015 278 9809
Info@tudelft.nl

Preface

This thesis is the culmination of my amazing stage of life in the city of Delft. It all started with my bachelor at the faculty of 3mE (Mechanical Engineering). Quickly after graduating, I noticed that I was deeply interested in nature and technology, and where better to combine these two than the master's degree at the faculty of 3mE; Biomechanical Engineering.

During the master period, I did an internship at Studio Roosegaarde for the simple reason that I deeply enjoy creative solutions, unsearched areas, and the freedom of design areas. Here I worked on different projects to develop designs and solutions, create interactive landscapes, and raise awareness of the current world problems. The internship thrived my skills in 3D drawings, visualizing, filming/video editing, photoshop, illustrator, designing, electrical schemes and hands-on building.

All the different interests and events came together when I started my thesis topic to create a 3D-printed ergonomic handle design for a steerable laparoscopic instrument with minimised part assembly. In order to come up with simple solutions, knowledge of various fields must be combined. In my opinion, a broad interest is the right direction to understand and develop the world around us. This results in a steep learning curve, which I experienced and fully enjoyed during this period of time.

It has been a roller coaster with the current COVID-19 situation, in where I want to thank all the people that supported me during this period of time, offline and online. Without the help of all those loving people, I could not have achieved what I achieved in the end. I want to thank Paul Breedveld for his supervision and guidance during the years. I want to address special thanks to Kirsten van Lussenburg and Costanza Culmone, who are very loving, positive and competent supervisors. Thanks for always being available and guiding me into the right path. Thanks for taking the time and putting so much effort into me during this process.
I want to thank Richard Alkemade for helping me out with 3D prints during the COVID-19 situation. I want to thank all the people I have met along the way during my study time and numerous hours of small talk outside the library that brightened my days and broadened my thoughts.

Finally, to my parents, family and friends, thank you so much for all the support throughout those years. They represent an essential factor in making life decisions, and so far I am happy with all the choices I have ever made.

I hope that you have a pleasant reading and a lot of inspiring thoughts throughout this paper.

Joost Alkemade
Delft, March 29, 2021.

Contents

Abstract

Introduction: This research aims to develop a 3D-printed ergonomic handle design for a steerable laparoscopic instrument with minimised part assembly. Steerable laparoscopic instruments are used in minimally invasive surgery (MIS). MIS is a technique where surgeons insert long slender surgical instruments through small incisions of five to ten millimetres in the abdominal wall. According to various studies regarding the ergonomics of laparoscopic instruments, improvements in the control and handle design are necessary. Non-ergonomic design and control, combined with extensive surgery, can cause physical discomfort, muscle fatigue, mental stress, and other complications to the surgeon that can adversely affect the patient. Improvements in the design can overcome inconvenient and uncomfortable movements of laparoscopic instruments to make MIS safer for surgeons and patients. In addition to the improvements in ergonomics, a reduction in assembled parts in current laparoscopic instruments can shorten the assembly time, resulting in lower manufacturing costs. 3D-printing offers design freedom to enable complex structures with minimised part assembly and has the potential to customise the instrument specifically to the surgeon.
Methods: The working principles and ergonomics of sixteen steerable laparoscopic instruments were analysed. Requirements were set up from the analysed laparoscopic instruments, handle design ergonomics and control ergonomics to develop an ergonomic handle design. Concepts have emerged from the requirements, and the most promising concept has been developed towards a final design. From the final proposed handle design emerged a working prototype, The LapaJoy. The 3D-printing technique of stereolithography was used to manufacture the LapaJoy. Steering, grasping, bending and locking tests were conducted to compare the retrieved data with the requirements to validate and evaluate the working principle and performance of the LapaJoy.
Results: The LapaJoy consists of five assembled parts and allows the surgeon to control the four different functions of the instrument. The surgeon can control the end-effector in two degrees of freedom, lock the end-effector's position, open and close the grasping forceps, and lock the grasping forceps in place. All four functions of the LapaJoy can be performed by a novel two-finger control system using the index finger and thumb. The results show that the LapaJoy can manipulate the end-effector in two degrees of freedom by 20° and lock the end-effector in any desired position. The instrument's grasper is functional, and the grasping forceps can be locked in place upon release of the grasper trigger. However, an analysation showed a reduction in the opening range of the grasping forceps with each opening and closing cycle. Furthermore, a material response wherein deformation of the steering segment's flexure occurred. The steering segment's flexure was deformed by 9.9° after applying almost 1 N to the grasping forceps in the vertical direction. In addition, fatigue and failure of the grasper and joystick design occurred during extensive use and testing.
Conclusion: By developing the 3D-printed ergonomic handle design with minimised part assembly, new knowledge was acquired in the possibilities of 3D-printing as a manufacturing technique for laparoscopic instruments. Future research is recommended to increase the steering angle and use more durable materials to create a more reliable product. The instrument's performance showed excellent potential in 3D printable laparoscopic instruments with minimised part assembly. The LapaJoy has the prospect of being an ergonomic, low cost, disposable MIS instrument.

Abbreviations

Nomenclatures

Abbreviations	Full form
MIS	Minimally invasive surgery
DoF	Degrees of freedom
FDM	Fused deposition modeling
3D	Three dimensional
IPA	Isopropyl alcohol
SLA	Stereolithography
SLS	Selective laser sintering

1 Introduction

1.1 Minimally invasive surgery

Minimally invasive surgery (MIS) is a technique where surgeons insert long slender surgical instruments (laparoscopic instruments) through small incisions of five to ten millimetres in the abdominal wall. It is widely adopted for operations since it has advantages over traditional open surgery. These benefits include less blood loss, shorter hospital stays, smaller scars, less postoperative pain, fewer infections and shorter recovery time [1, 2]. Conventional laparoscopic instruments for MIS contain a handle, a long rigid shaft, and an end-effector [1]. The conventional laparoscopic instrument is shown in Figure 1a. In open surgery, the total amount of positions and orientations an instrument can take is six, namely translation along each axis in three dimensions, and rotations around each axis in the three dimensions. Positions and orientations are defined as degrees of freedom (DoF) and are equal to the number of independent movements. When looking at MIS for example, the instrument must pass the abdominal wall. A trocar, a particular tube able to keep the abdomen inflated during surgery, is inserted in the incision of the abdominal wall and allows the insertion of instruments through the abdominal wall. However, the trocar constraints two of the instrument's translations. Therefore, the trocar reduces the degrees of freedom of the system to a four DoF system, as shown in Figure 2a. The conventional laparoscopic instruments can only reach inside the conical area of Figure 2a.

Besides the reduced DoF when using a conventional laparoscopic instrument during MIS, surgeons also have to cope with the fulcrum effect. The fulcrum effect inverts the movement of the handle compared to the end-effector due to the pivot point originated at the abdominal wall, as shown in Figure 2c. The fulcrum effect makes surgery challenging for tasks such as suturing [2, 3]. The limited four degrees of freedom and the fulcrum effect paved the way for innovative instruments. An example of such an instrument is the da Vinci Surgical System. The da Vinci Surgical System dampens hand tremors and enables extra degrees of freedom [4]. These robotic systems make surgical movements easier to execute compared to the surgical movements with conventional laparoscopic instruments. However, the da Vinci Surgical System also has its drawbacks such as, significantly higher costs, a cumbersome structure and time consuming troubleshooting of the hardware and software. Moreover, the surgeon is outside the operating area, and the conversion of instruments can cause delays since removing the da Vinci System is not as easy as conventional laparoscopic instruments [5, 6].

Innovations and research in laparoscopic surgical instruments have tried to implement some of the beneficial aspects of robotic instruments in surgical instruments at the cost of conventional laparoscopic instruments. Different instruments with an articulated end-effector were invented that are similar in design to those of the conventional laparoscopic instruments [1].

The articulating end-effectors improve the instrument's manoeuvrability by adding two extra degrees of freedom to the system as shown in Figure 1b. The tip of the instrument can now move in space with six degrees of freedom, enabling the surgeon to steer outside the conical area into directions that were not possible before.

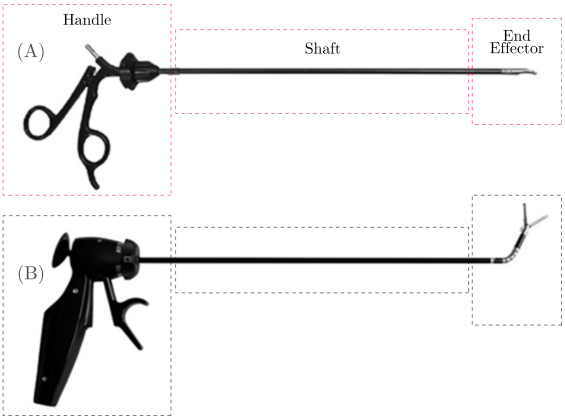

Figure 1: Laparoscopic instruments. A) Conventional laparoscopic instrument. B) Steerable laparoscopic instrument. Taken from [7].

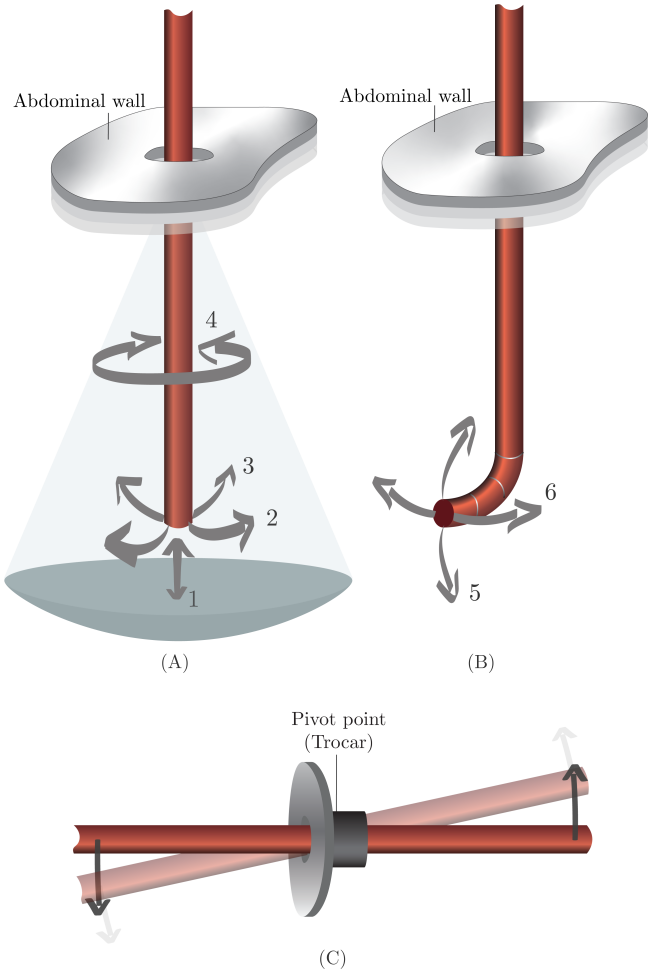

Figure 2: The possible movements of laparoscopic instruments in use. A) Rigid instruments with four degrees of freedom. B) Additional steerable tip adding two degrees of freedom. C) The fulcrum effect.

1.2 Steerable laparoscopic instruments

The innovations of steerable laparoscopic instruments led to a variety of designs, control mechanisms, and possible additional features. Figure 3 shows two different designs that can steer the end-effector in two DoF. Furthermore, the axial shaft can rotate around its axis by turning an intented turning knob and the instrument can grasp. The handle of the FlexDex is mounted on the surgeon's wrist, as shown in Figure 3a [8]. The handle of the LaproFlex fits inside the palm [9]. Steerable laparoscopic instruments can, for example, be controlled by a joystick, handle articulation, or lever rotation. They can also have different features such as locking the position of the end-effector or locking the angular position of the grasping forceps' jaws [1].

Moreover, different manufacturing techniques have been explored in order to simplify the fabrication and decrease the production costs. An example of a three dimensional (3D) printed laparoscopic instrument is the DragonFlex [10]. 3D-printing has been further explored as a manufacturing technique with the vision to develop disposable steerable laparoscopic instruments. 3D-printing is a manufacturing technique that can print complex designs without increasing the fabrication challenges. Therefore, multiple parts can be printed together as a single component drastically minimising the number of parts. An example is given by Bazuin who presented a non-assembled laparoscopic instrument in which the only post-production actions are the assembly of the cables and the removal of the support material [11].

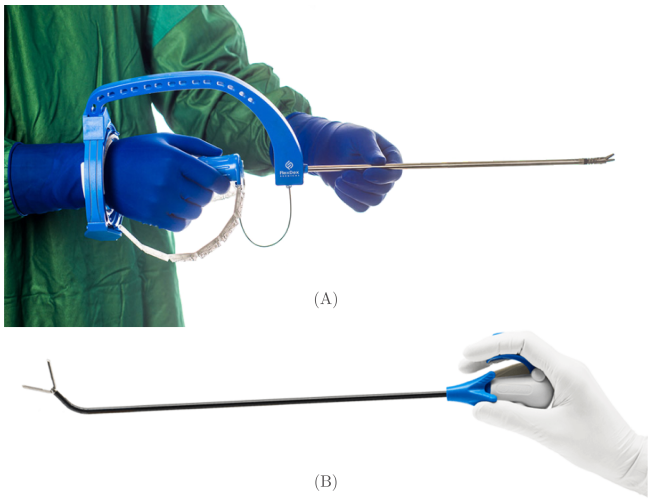

Figure 3: Steerable laparoscopic instruments. A) FlexDex. B) LaproFlex. Taken from [8, 9].

1.3 Ergonomics in laparoscopic instruments

All the different complex systems and designs raise concerns in the medical community about the ergonomic drawbacks [12]. The surgical performance is highly dependent on the design of the laparoscopic instrument. Performance depends most on the shape of the handle and the length of the instrument [13]. Therefore, the ergonomics of the handle design is important to ensure high surgical performances and to ensure the safety of the patients as well as the safety of the surgeons. If not designed correctly, the non-ergonomic designs can lead to physical discomfort, muscle fatigue, mental stress, musculoskeletal disorders for the surgeon, that can indirectly lead to consequences for the patient [12, 14]. Numerous studies were conducted on the ergonomics of laparoscopic instrument designs wherein researchers established guidelines for future designs based on surgeons' preferences. In those ergonomic studies, a list of ergonomic criteria was established, insight in the risk factors for surgeon injury was obtained, and knowledge about the effect of handle designs on the performance of laparoscopic instruments was gained [12, 15–17].

1.4 Problem definition

The benefits of MIS instruments for patients, such as less blood loss, minor scars, less postoperative pain, has been achieved at the expense of surgeons' ergonomic conveniences. The increased instrumental complexity has led to more ergonomic factors that must be taken into account. Although numerous studies have been done regarding ergonomics, more improvements must be made in the design. The improvements concern wrist deviation, hand position, control functions, force transmission, among other improvements of laparoscopic instruments to make MIS safer for the surgeons as well as the patients [18].

Non-ergonomic laparoscopic instruments that do not fit the tool to the hand stimulate inconvenient and uncomfortable movements executed by the surgeon. Furthermore, when continuously applying grasping forces, fatigue in the surgeons' hand, difficulties, and uncontrolled situations can occur [13, 16, 19–21]. Therefore, the laparoscopic handle design determines the quality of task performance and the surgeon's risk of injury.

In addition to the ergonomic problems, the assembly of control elements seen in most laparoscopic instruments leads to high manufacturing costs [7]. When looking at disposable instruments, the assembly takes up much time compared to the usage time, resulting in a decrease in the instrument's cost-effectiveness. The assembly time has to be investigated to increase the cost-effectiveness, which is of high importance in the economic aspect.

1.5 Goal

This study aims to design a fully 3D-printed ergonomic control handle for an existing steerable laparoscopic end-effector. The 3D-printing manufacturing technique, to develop the anthropology data-driven ergonomic control handle, allows for minimised part assembly and components. The handle gives the user the ability to steer the end-effector in two degrees of freedom, lock the end-effector's position, open and close the grasping forceps at the end-effector, and lock the jaws of the grasping forceps in place.

1.6 Layout of this report

This study shows all the taken steps to develop a 3D-printed ergonomic handle design. Chapter two analysis steerable laparoscopic instruments and their ergonomics from which the set-up requirements arose. Chapter three shows the development of the conceptual designs and the selection of the final conceptual design. Chapter 4 explores the development of the different prototype control systems towards the final prototype. The taken tests in Chapter 5 allows us to evaluate the performance of the LapaJoy. Chapter 6 discusses the design and points out recommendations towards a better design, after which Chapter 7 concludes the design.

2 Design analysis

2.1 Function design structure

A function design structure is an essential aspect of tool designing. The structure provides a tool to reflect on the working principle of a product without implementing already taken design choices [22]. Therefore, a graphical visualisation that focuses on steerable laparoscopic instruments' control functions was created to provide insight into the working principle of an abstract model without forcing early design choices. All steps taken, in this case, to control a steerable laparoscopic instrument are essential to accomplish a specific goal and therefore included in the function design structure.

The function design structure in Figure 4a shows all elements based on in- and outputs of a steerable laparoscopic instrument for the specific task grasping. Zooming in into the black box of Figure 4b there are three main functions: steering, grasping, and locking. The main functions cannot be broken down further. Figure 5 shows the pathways to generate the movement transformation between the in- and output of the three main functions. The action starts with either a hand movement or the human senses. Touch and visual evaluations are the feedback of the system. All three functions can be generated at any moment in time to create an easily manageable system. This function design structure can help during further design choices by simply visualising the known tasks step by step without any design restrictions.

2.2 Analysis of handle design ergonomics

An analysis of the ergonomics in handle design gives a better view of steerable laparoscopic instruments' design choices. The key principle of handle design is to fit the tool to the human hand. The simple act of gripping differs for individuals due to different hand sizes and applied forces onto the handle. Therefore, it is essential to design a handle that fits the different specifications between human hands [23]. According to Landsmeer, each grip can be distinguished in ergonomic principles as a power grip or precision handling [24]. Landsmeer introduced this distinction and explained the power grip as a rigid relation between the object and the arm. This relation means that movements of

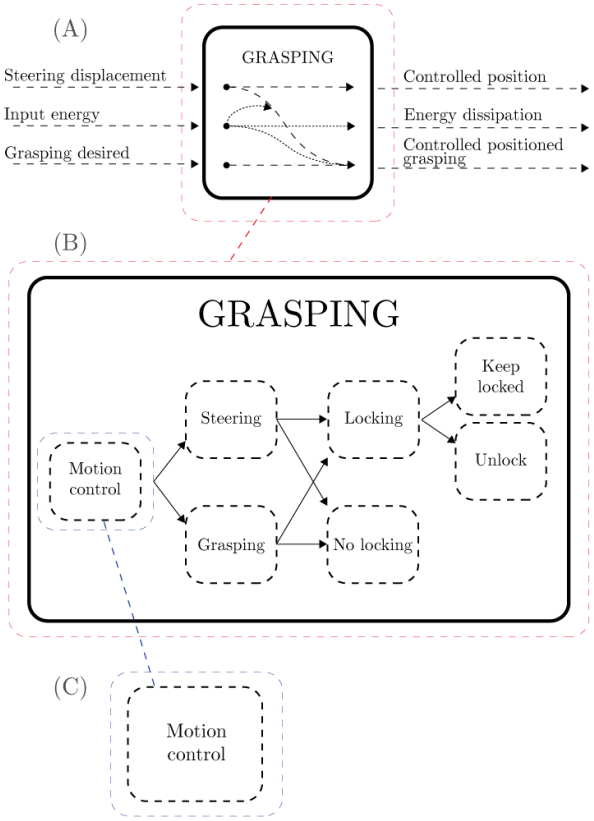

Figure 4: Black box model of steerable instruments.

the object arise by movements of the arm and not by the finger or palm muscles. By precision handling, the hand creates movements of the object independent from the arm [24]. The power grip is, for example, used to apply forces during suturing or holding the instrument securely. During the power grip, fingers are firmly wrapped around the object, where the fingertips are separated from the palm. A large contact area can avoid discomfort in the power grip. The precision handling creates fine movements for high accuracy tasks, such as gently manipulating organs or grasping tissue [23]. Thus, surgical instruments need to include both the power and precision handling to fulfil the task.

Not only the size is important, but the performance also depends on the handle's shape. In surgery, non-ergonomic laparoscopic instrument handles can stimulate inconvenient and uncomfortable movements resulting in poorer performance [13, 14]. Most used laparoscopic instruments have a scissor style shape that requires thumb manipulation [25]. In the study of Van Veelen et al. [15] they noted that the scissor handle is associated with extreme wrist overloads during precision tasks, where surgeons put themselves in non-ergonomic postures. Instead, using the fingertips while grasping, rather than the base of the finger, reduces the discomfort for the surgeon [18]. Figure 6a shows, for example, that the task forces the wrist into a position where ulnar deviation occurs. In comparison, figure 6b shows the ergonomic hand posture. Studies have shown that the forced deviation of the wrist out of the neutral position results in fatigue, discomfort and decreases the efficiency of the forearm muscles [26]. Instruments, of which the handle is in the extension of the forearm

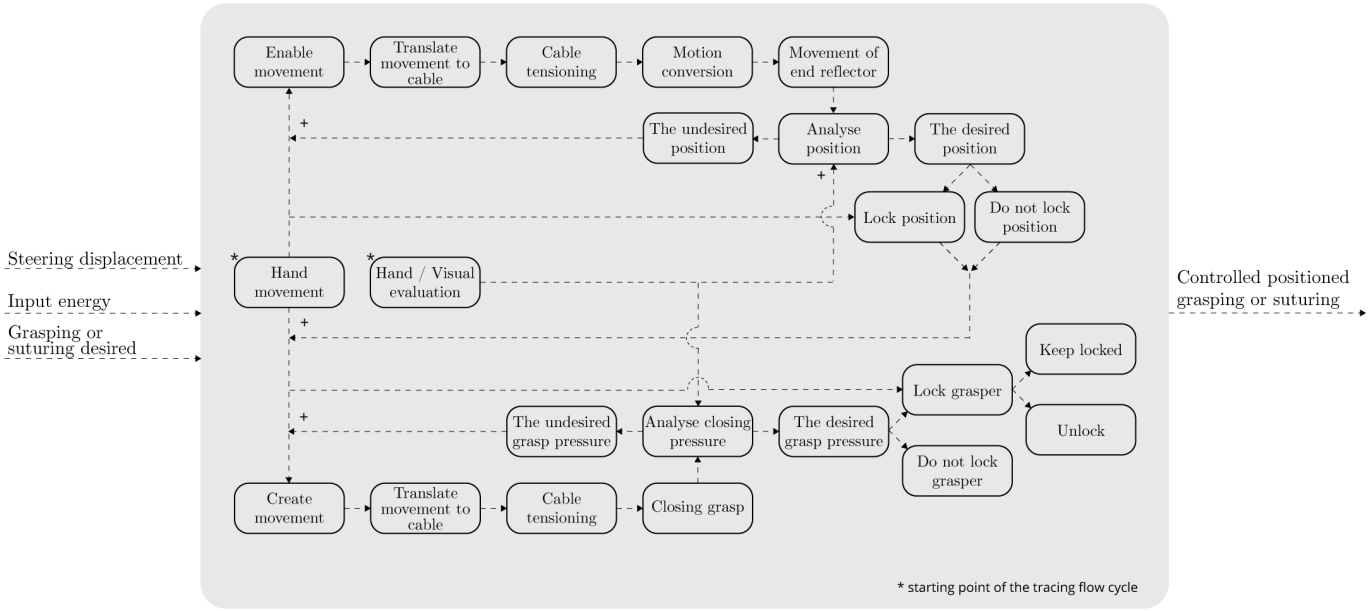

Figure 5: Solution neutral function structure design.

(inline), can cause extreme wrist deviation, greater shoulder involvement, other non-ergonomic postures, limited port positioning options, and limited movements during surgery [1, 14].

The forces that are required during surgery when using laparoscopic instruments creates another ergonomic problem. Laparoscopic instruments with small contact surfaces are not ideal for compressive forces that the hand and fingers apply to the instrument. When using a laparoscopic instrument during MIS, more significant peak and total muscle effort are required than during open surgery [15]. To reduce tremor and execute tasks with high precision, surgeons keep a forceful grip. The compressive forces then obstruct the blood flow and nerves in the surgeon's fingers. Less blood flow and obstruction of the nerves leads to numbness of the fingers which can occur during surgeries [27, 28]. A pressure applied greater than 3 kg/cm^2 causes pressure areas in the surgeon's finger, and applied pressure of more than 5 kg/cm^2 causes pain [29].

Electromyography (EMG) data and surveys showed the response of fatigue in muscles. A three to five times greater muscle contraction force for grasping in laparoscopic surgery than for open surgery was registered in EMG studies of the hand and forearm [26]. Moreover, muscle fatigue was more prevalent among laparoscopic surgeons having less than two years of practice [30]. Experience improves the technique and reduces the level of fatigue. However, the improvement of the technique only slightly reduce the fatigue of the muscles and is unfortunately not enough to prevent fatigue of the surgeon [31].

Furthermore, the posture is important since many of the handle aspects should be designed on the surgeon's posture. Figure 7 shows the ergonomic posture, and the data is retrieved from the study of Bullinger [32]. According to Bullinger, an elbow flexion between 90° and 120° allows for maximum strength. This is also the posture that can be held for the longest time [32]. The angle is important to determine later on the handle dimensions.

It is impossible to design an ergonomic handle that fits all users. Therefore, an anthropometric study (the scientific study of the human body measurements) must be included to develop a convenient laparoscopic handle for the vast majority.

2.3 Design analysis of steerable laparoscopic instruments

An overview of the state-of-the-art of mechanical driven hand-held steerable laparoscopic instruments was created to get a broader view of the different handle control, Table 1. The overview only consists of functioning prototypes or commercially used products, which means no patents or concepts drawings were included. Furthermore, the overview does not address pre-bent laparoscopic instruments of which the shaft can only rotate since no end-effector articulation occurs. The steerable laparoscopic instruments were categorised from the ergonomic point of view, considering their working principle in steering, grasping, and locking. The instruments were numbered below the schematic drawing shown in Figure 8.

2.3.1 Hand movements for steering

All found laparoscopic instruments can steer in at least one DoF. The instruments show a total of seven different steering movements for motion control. As shown in Figure 8, the subcategories for the handle movements for steering were divided into one DoF lever, handle articulation, joystick, trackball, and a steering wheel. A one DoF lever, such as SerpENT (1), and the Radius

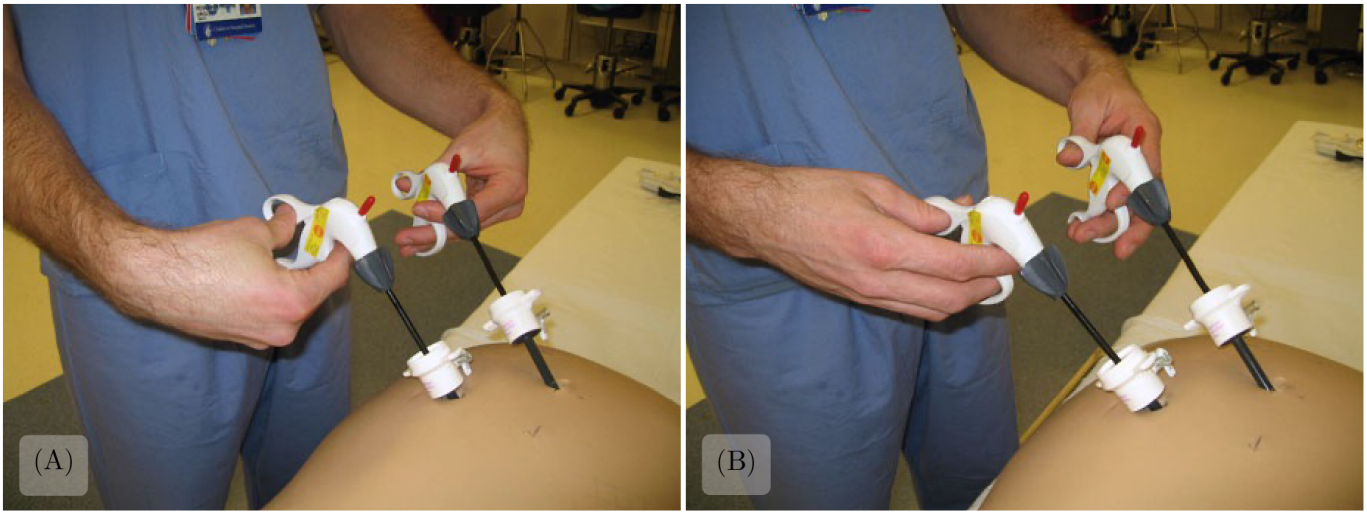

Figure 6: Different hand postures during use. A) Non-ergonomic wrist angle with pressure on carpal tunnel. B) Ergonomic wrist angle. Taken from [16].

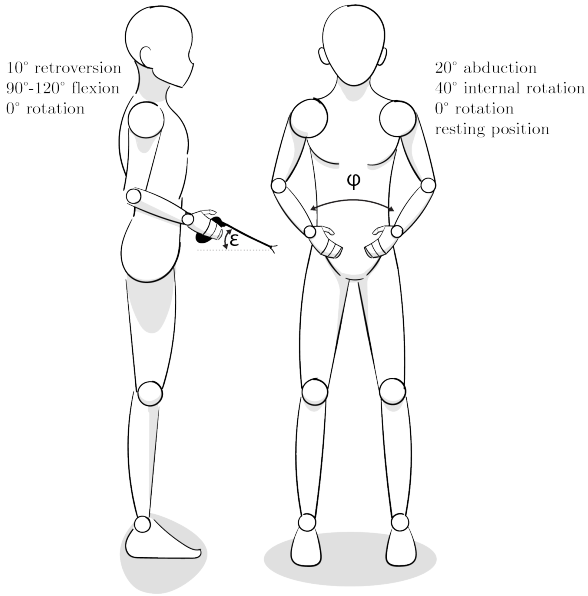

Figure 7: Ergonomically ideal posture for the surgeon during laparoscopic surgery. Symbol ϕ indicates manipulation angle. Symbol ε indicates elevation angle.

Surgical System (2), can create a steering motion in only one DoF. The one DoF lever that is used to steer the end-effector of the instrument can either move in the horizontal direction, as in the SerpENT (1) or vertical direction, as in Radius Surgical System (2) direction. The one DoF lever results in a one DoF articulation of the end-effector in either horizontal or vertical direction [1]. There are two updated versions of the Radius Surgical System, the R2 Drive and R2 Curve, based on the same working principle [34, 45].

The handle articulated control was divided into the pistol grip and the inline grip. Handle articulation is defined by the entire handle's movement to steer the end-effector of the instrument in two DoF. Inline grip means that the handle is placed horizontally in the extension of the axial shaft, Figure 10a. A pistol grip handle is under an angle with respect to the axial shaft, as shown in Figure 10b. All instruments with articulated control require body wall reaction or different external forces to stabilise and counter the reaction forces of the steering movements of the surgeon's hand. However, these forces can be minimised as seen, for example, by the FlexDex (10) [1]. In the design of the FlexDex, a frame connects the instrument to the forearm of the user providing a three DoF articulation system. The wrist articulation is located in the centre of the surgeon's wrist. The handle articulation does not require body wall reaction to counteract the surgeon's steering movement at the abdominal wall and minimises the required external body wall forces [1].

The joystick and trackball controls are two DoF articulation systems that are controlled mainly by thumb movements. Joystick control means that handle grip remains stable where only a single small stick or element that is finger controlled transfers the movement to the end-effector. In the found literature, the joystick transmits the motion by cables to the end-effector [37]. The trackball control is based on the ball and socket joint principle. The ball and socket joint transmits movements of the trackball to the rods inside the axial shaft. The rods transmit the motion to another ball and socket joint, resulting in end-effector articulation [43].

The rotation of the steering wheel in the last category of Figure 8 results in the articulation of the end-effector. The pitch and yaw movement of the SATA's end-effector, for example, controlled by the index finger and thumb that either rotate a wheel, results in a pitch and yaw movement of the end-effector [44].

2.3.2 Hand movements for grasping

Different input movements and design choices were found in the literature to execute a grasping task. As shown in Figure 9, the hand movements for grasping are: scissor front, scissor back, scissor parallel, lever handle into the grip handle, lever handle outside the grip handle, pistol trigger, parallel lever handle, and pinch tweezer. In all cases, the kinematic system consists of a handle that pivots around a point. The only distinction in the kinematic system can be made based on a single

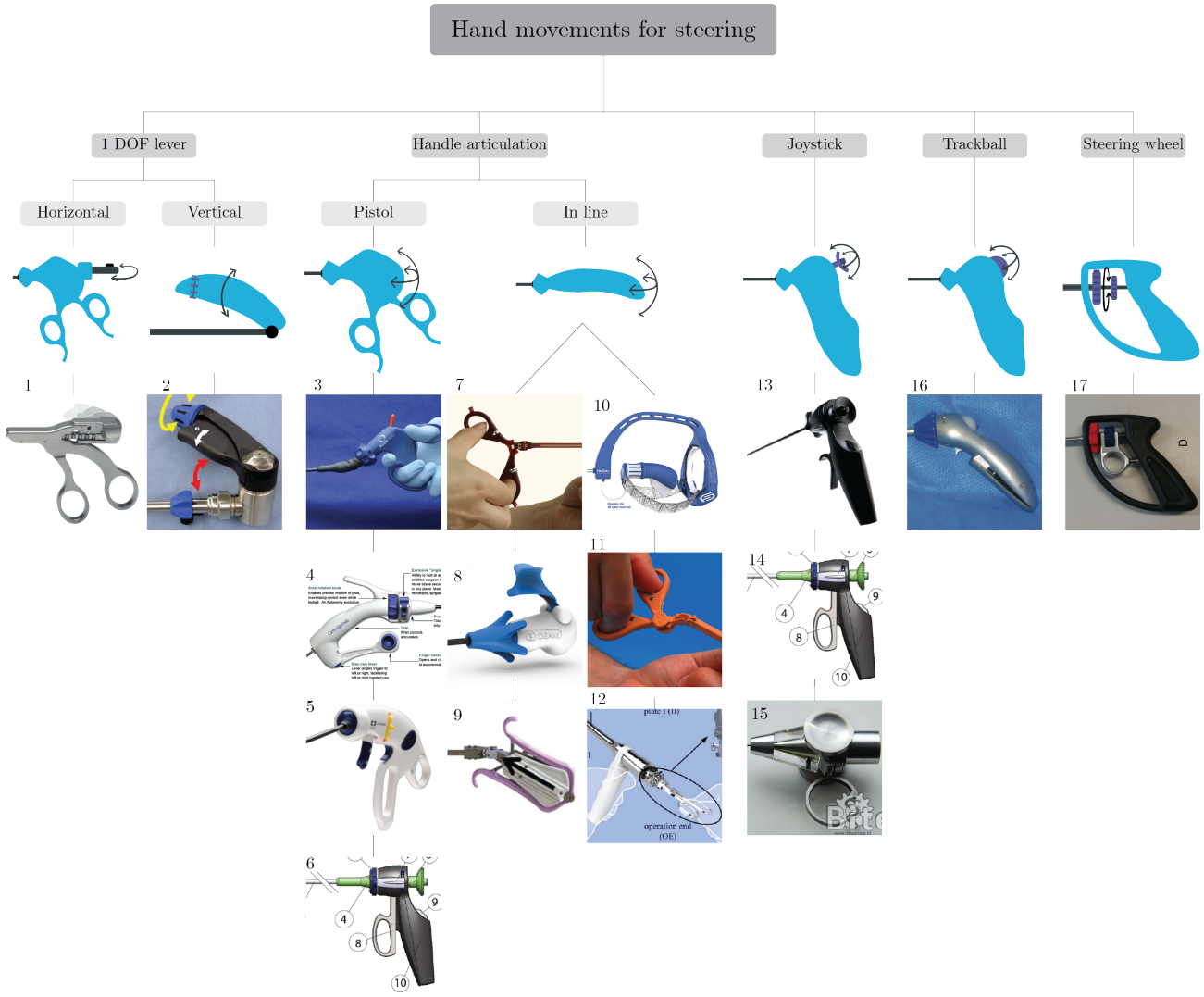

Figure 8: Steerable laparoscopic instruments found in literature. 1) SerpENT [33]. 2) Radius Surgical System [34]. 3) RealHand [1]. 4) Autonomy Laparo-angle [35]. 5) SILS Clinch [36]. 6) Duoflex [37]. 7) Volt [38]. 8) LaproFlex [9]. 9) Maestro [39]. 10) FlexDex [40]. 11) Dragon Flex [7]. 12) Easy Grasp [2]. 13) Miflex [41]. 14) Duoflex [37]. 15) I-Flex [42]. 16) Intuitool [43]. 17) SATA [44].

lever handle (lever handle, trigger, front/back scissor) or parallel lever handle (parallel scissor, parallel lever handle, pinch tweezer). However, the categorisation was based on the design choices to analyse different input movements of the instrument. Eleven out of the sixteen instruments can rotate the axial shaft to change the axial angle of the grasping forceps [1,2,9,34,35,37,43,44]. The rotation of the grasping forceps adds an extra DoF to the system to avoid wrist rotation. The following instruments can rotate the axial jaw angle: Radius Surgical System, RealHand, Autonomy Laparo-angle, SILS Clinch, Duoflex, LaproFlex, FlexDex, Easy Grasp, Miflex, Intuitool, SATA. Most of the instruments have a rotational knob to realise the shaft's axial rotation except the Easy Grasp. The Easy Grasp rotates the entire instrument separately from the scissor handle. This disconnection makes it possible to rotate the grasping forceps while keeping the handle in a fixed position [2].

2.3.3 Hand movements for locking

Within the laparoscopic instrument designs, two different locking systems occur, namely a locking system to lock the grasping forceps' jaws and to lock the steering angle of the end-effector. Locking the controllers avoids fatigue of the surgeons' hand, difficulties, and uncontrolled situations during surgery when applying forces onto the tissue [20, 21]. Not locking the grasping forceps, for example, can be inconvenient for some tasks such as suturing [46]. Due to reasons as such, design choices were made to whether or not include locking mechanisms.

Another essential aspect to take into account is the finger used to control the functions. When the same finger is used to control multiple functions of the laparoscopic instrument, tendonitis can occur [15]. Figure 9 shows that in total, six different steering lock control movements were found in the literature, of which six out of the sixteen instruments are equipped with a steering lock option. Eight out of those sixteen instruments can lock the grasper [1, 34, 35, 37, 46]. In total, five instruments can execute both locking tasks.

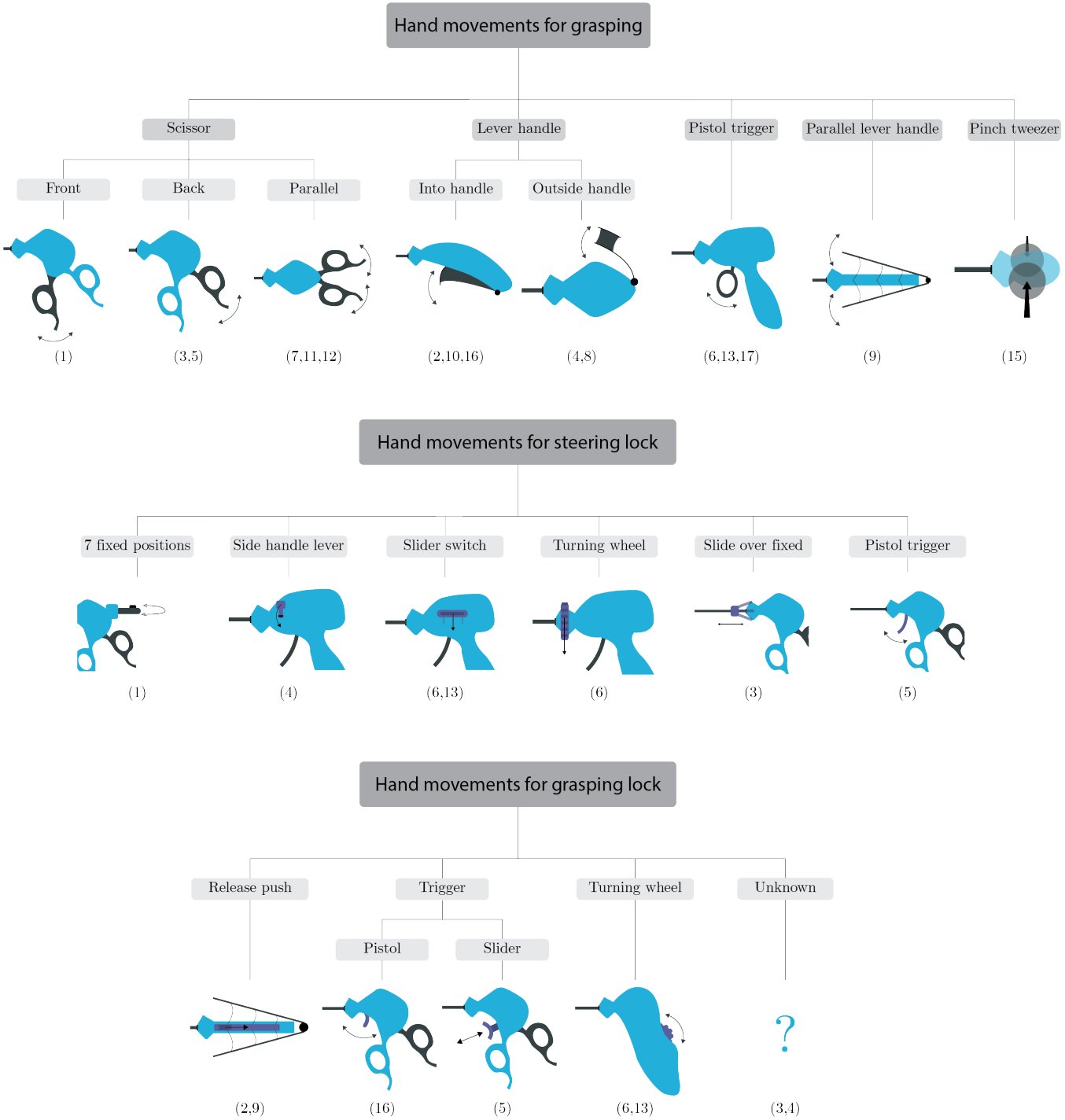

Figure 9: Grasping hand movements, steering lock hand movements and grasping lock hand movements.

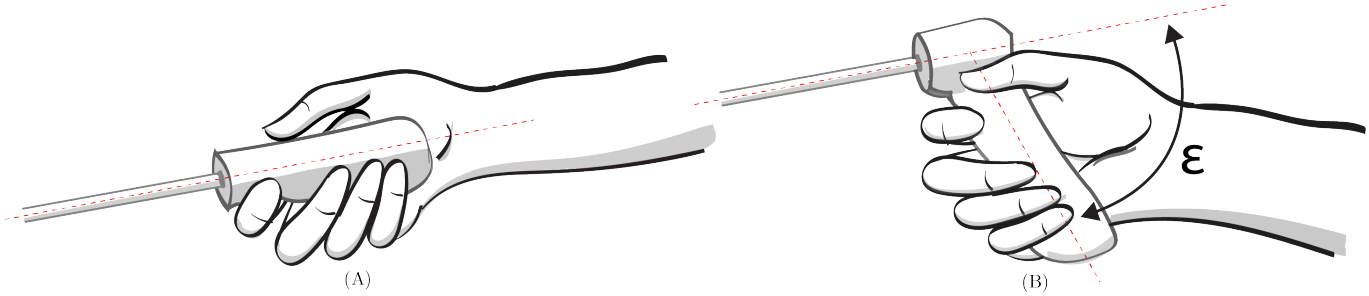

Figure 10: Two different grip handles. A) Inline grip. B) Pistol grip. Symbol ε indicates angle between shaft and handle.

Device	Handle design	Axial shaft rotation	Steering lock	Grasping lock
SerpENT	Pistol	No	Yes	No
Radius Surgical System	Lever	Yes	No	Yes
RealHand	Pistol	Yes	Yes	Yes
Autonomy Laparo-angle	Pistol	Yes	Yes	Yes
SILS Clinch	Pistol	Yes	Yes	Yes
Duoflex	Pistol / Joystick	Yes	Yes	Yes
Volt	Inline scissor	No	No	No
LaproFlex	Inline handle	Yes	No	No
Maestro	Inline handle	No	No	Yes
FlexDex	Inline handle	Yes	No	No
DragonFlex	Inline scissor	No	No	No
Easy Grasp	Inline scissor	Yes	No	No
Miflex	Pistol / Joystick	Yes	Yes	Yes
I-Flex	In palm joystick	No	No	No
Intuitool	Pistol / Trackball	Yes	No	Yes
SATA	Pistol	Yes	No	No

Table 1: Summary of state-of-the-art manual mechanically driven steerable laparoscopic instruments.

2.4 Design requirements

Considering the design analysis of Section 2, design requirements were set out. The design requirements were divided into three subsections of control, dimensions, and production, shown in Table 2.

2.4.1 Control design requirements

Single hand control is required to control the steerable laparoscopic instrument to execute other tasks with the second hand or control two steerable laparoscopic instruments at once. The handle should then rest continuously in a half-closed hand, similar to a resting hand position. It would be favourable if right-handed and left-handed users can control the laparoscopic instrument since around 10% of the world population is left-handed [47]. If a handle is not designed for both left and right-hand users, a 3D-printer has the advantage that the design can be mirrored and then printed.

External forces that the instrument exerts on its environment should be minimised at all times. The steering forces that occur during handle articulation result in the slender rod's reaction forces onto the body wall. The handle articulation now results in less direct steering feedback due to loose and flexible tissue of the body wall that is manipulated by external forces. Besides less direct feedback, the handle articulation also becomes a non-rigid steering system. Therefore, it is impossible to create a rigid steerable system with handle articulation unless a frame connects the instrument to the controlling hand of the surgeon or all forces are opposed in the hand itself. However, mounting the instrument to the surgeon as seen with the FlexDex, for example, the instrument limits the ease of use and is therefore not a design consideration [1].

The handle should allow for end-effector **articulation of 60°** in two DoF to minimise non-ergonomic postures, uncomfortable movements and manoeuvres. An end-effector articulation of 60° is comparable to state-of-the-art steerable laparoscopic instruments [1, 20, 48]. **The thumb should control the steering**. The thumb movements are executed by strong and short muscles located in the palm [49]. Research showed that handle articulation requests greater effort than joystick control [50]. Furthermore, thumb control is usually preferred by users [21] and outperformed handle articulation control in terms of motion, accuracy, and the perception of steering [51]. Moreover, the thumb is the best suitable finger to control the steering, since the thumb is the only finger able to perform flexion/extension, abduction/adduction, opposition/reposition.

Another important control design aspect is the movement of the end-effector relative to the control input. A distinction can be made between parallel control and reverse control. Parallel control is a steering approach where the steering input with respect to the shaft creates an end-effector articulation output parallel with the input. Manipulating the input in an upward pitch direction results in the end-effector's downward pitch direction if parallel articulation is applied. Reverse control means that when controlling the handle in an upward direction, the end-effector moves in the same upward direction. Parallel and reverse control are shown in Figure 11. According to studies, it turned out that parallel control is less intuitive than reverse control [52, 53].

The joystick or trackball controlled by the thumb can be positioned on the left side or at the back of the handle in case of right-handed use, as shown in Figure 12. If the thumb is located sideways to control the steering mechanism on the side of the handle, the steering cannot

be classified as reversed control since the output is not in the same direction as the input. Furthermore, looking at the hand at rest, the wrist is 35° bend relative to the forearm, and the thumb is directed forward, parallel to the forearm and a little off centre from the line as shown in Figure 13. The requirement was set to have

	Subfunctions / Subsystems	Requirements	Wishes
Control	Handle	Single hand control.	Adjustable for left and right handed.
	Steering	Avoiding external forces.	
		Allow for a two DoF end-effector articulation of 60°.	
		Joystick or trackball controlled by thumb.	
		Reverse controlled steering system that is located on the back of the handle.	
	Grasping		Grasping controlled by index finger.
	System	Grasp, steer, lock the jaws of the grasping forceps, and lock the end-effector in place. Possibly all at the same time.	
	Locking		Lock in any position, achieved by continuous locking.
	Ergonomics	Power grip handle to firmly hold the instrument combined with precision handling handle for fine control movements.	
		Handle design that stimulates a straight wrist and allowing the hand to be in a resting hand position.	
		Multiple finger control to always maintain full instrument control and to avoid single finger fatigue.	Lock the steering with the same finger that controls steering. Same holds for the grasper. (Two-finger control).
		Logically ordered and easily accessible control system layout.	
		Entire palm is involved in holding the handle design.	
Dimensions	Ergonomics	Handle diameter of 35 mm.	Handle diameter: Scalable to the preferred size of the surgeon.
		95% of the Dutch population is able to reach and control the functional elements*.	
		Handle angle between: 35° to 45°.	
		Additional grip angle to compensate for metacarpals head of: 12°.	
		Avoid compressive forces on the concentrated contact areas by maximising contact areas.	Prevent applied pressure force of less than 3 kg/cm^2 that causes pressure areas on the surgeon's finger.
Production	Assembly	≤5 parts assembly.	Non-assembly design.
		Accessible assembly design.	
	Single use		Minimal use of material.
			Designing with shell structures.
	Manufacturing method	3D-printing technique: Stereolithography.	
	Material	Formlabs resins: Durable and Tough 1500.	

Table 2: Functional design requirements. * Dimensions not yet defined since no control layout is known.

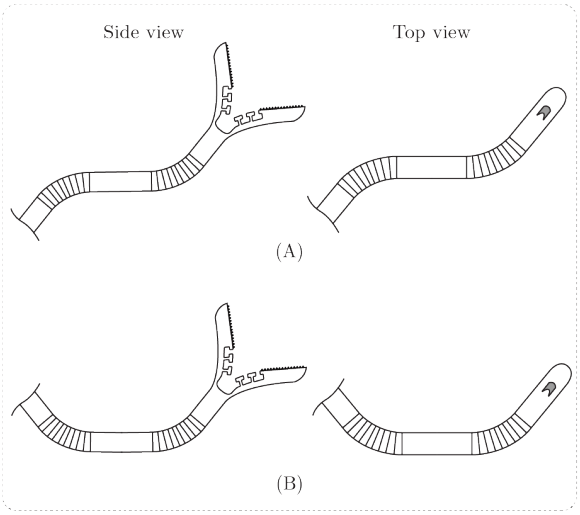

Figure 11: Different input motion controls that result in the movement of the end-effector. A) Parallel control. B) Reverse control.

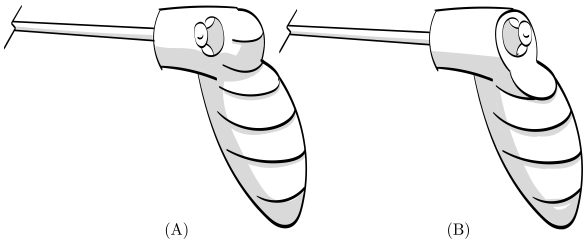

Figure 12: Schematic drawing of joystick placement onto the handle.

a **reverse steering control** system that is placed on **the back** of the instrument.

Furthermore, the control system makes it possible to **grasp, steer, lock** the jaws of the **grasping forceps**, and **lock the end-effector** in place. The control tasks should possibly be executed at any time and simultaneously to avoid inconveniences during task execution. Locking the end-effector and grasping forceps relieve the surgeon from tiresome steering and grasping postures. Locking the grasping forceps can also be convenient, for example, for tasks such as suturing to relieve the surgeon from gripping fatigue [46].

The working principle of locking must be considered. However, the specific design choice for the steering lock and grasping lock hand movements are not yet decided. There are two options for the locking feature of steering and grasping: discrete and continuous locking. Discrete locking is distinguished by a pin and hole system and is only possible with different interval positions. Continuous locking, on the other hand, has no locking interval positions and can take any desired locked position. The desire is to **lock in any position**, which can be achieved by continuous locking.

From an ergonomic aspect, it is important to consider the most ergonomic handle available to hold the instrument. A **power grip handle** should be implemented to hold the instrument firmly and precision handling to execute fine movements with high accuracy. An inline grip handle, seen in the FlexDex and Maestro,

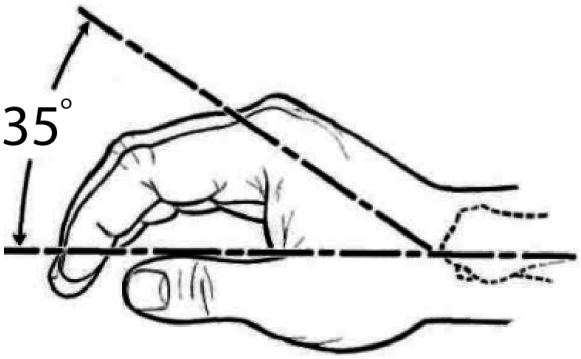

Figure 13: Hand at rest. Taken from [54].

for example, requires ulnar deviation and greater shoulder involvement during handle articulation [14]. To minimise the ulnar deviation of an inline grip handle during end-effector manipulation, larger angles with less input can be generated using an amplified articulation control, but ulnar deviation will still occur. The wrist must be placed in a position that **prevents ulnar deviation** such that the hand is in a resting position.

To maintain full control while executing different control tasks simultaneously, such as steering and grasping, **multiple finger control** is necessary. Using only one finger for the different tasks can lead to the finger's previously mentioned overload and must be avoided. To minimise effort and avoid confusion of the multiple control systems, a **logically ordered and easily accessible** control system layout must be designed. The logically ordered control system layout allows for anatomically correct movements and prevents the surgeon's high demand that results in fatigue. To minimise the chance of confusion between the different controlled features, it is highly desirable to lock the steering control with **the same finger** that controls the steering movement. This also holds for the grasper, where another finger controls the grasping forceps and locks the grasping forceps in place. Furthermore, should the **the entire palm** be involved in holding the handle design since it reduces the fatigue of the thenar [55].

A wish was made for two-finger control, and it is important to discuss the suggested finger to control the grasper. The features should be controlled by the fingers best suited to the specific task. As previously mentioned, the thumb is the suggested finger for steering control. The middle finger and index finger are the best-suited fingers for precise manipulation tasks [14]. However, two studies state that it is difficult to control the little, ring and middle finger simultaneously and independently [56, 57]. Accordingly, the index finger is the most suitable finger to control the grasper in a two-finger configuration. A flow chart in Figure 14 gives an overview of the fingers in control of the different control systems.

2.4.2 Dimension design requirements

As mentioned in Section 2.2, ergonomics should be based on anthropometric data. Creating an instrument

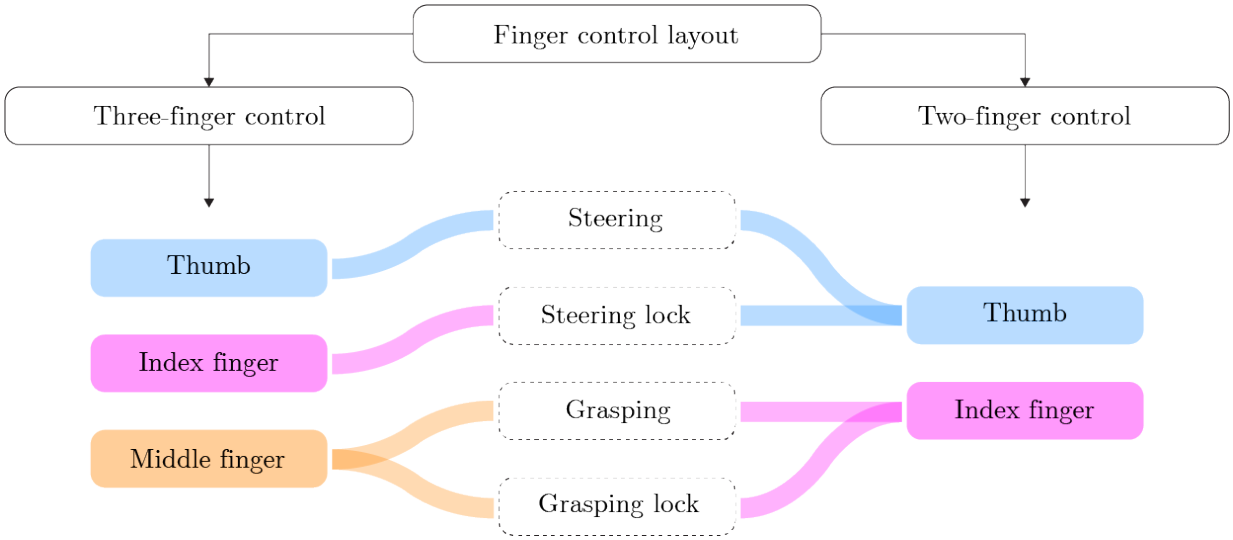

Figure 14: Flow chart of the finger control layout.

handle with a specific diameter that is convenient for 95% of the target group is a well-considered compromise [58]. A percentile value of 5% indicates the value of which a given percentage of the observation in a target group falls. Meaning that for a P5 value, 95% of the population can at least measure up to the size of the handle. In the study of Patkin, the optimal power grip handle has a diameter of 30.00 - 40.00 mm [23], whereas, for Seo and Armstrong, 40 mm is the diameter of an optimal handle [59]. However, 95% of the Dutch population between 25 and 65 years old can enclose the grip of a cylinder by the thumb and index finger of a handle diameter of 35 mm. These values were based on the data of Dined that provides an overview of anthropometric data [60]. The **diameter** of the handle was chosen to be **35 mm** considering the Dined data and the studies mentioned above. Also, **95%** of the Dutch population is able to control the functional elements, which means that the fingers should be able to reach the control buttons.

The manipulation angle is the angle between the two inner arms indicated by angle ϕ in Figure 7. Manasnayakorn et al. found that a manipulation angle ranging from 45° to 60° is the most ergonomic angle [61]. To ensure the shortest execution time and optimal performance quality, the elevation angle, the angle between the shaft and the horizon indicated by angle ε in Figure 7, should be of the same magnitude as the manipulation angle. Thus for a 30° manipulation angle, the elevation angle should be 30° as well [61]. According to the study of Fingerhut et al., the best ergonomic elevation angle to work with is 40° to 45° [62]. It is relevant to address the importance of the elevation angle. The elevation angle is dependent on the length of the shaft, the height of the operating table, and the surgeon's length. The elevation angle was therefore not included in the design requirements due to the interdependent parameters.

Another critical angle to be considered to avoid ulnar deviation was the angle between the shaft and the handle, as shown in Figure 10b. An angle up to 50° reduces ulnar deviation [15]. According to van Veelen et al., the **grip angle**, which is the angle between the handle and shaft, must be between **35° and 45°** [15].

Furthermore, it is essential to take the metacarpals head into account for the handle design. The line through the heads of the metacarpals of the index and little finger with respect to the longitudinal axis of the hand creates an angle of 75° [14]. According to Tilley and Dreyfuss, the angle between the middle and little finger perpendicular to the line of the longitudinal axis of the hand is 12° [63]. The ergonomic handle will have an additional **12° angle along the grip angle** that is between the 35° and 45°. The additional 12° angle will compensate for the position difference of the metacarpals head between the middle and little finger. The additional handle grip angle follows the vertical finger grip curvature shown by the dashed line in Figure 15.

Another problem that surgeons face is the high-pressure loads applied to the instrument, as explained in the analysis of handle design ergonomics. The compressive forces on the instrument's concentrated contact areas can obstruct the blood flow (ischemia) that can lead to numbness and tingling of the fingers and should be minimised [**?**]. **The contact areas** for this handle design must therefore be **maximised** as much as the design allowance. A wish was made to have an applied pressure force of less than 3 kg/cm^2 to avoid pressure areas on the surgeon's finger.

2.4.3 Production design requirements

The handle design should have a minimised amount of assembled parts, wherein a wish was made for a non-assembled main body. However, simple design and easily accessible assembly are of high importance to minimise the assembly time. Circumstances in the design can arise wherein it might be more convenient to have more assembled parts that are easier to assemble than less assembled parts that are more difficult to assemble, resulting in a longer assembly time. Therefore, **less than 5 part assembly**, with easily accessible assembly was required. **3D-printing** is the

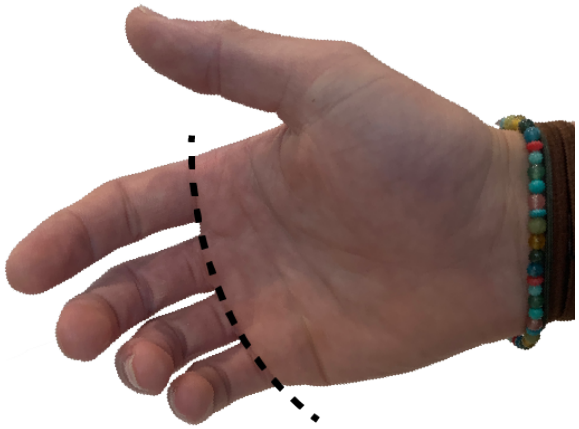

Figure 15: Drawn line between the heads of the metacarpals.

ultimate manufacturing technique for minimising the assembly and number of parts. For this design, a wish was made to minimise material usage by, for example, shell structures since the instrument will be a disposable product.

Stereolithography (SLA) will be used as the printing technique to create the mechanisms and prototype. SLA is a technique where a photopolymer resin is contained in a vat. The desired layers are created by a UV laser beam that solidifies the curable resin [64]. The specific printer is the Form 3B printer from Formlabs, and the materials that can meet the design requirements are **Durable** resin and **Though 1500** resin from Formlabs. **Durable resin** is flexible, impact-resistant and creates a smooth surface finish, which is ideal for the flexures printed within the design. However, the springback time of the material is low. A low springback time results in a slow return of the initial shape state and is undesirable. It is, therefore, that **Though 1500 resin** will be used for spring designs within the instrument.

2.4.4 3D-printing technique

Either **Durable, Tough 1500** or both resins from Formlabs will be used as material. To meet the design requirements of a minimised and simple assembly design, 3D-printed joint configurations, bending elements, stiff elements, and grasping control mechanisms have to be investigated. Also, to control the different features, the positioning and the printing feasibility have to be kept in mind while brainstorming and creating concepts. The 3D-printing possibilities to meet the requirements were further investigated in Section 4, the design process.

3 Conceptual design

3.1 Handle design concepts

The pistol grip handle is under an angle to the axial axis of the shaft. Unlike the inline grip, the pistol grip stimulates a straight wrist and avoids ulnar deviation due to the handle angle. The pistol grip was therefore

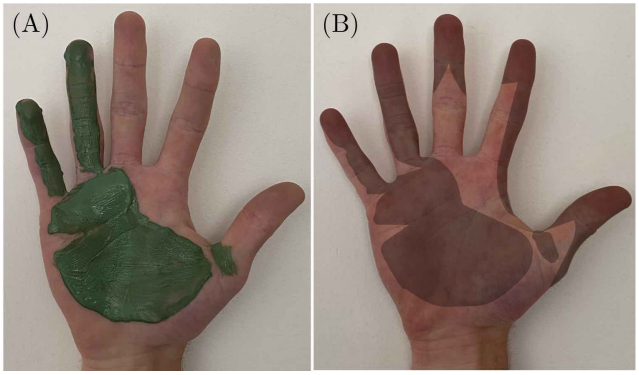

Figure 16: Visualisation of important contact areas. A) Visualisation of contact areas by pressing a soft clay ball, painted in green, into form of the force grip. The important pressure areas holding the instrument concerns the palm, thenar, ring and little finger. B) Most important contact zones of the force grip combined with the areas for controlling the laparoscopic instrument.

chosen as handle configuration.

Furthermore, the handle has to be designed such that large contact zones of the thenar, palm and fingers can avoid the discomfort of the power grip, meaning that the pressure will be evenly distributed over the handle design with a diameter of 35 mm. The crucial areas for manipulating the laparoscopic instrument, according to Matern and Walker [14], were combined with the pressure areas for holding the instrument, Figure 16b. In addition, if the middle finger will be included in the power grip, the entire finger will be wrapped around the handle, similar to the little and ring finger.

Models were made from clay to get a first visual insight into the handle shape. The thumb, middle finger, and index finger were not yet assigned to a specific position in the handle designs. The ring and little finger are usually assigned to hold and direct the instrument [14]. Figure 17 shows two different moulded handles used for the conceptual drawings; one with the shaft above the index finger and the other with the shaft placement between the middle and index finger. In the case of the shaft going through the middle finger and index finger, the controlling systems were separated by a rod. The separation potentially prevents confusion.

3.2 Control design concepts

An investigation into previously designed laparoscopic instruments gave a broad view of the design possibilities [18]. Considerations were made based upon requirements and ergonomic design choices, which decreased the possible design combinations found in the literature.

The category, one DoF lever, in Figure 8 was not included in the design overview of Figure 18 since it cannot steer in two DoF. The scissor category within the grasping hand movements was not included in the design overview regarding ergonomics. Van Veelen et al. noted that the scissor handle is associated with extreme wrist overloads during precision tasks, where surgeons put themselves in non-ergonomic postures [15].

Furthermore, different grasping mechanisms from

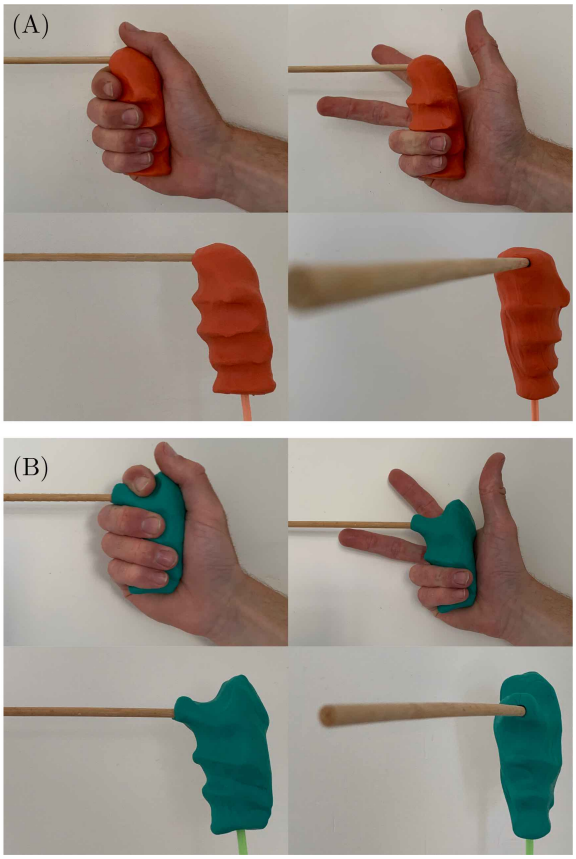

Figure 17: Various shaft layouts. A) Shaft above index finger. B) Shaft placement between the middle and index finger.

the literature were not included in the design overview. The pinch tweezer was eliminated since two fingers are occupied with controlling one task. The parallel lever handle was not included in the design overview since the palm has to move inward, which leads to movement of the entire hand that can result in unwanted movements.

The seven fixed positions and the slide over fixed control mechanism that can only take one locked position were excluded from the overview based on the number of possible lock positions. All designs found in the literature to lock the grasper were included in the design overview. The overview is shown in Figure 18.

Different combinations of solutions given in the design overview were combined into design ideas. The kinematic systems, in the concept drawings of Figure 21-20, visualise the finger movements and indicate the location of the control mechanisms to see the full potential of different control combinations.

For this stage of concept generation, the kinematic system and arrangement of the control buttons were considered to come up with conceptual designs. The combinations were made within the design overview and applied in such a manner to fulfil the ergonomic requirements. As stated in the requirements, the handle must have the ability to control the different functions simultaneously. Considering two fingers that hold the handle, three remaining fingers can now control the four different tasks of grasping, steering, grasping lock, and steering lock. As an example, the design in Figure 19a has four different control buttons (indicated by colours) to execute all tasks. Only three fingers can control the features, which results in a non-continuous control system.

It is possible to include the palm to control the grasper, as shown in Figure 19b. For example, the thumb controls the steering, the index finger controls the locking of the end-effector, the middle finger controls the grasper, and the palm controls the locking of the grasper. With this configuration, it is possible to execute all four tasks simultaneously. However, this design has the disadvantage that the entire palm involved in the control movement, which results in unwanted movements of the entire instrument.

A different control approach, shown in Figure 19c, results in three fingers executing all four tasks while holding the instrument stable. The thumb controls the joystick, and the index finger controls the steering lock, for example. The middle finger controls the grasping forceps and locking of the grasping forceps. A system as such uses interlocking mechanisms that can lock the jaws of the grasping forceps using the same finger that controls the grasping movement by locking the slider/trigger in place. However, the required grasping force must be achieved in the locked state and the unlocked state. The dual control system of grasping and locking must be designed such that the grasping force does not exceed the maximum applied pressure while creating the extra displacement to lock the grasper in place.

To meet the requirement of a simultaneous control system, with a two-finger control design as wish, a different advanced control system than the control systems in Figure 19 must be designed. The advanced system must be designed such that two fingers control four tasks. The tasks should be related to each other, meaning the finger either controls steering and locking of the end-effector or controls grasping and locking of the grasping forceps. Different aspects have to be considered, such as friction, interlocking, locking upon release, and design stiffness to develop a two-finger control design.

3.3 Conceptual control layout

The priority of the design process was to create an innovative two-finger control system for the ergonomic handle. However, if it appeared that two-finger control was not feasible in this phase of design, three-finger control was the alternative. Therefore, both the three and two-finger control were investigated, and design layouts were drawn. The concept drawings were divided into three and two-finger control. Two-finger control layouts are shown in Figure 20. The three-finger control concepts are shown in Figure 21 and Figure 22.

The two-finger control design was a concept where the joystick can be locked without any external control buttons. For this manner, the steering control was designed such that it can also lock itself, leaving it a simultaneous system where only two fingers control all features. Two-finger control designs lead to the most simplistic design layout possible that avoids confusion and single finger fatigue. The concept drawings are

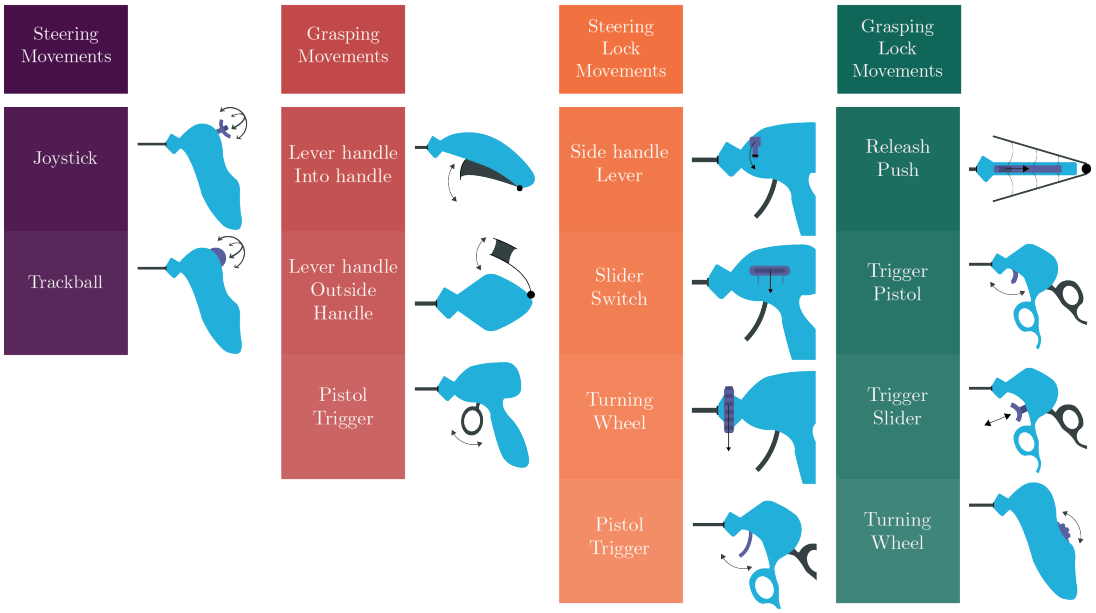

Figure 18: Design overview of the chosen design combinations.

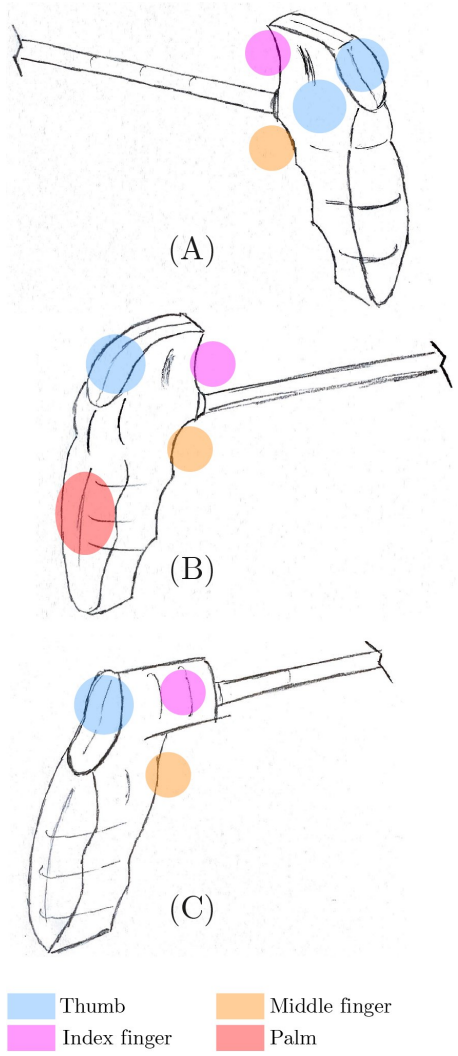

Figure 19: Conceptual drawings of potentially feasible control layout examples. A) Handle design with a non-continuous control system, thumb controls two features. B) Continuous control system design that includes the palm. C) Continuous three-finger control system design.

shown in figure 20 where the thumb controls the steering feature, and the index finger controls the grasper. The joystick control was further developed to see the full potential of the two-finger control in Section 4.

In Figure 21 and Figure 22, two different handle designs were drawn. One design was drawn with the rod above the index finger, and the other design with the rod between the index and middle finger. All grasper controls in Figure 21 can be interchanged between the two different handles. The steering lock control concepts were designed based upon the specific handle and cannot be interchanged between the two handle designs. Moreover, the trackball and joystick concepts for steering control can be interchanged between the handle designs.

The designs in Figure 21 and Figure 22 show the kinematics of the three-finger control systems where the different colours represent the finger that is in control. Figure 21 shows the possibilities of three-finger control concepts to lock the grasping forceps. Figure 22 shows the three-finger control concepts to lock the steering control. A combination between the control layouts of Figure 21 and 22 results in the three-finger control layout. With a thumb controlled joystick design and pistol grip handle, the index finger is the closest finger to the joystick. Since either the cables must be locked or the joystick itself must be locked to keep the end-effector in place, the index finger was chosen to control the steering lock in a three-finger control design. The above-mentioned positioning for the three-finger control layout prevents design complications such as cable placements. All conceptual grasper in two and three-finger control layout designs were designed such that besides grasping, the system can also lock itself.

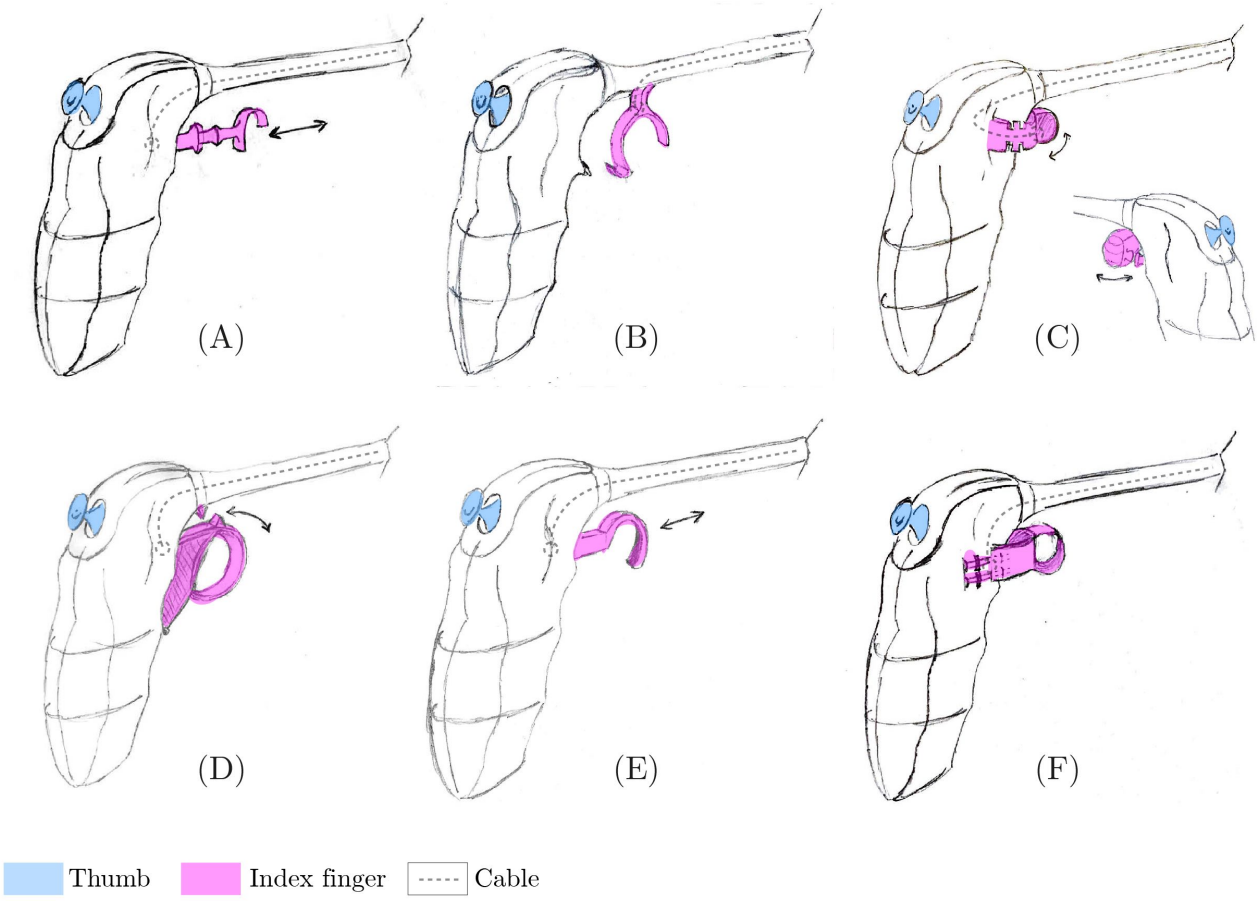

Figure 20: Two-finger control concept drawings of the entire system control.

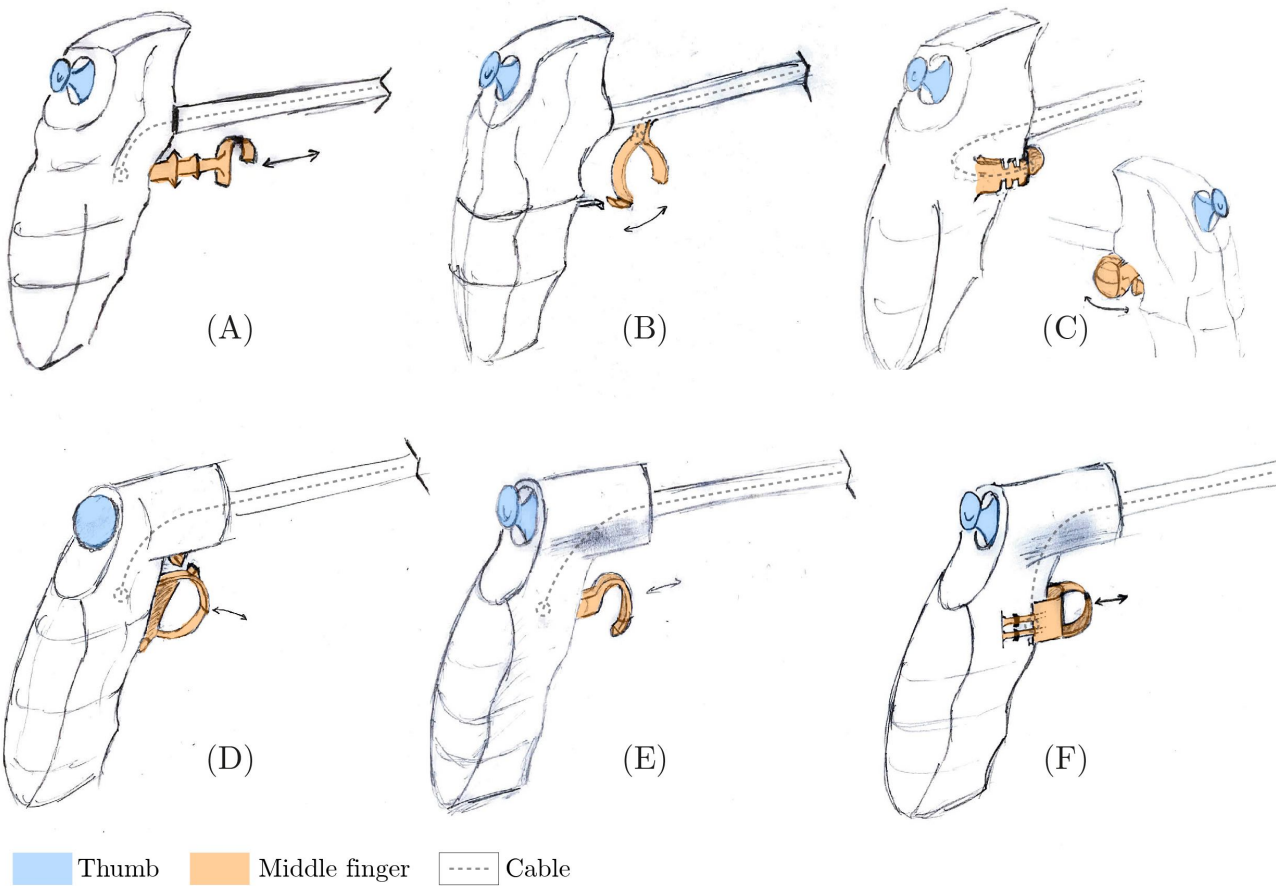

Figure 21: Three-finger control concept drawings of the grasping lock control.

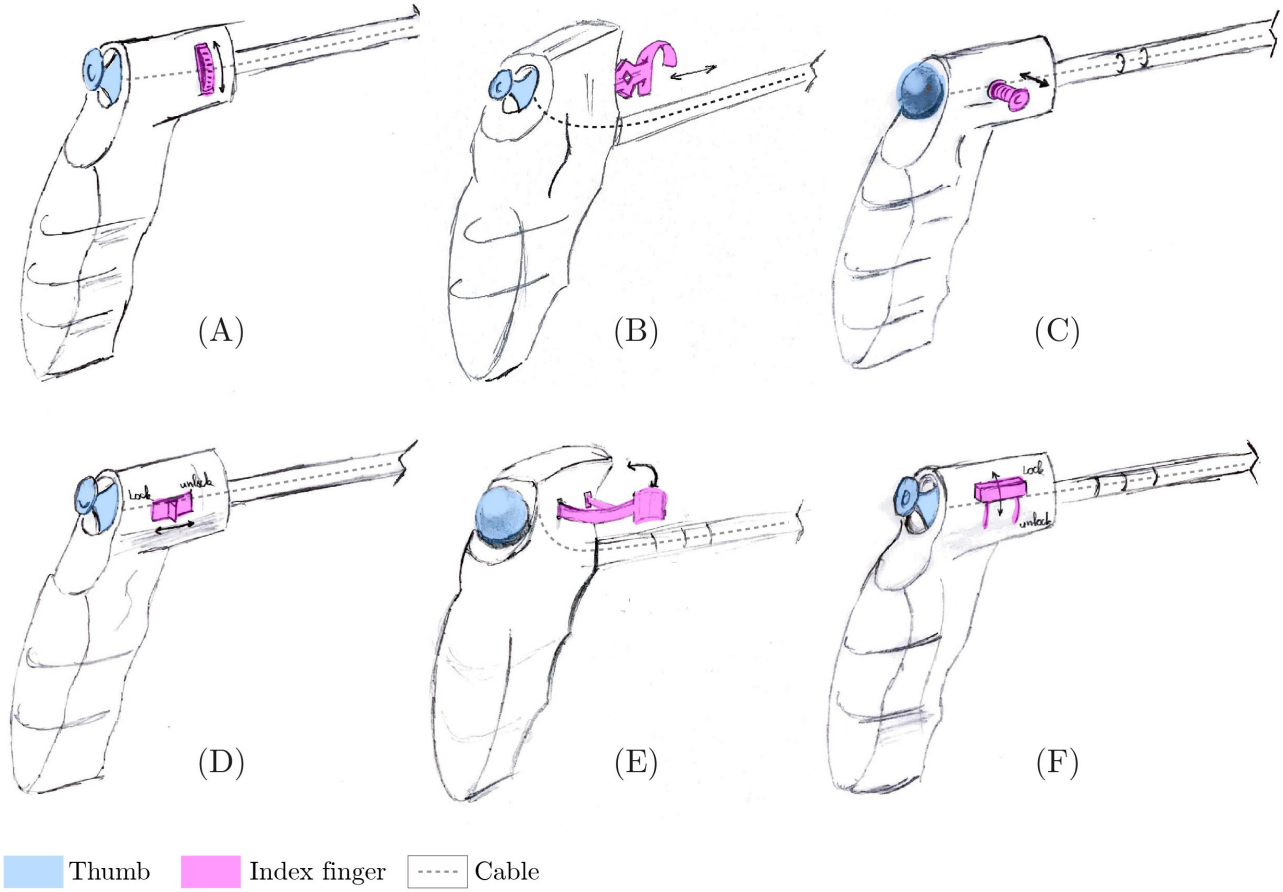

Figure 22: Three-finger control concept drawings of the steering lock control.

3.4 Concept selection

3.4.1 Steering control selection

The concept selection is explained within this section and presented in Table 3. The table provides an overview of the criteria whereupon the concepts were judged. The concepts were graded accordingly on a scale from five to one.

First of all, the difference between trackball design and joystick design must have been considered by investigating the working principle of the two control systems. A trackball design consists of a ball and socket joint that transmits the movements to the rod inside the axial shaft where the entire trackball system contains multiple rotating and moving components [43].

A joystick, on the other hand, transmits the motion via a moving stick that includes cables to the end-effector with fewer parts than a trackball. Therefore the joystick was chosen to control the steering system. The trackball and joystick control designs were not scored in Table 3. The concept selection towards the final conceptual design could then be made for the two and three-finger simultaneous control systems.

3.4.2 Two-finger control selection

For the two-finger control design, the index finger was assigned under the shaft to mimic the naturally closed grip towards the palm [14]. Also, in this two-finger control configuration, no confusion of the different control systems can occur. None of the kinematic systems interferes with each other, so the shaft does not have to separate the control systems. **Design A, E** and **F** of Figure 20 looked promising in terms of ergonomics and placement of the controls. Those three grasper designs are based upon sliding mechanisms that move in and outward. **Design A** consists of a sliding mechanism that moves into the handle and locks when the slider trigger is locked into the interlocking mechanism. **Design E** also consists of a sliding mechanism but is based upon a constant friction design when moving in- and outward. **Design F** is based upon a slider trigger that moves on the outside of the handle and also interlocks that slider trigger. The sliding mechanisms consist of a sliding part and a guiding path. These mechanisms need to be assembled in order to function which does not contribute to the requirements of minimised assembly design and were therefore excluded from the concept selection.

Design B, C and **D** of Figure 20 have a rotational motion input. The rotational movement can be easily achieved by 3D printing flexures that transmit the rotational movement through elastic body deformation. All three designs have a different grasp and release direction. The grasping control in **Design B** is close to the shaft, where the cable of the grasper can run through the shaft to the grasping forceps without any bypasses. The grasper's input motion in **Design C** moves into the same direction as the enclosing motion of

the hand that results in the manipulation of an enclosed handgrip, which is ergonomic in use [65]. However, designs as such come with drawbacks. Multiple cable bends are necessary within **Design C** to run from the grasper towards the grasping forceps. The wire experiences additional friction within the cable trays under tension since the cable is bent around corners. The decrease in feedback due to cable friction is undesirable. **Design D** is attached to the handle, and the cable must also run through the handle to reach the shaft, resulting in less efficiency due to wire bending. A similar grasping system as shown in **Design B** was further explored in the preliminary design since a flexure joint can realise the motion, and the cable runs from the grasper directly through the shaft.

3.4.3 Three-finger control selection

The selection of the three-finger control design was also based upon multiple design criteria. The combination of the most suitable grasper and steering lock control results in the final conceptual design. The same reasoning for the grasper in two-finger control design was applied to the three-finger grasping control design selection, Table 3.

Design A in Figure 22 contains a turning wheel. A turning wheel contains moving parts and must be assembled, which does not contribute to the desire for a minimised assembly design. Since the task is locking, the feature must either be in a locked or unlocked state. The either locked or unlocked state is different from grasping, which must be able to take any position. Looking at **Design B**, it is possible to develop a compliant snap-through system that can function as a continuous locking system, either in a locked or unlocked state. A snap-through working principle can also be developed for the control systems of **Design C, D, E** and **F**, Figure 22. However, the various designs show different index finger movements to control the task.

To create a system where the least muscle fatigue occurs, the index finger motion must be prevented from abduction and extension extremities. Since the three other fingers are in an enclosed grip position (flexion), the index finger should be flexed to ensure physical comfort and prevent muscle fatigue. The design that allows a flexion motion of the index finger is seen in **Design B** and was therefore chosen as the final conceptual steering lock feature. An informed and logical choice was made for the three-finger control handle design to avoid confusion of the different controls. The shaft, by three-finger control, runs between the index and middle finger to provide the separation of the controlling systems. Moreover, this system is beneficial in the three-finger control layout since none of the kinematic systems can now interfere with each other. The final conceptual design of the control system placements for two and three-finger control are shown in Figure 23.

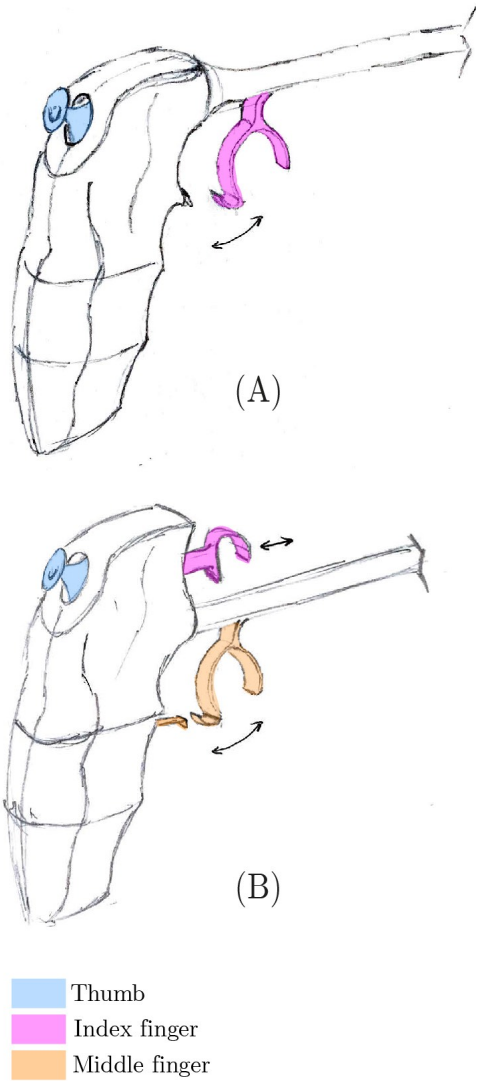

Figure 23: Conceptual design selections of two-finger and three-finger control. A) Final conceptual handle design with two-finger control. B) Conceptual handle design with three finger control.

3.5 Final conceptual design

Multiple conceptual designs were proposed wherein two-finger, and three-finger control concepts were both elaborated. The two and three-finger control designs in terms of hand movements can both be achieved. However, a two-finger control contains fewer control buttons, results in more straightforward control with less confusion between the control systems. Therefore, was the two-finger control, shown in Figure 23a, selected as final conceptual design and further elaborated in Section 4.

4 Design process

4.1 Preliminary design

4.1.1 Joint configurations

The grasping control must enable one DoF motion to realise the grasping forceps' opening and closing movement. The joystick must enable the control of the end-effector in two DoF. Possible joint mechanisms

	Requirements	A	B	C	D	E	F
Two Finger grasping control.	Ergonomic movements	4	4	5	4	4	4
	Ease of use / Muscle fatigue.	4	4	5	4	4	4
	Placement of controls.	5	5	5	5	5	5
	Assembly / No moving parts.	1	5	4	4	1	1
	3D printability.	5	5	3	4	5	5
	Cable bents / Cable connections.	3	5	1	3	3	2
Score		**22**	**28**	**23**	**24**	**22**	**21**
Three finger grasping control.	Ergonomic movements	4	4	5	4	4	4
	Ease of use / Muscle fatigue.	4	4	5	4	4	4
	Placement of controls.	5	5	5	5	5	5
	Assembly / No moving parts.	1	5	4	4	1	1
	3D printability.	5	5	3	4	5	5
	Cable bents / Cable connections.	3	5	1	3	3	2
Score		**22**	**28**	**23**	**24**	**22**	**21**
Three finger steering lock control.	Ergonomic movements	2	5	4	3	3	3
	Ease of use / Muscle fatigue.	3	5	4	5	5	4
	Placement of controls.	4	5	4	4	4	4
	Assembly / No moving parts.	1	4	4	4	4	4
	3D printability.	2	4	4	4	3	4
	Snap through simplicity/ Steering lock control design simplicity.	2	4	4	4	3	4
Score		**15**	**27**	**24**	**24**	**22**	**23**

Table 3: Graded concepts based on established criteria for concept selection.

that enable rotational movements in one DoF and two DoF were suggested by Jelinek et al. The suggested mechanisms highlight different joint configurations categorised by several joint types [48]. As shown in Figure 69 of Appendix B, the motion can be established by rolling, sliding, the combination of rolling and sliding, or bending. A planar joint that allows for one DoF can fulfil the desired grasping motion. A spatial joint category, divided into the perpendicular mirrored joints and revolved joints, allows the transfer of the movement from the steering control to the tip in two DoF.

4.1.2 Minimal assembly joint configurations

The requirement to have a 3D-printed minimised assembly design excludes some configurations from the joint classifications due to complexity. The grasper control, which should allow for one DoF motion, is feasible by the bending flexure joint. The bending flexure joint is a simple design that requires no assembly.

The joystick control requires spatial joint connections to realise the joystick movement. The bending flexure joint is a non-assembly configuration. However, a flexure joint does not have a single centre of rotation where the joystick pivots around. The joystick's path is then not defined by a circular motion with a constant radius. The flexure joint can therefore be a disadvantage in a further design stage for two-finger control design. The rolling belted joint and sliding hinged joint do not require assembly in theory. However, both joint types are complex to print, and simpler solutions can be found.

The working principle of a rolling friction joint is based on normal force and must be assembled under preload. The rolling sliding joint contains a smaller friction surface area than the sliding curved joint. On the other hand, the rolling sliding joint tends to slide if not enough pressure is applied during assembly between the two surfaces. The system becomes prone to error if no pressure is applied during assembly and was therefore excluded from the design. The rolling toothed joint and sliding curved joint are the best constraint joint types. However, the rolling toothed joint contains multiple angled surfaces where the sliding curved joint consists of a single surface which is constrained by curved features. The sliding curved joint was chosen due to its simplicity.

4.1.3 Handle design

The P5-value for the handle diameter is 35 mm. The desired handle angle with respect to the axial shaft is between 35° and 45° [15]. For this design, a 45° angle was chosen.

The difference between smooth grips and grips with finger grooves was investigated. Finger grooves can be

a disadvantage since they may not fit every surgeon's hand size, which results in non-ergonomic postures and injuries. The two handles were designed with and without finger grooves. According to Gonzales et al., the finger grooves must have a length of 30 mm and a width of 24 mm [66]. However, the little finger width size of the 95th percentile male was 6 mm smaller than the suggested finger groove of 24 mm. The little finger handle groove was therefore chosen to be 20 mm in width. Adding up the finger grooves widths makes a total width of 92 mm, which becomes the handle's total length with finger grooves.

According to Matern & Waller, the 95th male percentile of the hand with is 93 mm [14]. However, a total width of 92 mm was also chosen for the handle without finger grooves. Both ergonomic handles have an additional 12° angle along the grip angle, which compensates for the position difference of the middle and little finger's metacarpals head. The ring finger's metacarpals head starts at a distance of 48 mm from the top of the handle grip. At this distance starts the 12° angle compensation until the bottom of the handle. Furthermore, at the distances 24, 48, 72, and 92 mm from the top of the handle, points were placed through which a spline was drawn to create an ergonomic curvature through the metacarpals head.

The two different handle grip designs that meet all requirements are shown in Figure 24. No control features were yet drawn in the handle designs, but the handle must leave space for the carpometacarpal joint (proximal base joint in the wrist) and thumb metacarpal to move freely and control the joystick. A side note to make within the handle design is the handle preference of the surgeon himself. Since 3D-printing is the manufacturing technique, the handle designs with and without finger grooves can be easily created. The surgeon can choose his preferred design with or without finger grooves. However, a design that is not user-friendly for a range of hand sizes is contrary to the requirements. Therefore, this research makes use of a handle design without finger grooves to fit most hands possible.

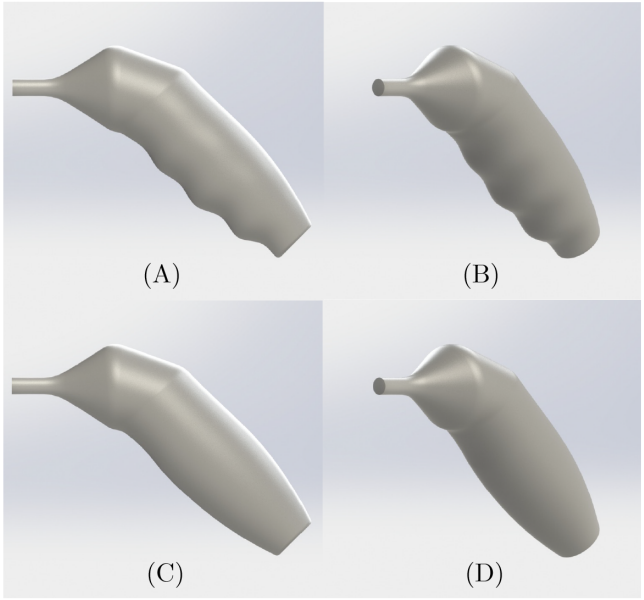

Figure 24: Various handle designs. A-B) 3D drawing of the handle design with finger grooves. C-D) 3D drawing of the handle design without finger grooves.

4.1.4 Joystick design

Different design principles must be combined to achieve a functioning 3D-printed joystick with a minimised assembly that can lock itself. Since a two-finger control system was chosen, the thumb must control the steering and locking system at once. First, a difference between active and passive continuous locking must be clarified.

Passive continuous locking is defined by a constant friction force that is always present and cannot be switched off. The active continuous friction force is defined by switching between locked and unlocked state upon push and release of the joystick. Although friction is not dependent on the surface area but dependent on the friction coefficient and normal force, friction can be generated from various aspects. An example of such a passive control system can be a ball and socket joint, which is designed such that friction force is always present between the ball and socket joint. However, the disadvantage of passive friction control is; constant resistance during manipulation can lead to less precise control. Active continuous friction control, on the other hand, can be switched on and off. The friction force is not present during manipulation, after which releasing the joystick, friction is again present. A schematic drawing of the active friction control system is shown in Figure 25.

Initially, a simple design with easy assembly was created to show the joystick's working principle. A dome placed over the joystick generates pre-tension since pre-tension cannot be printed within the design. The pre-tension must be present to build up pressure between the joystick and dome to ensure friction within the system. Figure 26a shows the 3D drawing of the joystick working principle, and Figure 26b the 3D-printed joystick. Based upon the conceptual working principle, a fully functional joystick design was further elaborated in Section 4.2 detailed design.

4.1.5 Grasper control design

By testing different grasper configurations, discussed in Appendix C, it was concluded that the kinematics of these initial concepts did not suffice. Unintended movements occurred, and continuous friction within the design led to a reduction in ease of use. Therefore, a one DoF bending flexure was chosen within the grasper system to pull the cable. The one DoF bending flexure avoids lateral movements the grasper design while it can close the grasping forceps. The grasper must also be locked, which can be done by another one DoF bending flexure. Therefore, the entire grasping system becomes a two DoF system that can grasp and lock the grasping forceps.

Grasping must feel natural to the surgeon. Therefore, within the new design, the index finger moves inwards towards the palm to grasp. Whereupon release of

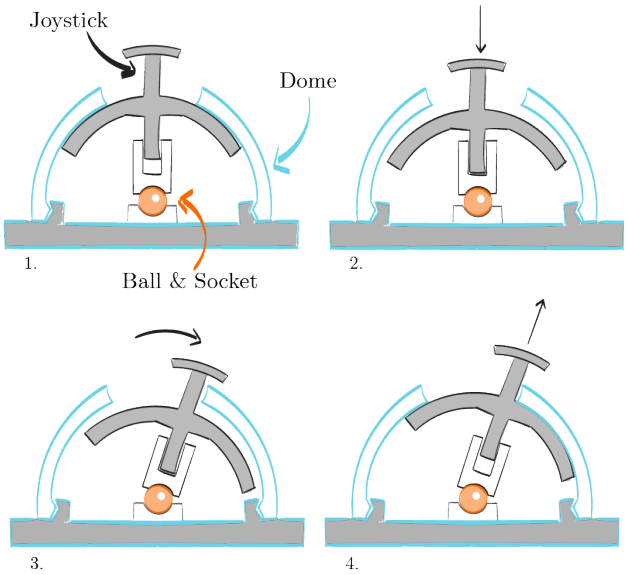

Figure 25: Schematic drawing of the joystick working principle of the mid plane section. 1-4) Steps taken to move the end-effector. 1) Neutral locked state. 2) Unlocked state. 3) Movement of the joystick in unlocked state. 4) Locked state in the desired position.

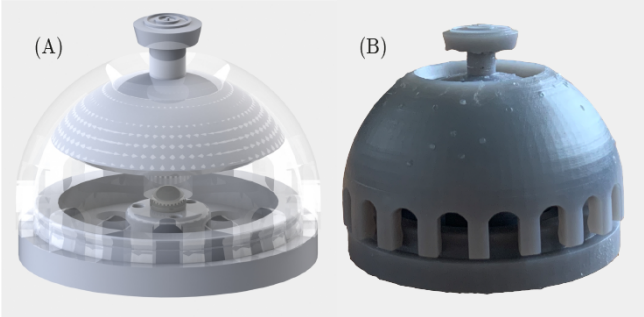

Figure 26: The assembled joystick design. A) 3D drawing of the joystick design to validate working principle. B) The assembled joystick design manufactured by 3D-printing.

the trigger, the grasper locks automatically. From the locked position, the right index finger must push slightly to the left to unlock the grasper and move the trigger into a forward direction to open the grasping forceps again. The steps are shown in Figure 27.

Based upon the finger movements and the two straight bending flexures, a first hands-on prototype was created on a large scale, Figure 28a-b. The working principle's actual representative scale was drawn in SolidWorks, Figure 28c-d, and 3D-printed, Figure 28e-f. The compliant kinematic system of the flexures showed great bending properties, and the locking system worked accordingly, Figure 28f.

4.2 Detailed design

4.2.1 Grasper control

Figure 29 shows an exploded view of the final detailed design to clarify the indicated parts to avoid confusion. The grasper's trigger placement depends on the flexion of the finger, the length of the index finger from

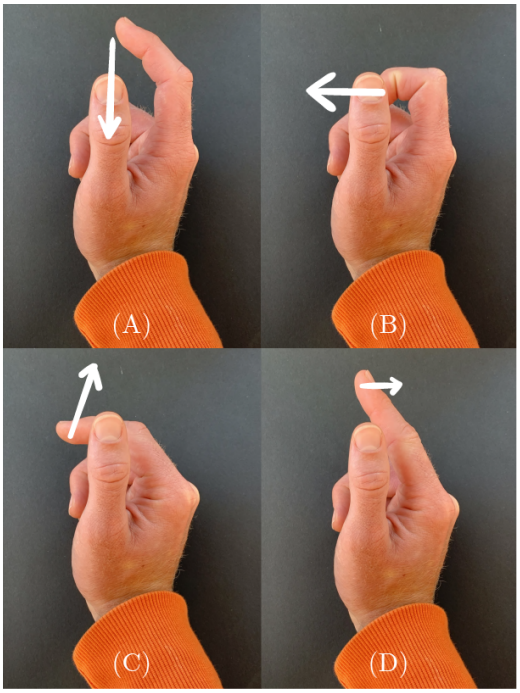

Figure 27: Steps of the grasping movements. A) Initial state to grasping state. B) From grasping state to unlocked state. C) From unlocked state to initial position. D) Initial state.

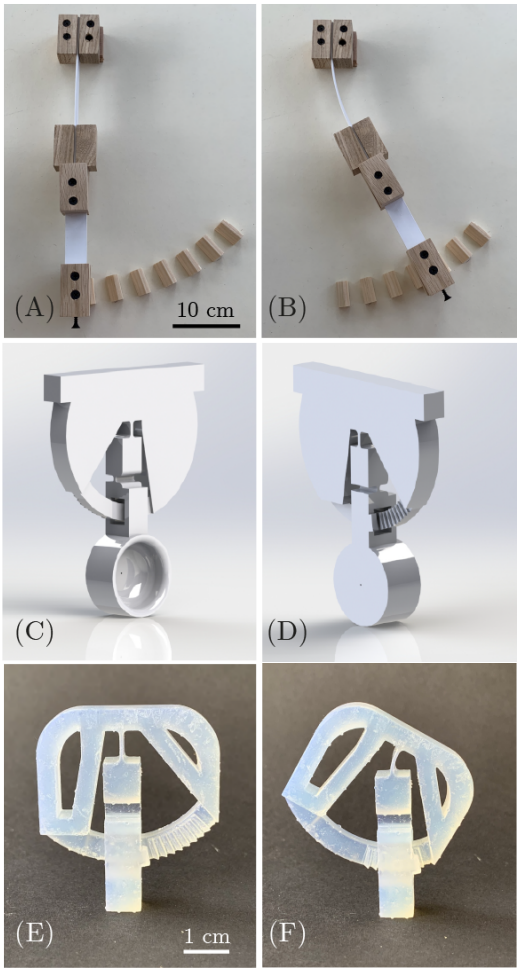

Figure 28: The grasper control. A-B) Prototype in large scale of working principle. C-D) Simplified 3D drawing of a prototype in SolidWorks. E-F) 3D-printed working principle in small scale.

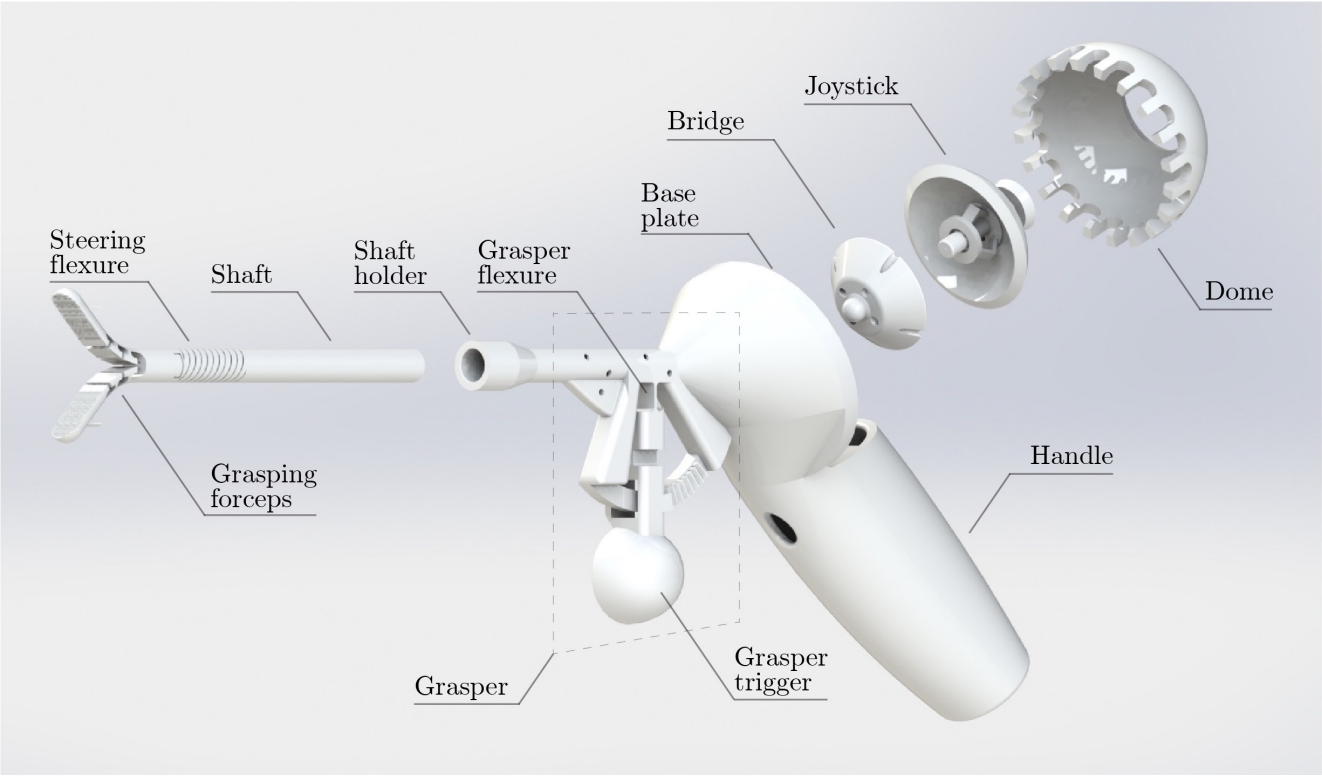

Figure 29: Exploded view of the 3D design with all part names indicated.

the metacarpophalangeal joint (MCP) to fingertip, the height of the horizontal rod of the instrument, and the handle itself. First of all, the grasper's placement must be kept in mind to combine flexure lengths and dependent dimensions.

For 95% of the Dutch population between 20 and 60 years old is the length of the index finger 64 mm or greater [60]. Therefore, the grasper's trigger is located along the index finger's axis, at 44 mm from the MCP joint. The distance compensates for the index finger's flexion to control the grasper. The index forefinger width of 95% of the Dutch population between 20 and 60 years old is 20 mm, or smaller [60]. The trigger cup was chosen to be 20 mm in diameter to fit the index finger.

The control cable connected to the grasper control is connected to the grasper control at a distance of 6 mm from the flexure's centre of rotation to realise a cable elongation that closes the grasping forceps entirely upon the trigger's full range of motion. Compensation of 50% for friction, twisting of the flexure, cable slack, and extra grasping force if needed has been taken into account with the 6 mm distance. Appendix E shows the distance calculation.

4.2.2 Bridge

The bridge is an assembly part of the joystick and provides the connection between the joystick and handle, Figure 30. The combination of the bridge and the base plate works like a ball and socket joint that allows for two DoF motion of the joystick that pivots around a single point. It must pivot around a single point to follow the constant curvature of the dome. A pin in hole connection between the bridge and joystick makes sure the joystick can be pressed inwards to release itself from the dome. The cables are connected to the bridge, making sure that no cables are shortened by pressing the joystick into the bridge.

The angular position of the joystick determines how far the joystick is pushed and should not exceed 45° in total [63]. Since the joystick should not exceed 45°, an amplification system must be implemented within the steering control system to meet the end-effector articulation requirement of 60°. The cables are lined up such that all cables have the same distance towards the centre. The cables' radial distance towards the centre point of the steering section must be greater than the cables' radial distance towards the end-effector's centre point. The difference in cable distance towards the centre point increases the distance travelled of the end-effector output compared to the steering input. Too much amplification could potentially result in less control and overshoot. Therefore, it was chosen to implement an amplification factor of three. The input of 20° now achieves an output rotation of 60°. The cables at the bridge with a certain radius (R_i) are pulled or pushed when the joystick is tilted, which results in pushing or pulling the cables at the end-effector with a certain radius towards the centre (R_o). If the joystick is tilted with an angle, defined by angle θ, the end-effector is manipulated with an angle of $\alpha = \theta \cdot \frac{R_i}{R_o}$. As seen from the relation of the bridge radius and end-effector radius, the bridge radius must be three times as large as the end-effector radius to create the desired amplification factor. All further dimensions of the joystick and dome are based on the bridge's minimised achievable dimensions to generate a system as small as possible.

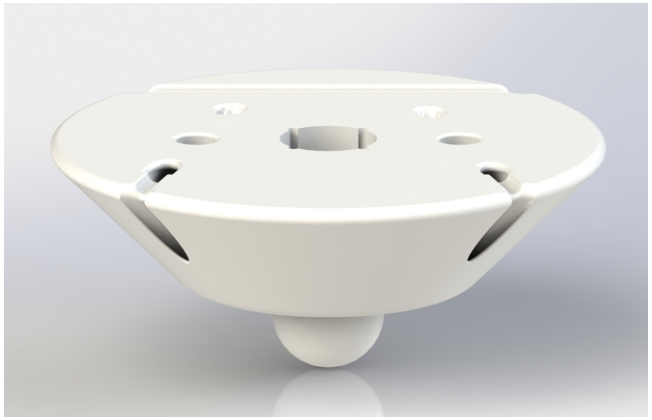

Figure 30: 3D drawing of the bridge.

4.2.3 Joystick

The joystick consists of a steering knob, a disc, a pin, and a spring, all combined as non-assembly. The steering knob is controlled by the thumb and is outside the dome. The disc, indicated in Figure 31a provides the friction. The disc was maximised to the design allowance. The pin below the disc slides into the bridge to interconnect the joystick and bridge, making the steering control feasible. The spring was included in the joystick's design to create preload between the dome and the disc. The spring was directly printed onto the joystick as shown in Figure 31a for minimal assembly, where only the spring design is shown in Figure 31b.

An important aspect of springs is the springback time. According to the manufacturer and own gained perception best achievable with Tough 1500. The best-suited spring properties were obtained by printing different thicknesses of the spring flexures and based upon the results of cured and uncured springs. The spring is compressed by the difference in radial distance of the dome's inner wall and the disc's outer wall towards the rotation centre. The curvature of the disc's outer wall and the dome's inner wall is identical.

The P5 value of the thumb is 55 mm in length from root to tip [63]. The joystick is at a distance of 30 mm from the thumb's root to compensate for the flexion and the distance from the thumb's tip to the middle of the upper part. Furthermore, the joystick is placed 8 mm to the left to realise the resting hand's posture, Figure 13 [54, 63].

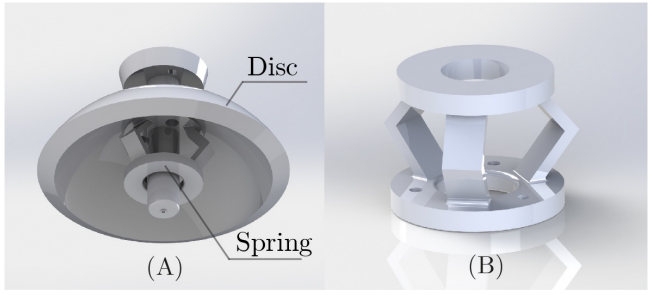

Figure 31: Joystick control design. A) 3D drawing bottom view of the non-assembly joystick design. B) 3D drawing of the spring.

4.2.4 Dome

The dome provides friction to the system. The pressure is built up between the disc and the dome by compressing the spring. The dome's top hole allows for the joystick's range of motion of 20° in all directions. The dome connection onto the handle consists of a click system for minimised and easy part assembly. Cutouts were made at the bottom of the dome to create separated flexible teeth, to click the dome onto the base. The dome's clamping teeth contain a small sphere that makes contact with the base at two points. The connection compensates for imperfections and can find its locking position, as shown in the schematic drawing of Figure 32. The dome is shown in Figure 33.

The dimensions of the dome were based on the smallest possible dimensions achievable for the joystick, which in its turn was based on the bridge dimensions. Therefore, the dome's outer radius was set to 25 mm, with a wall thickness of three millimetres for its stiffness.

Figure 32: Schematic drawing of dome connection to base. Blue: dome. Orange: connection base.

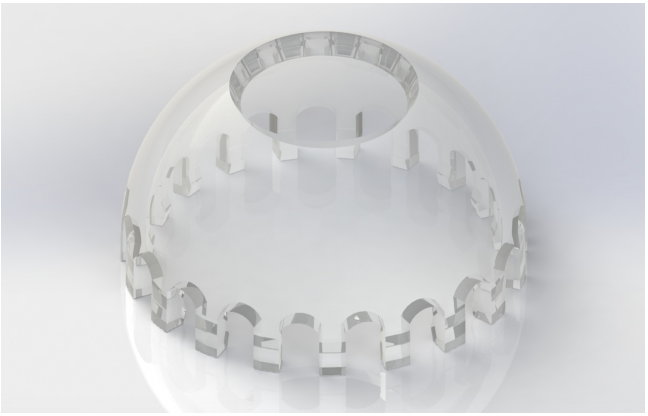

Figure 33: 3D drawing of the dome.

4.2.5 Handle

The joystick and grasper were both optimised for ergonomic use, and they showed promising results. The handle meets the requirements and could now be combined with the joystick and grasper into the overall handle design, Figure 34.

Some adjustments at the end of the handle were made to combine the joystick and the handle. A base, placed at the determined distance from the handle grip, was created to assemble the joystick and dome onto the

handle by a click on system. The angle of the base plate in relation to the handle was a trade-off between several relations, namely: the joystick's reachability for the thumb was determined by the base plate's angle and the distance from the handle, indicated respectively by α and L_T in Figure 34. The angles of the cable trays were determined by the angle of the base plate and the shaft. Straight aligned cable trays minimise cable friction, and they show better results in terms of clogging when printed.

The grasper was connected below the rod such that the grasper could rotate over the entire translation distance. The cup was at the determined dimension of 44 mm in line with the index finger's direction and directly attached below the rod to where the flexure was connected.

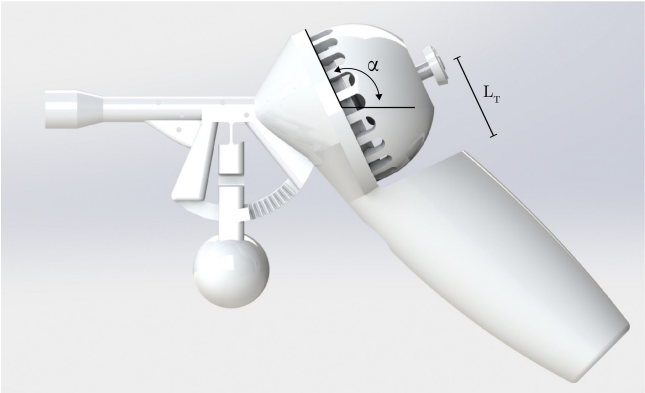

Figure 34: Assembly of the 3D-printed ergonomic handle.

4.2.6 Grasping forceps, flexure, and shaft

In the study of L. Bazuin, extensive research was done on the grasping forceps to create a 3D-printed non-assembly steering instrument [11]. Based on this research, the best proven grasping forceps were applied to the design of this study, Figure 35.

The developed flexure in the research of C. Culmone was connected to the grasping forceps [67]. The other side of the flexure was connected to the shaft. The cable trays within the grasping forceps, flexure and shaft have a diameter of 50 μm.

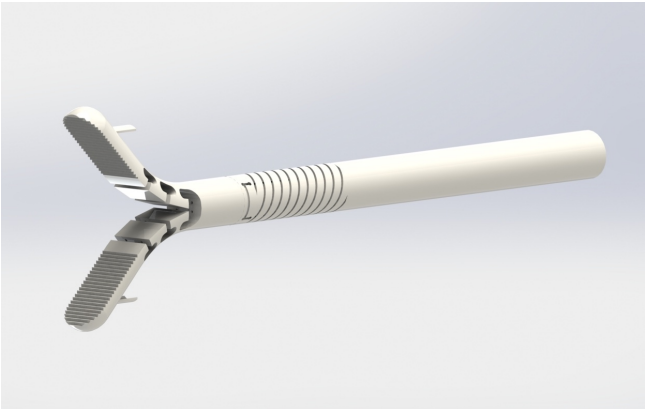

Figure 35: 3D drawing of the shaft, flexure, and grasping forceps.

4.2.7 Control cables

Multiple cables must be guided through various cable trays to steer the end-effector and control the grasping forceps. The minimum amount of three cables of one joint and a single segment realises the end-effector movement in two DoF. The three cables must be equally divided over 360°. However, six attachments points are necessary when using three cables, Figure 36a. To create two attachments with the same cable configuration, one cable can be used, which results in two cable attachments in different parts of the instrument, Figure 36b. Four cable trays and only one cable can be used to make sure that the cable attachments are within the same section of the instrument, shown in Figure 36c. There was chosen for design c of Figure 36. The two cable ends of the steering group can be connected onto the bridge since the bridge allows for the spatial possibility to clamp both cables.

The shaft contains four cable trays to control the grasping forceps. The two separate cables for the grasper control run back and forth throughout the shaft. A specifically designed loop at the grasping forceps tightens the cable. Two cables result in four cable ends at the grasper side. The cables can be combined into one bundle and connected to the grasper by a micro cable clamp that can be placed in the intended fitting.

Figure 37 shows all cables and connections in the transparent preview of the design to visualise the connections between the parts. The different colours show each controlled part by each finger. The handle consists of a master-slave system. The control buttons are the master, and the grasping forceps and end-effector are the slave. The cables connecting the master and slave all remain the same colour to visualise the different connections.

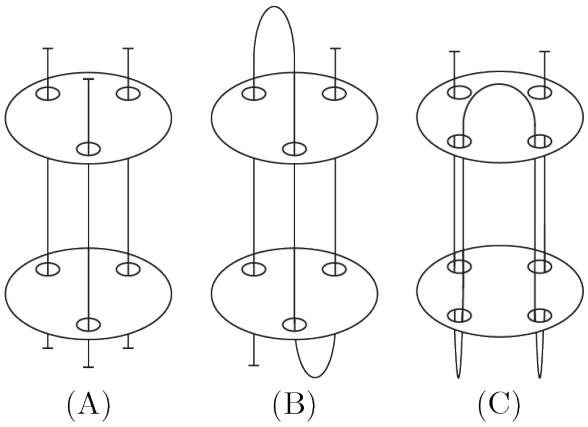

Figure 36: Various cable attachment and layout possibilities. A) Three cable layout. B) Single cable layout, different section attachment. C) Single cable layout, same section attachment.

4.3 Final Design

4.3.1 Manufacturing method

To validate all final parts, different experiments regarding the print directions, flexure thickness and curing time were researched until all parts worked

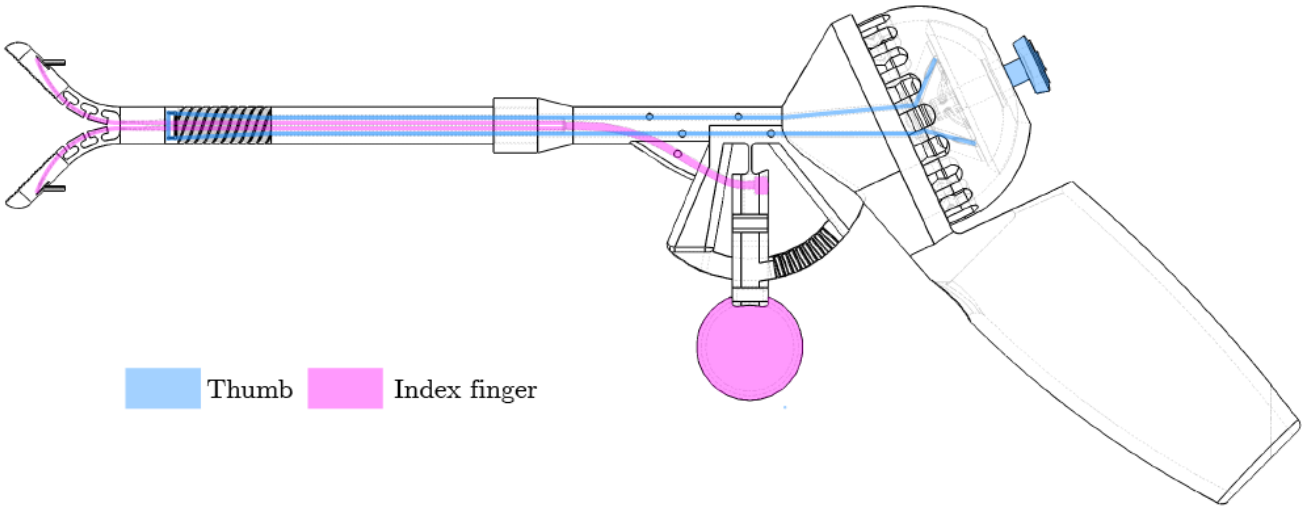

Figure 37: Master to slave control with associating cable connection.

properly. The individual parts with the correct print directions are shown in Figure 38. Figure 39 shows a render of the assembled instrument, called the LapaJoy.

The ergonomic handle was printed using the Formlabs Form 3B printer based on the stereolithography technology with Tough 1500 resin. The layer thickness was set to 50 μm, where the handle is limited by the maximum build volume of 145 x 145 x 185 mm. The entire handle was based on the limiting print dimensions and the ergonomic dimension requirements. The handle at the bottom backside must have been slightly cut-off to stay within the building volume while remaining the included shaft attachment and all ergonomic dimensions. If the handle's shaft connection would be shorter than the current design, the bending of the cables from grasper to shaft would be more curved. The more curved cable results in higher friction due to the cable tray walls' that create a greater normal force onto the cable. The print direction of the handle with the sliced part is shown in Figure 40.

The print was cleaned by the Formlabs cleaner within isopropyl alcohol (IPA) for 20 minutes. Afterwhich the print was cured. The print should stay within the Form cure for 60 minutes at 60° Celcius with exposure to the ultraviolet light (UV) to fully cure the instrument. The wavelength of the Form cure was 405 nm. However, the grasper's flexure does not allow for a curing time as such, and the curing time was therefore adjusted to 3 minutes total at 60° Celcius. The inside of the handle was still uncured due to the short exposure period without direct UV light. Therefore, the uncured soft parts were exposed to UV light by a UV torch (Convoy S2+, 365 nm). The final cured prototype is shown in Figure 41.

The curing period of the assembled parts, the dome, bridge, and joystick were different from the handle itself. The dome and the bridge were cured by the complete cycle of 60 minutes at 60° Celcius with continuous UV light exposure. The joystick was cured for three minutes to maintain its spring properties. The disc was shielding the spring from direct UV light. The nylon coated stainless steel cables from Cenfill used for the prototype have a diameter of 0.18 mm and were implemented for the steering and grasping control.

The grasping forceps, flexures, and shaft were printed as a single component using the VAT photopolymerization printer EnvisionTEC Perfactory 4 Mini XL ERM because the resolution that must be achieved for the cable trays (50 μm) is not feasible with a Formlabs Form 3B printer. The resin that was used for this print was EnvisionTEC NanoCure R5.

4.3.2 Prototype assembly

The LapaJoy consists of 5 parts, Figure 42. The assembly of the different printed parts can be divided into cable assembly and part assembly. Part assembly consists of clicking the different components into each other without any extra assembly tools. However, it was not possible to first assemble all cables or first assemble all parts. The assembly of cables and parts is dependent on each other.

First, the cables from the grasping forceps must be inserted through the shaft towards the grasper. The steering cable starts at the bridge and goes two times back and forth from the bridge to the steering segment in the shaft. The cables were not attached at this moment of time in the assembly process. The shaft can then be attached to the handle by placing the shaft in the hole connection. The single cable used for steering control must achieve independent cable actuation. The steering flexure of C. Culmone in the shaft includes an innovative fixation module [67]. The cable was looped into a cross-shaped groove within the module in the shaft's transverse plane, which leads to reciprocal friction. The friction-based fixation was also used for the

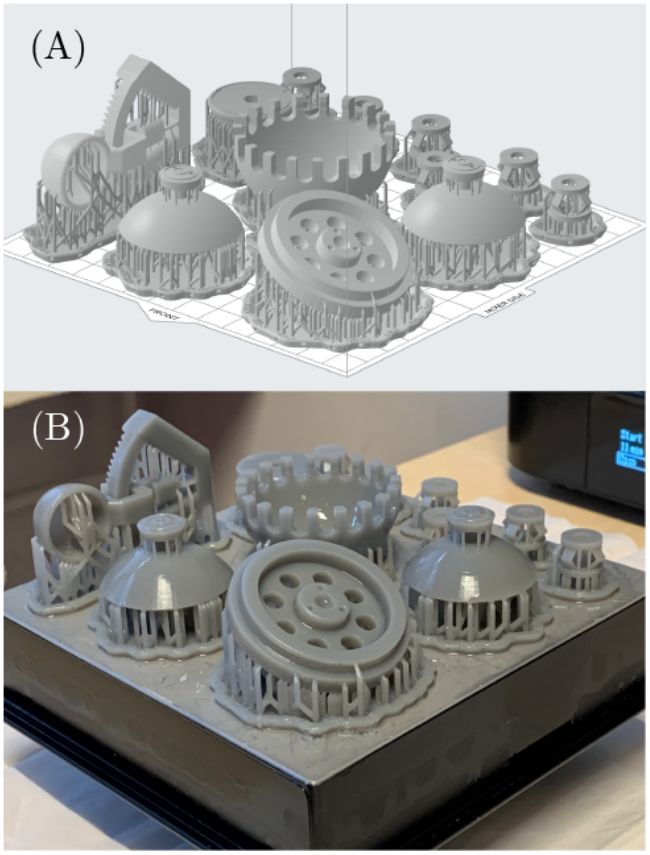

Figure 38: 3D-printed parts. A) Image of the parts in Preform software with the final print directions. B) The printed parts with the final print direction.

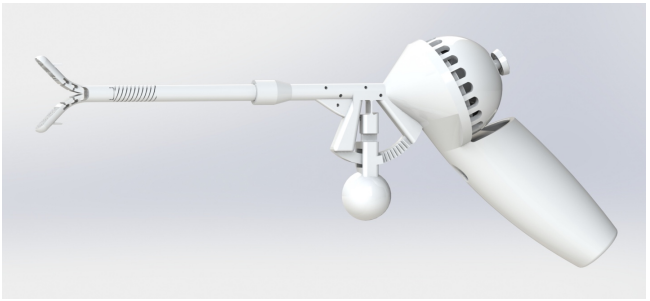

Figure 39: 3D image of the LapaJoy.

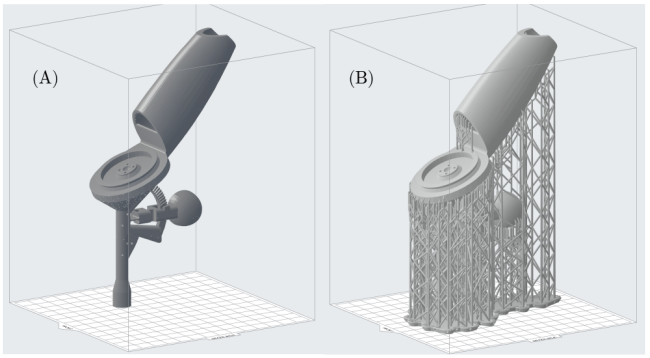

Figure 40: Image of the handle in Preform software. A) Print direction of the handle. B) Print direction of the handle with included supports.

Figure 41: Final result of the 3D-printed cured handle.

other cable within the steering segment module, which was rotated 180 degrees relative to each other resulting in four independent cables.

A supportive removable part was added below the bridge to simplify the positioning in the neutral position, Figure 43a. The two cable ends were connected and fixated to the bridge by set screws (3 x 3 mm) in the intended holes. The cable part linked across the bridge was not secured by set screws but was made independent by glueing 43b. The cables were straightened by the weight of a 17 gram bolt and not assembled under high tension since cables must run straight throughout the design without pretension in the system.

The two control cables of the grasper, which were looped in the grasping forceps, result in four cable ends. The cable ends were bundled and clamped together, Figure 43c. The cable clamp was then placed in the therefore provided hole at the calculated distance of the rotation point of the flexure, Figure 43d. The joystick and dome can be attached by clicking them onto the handle in place. These parts require no further assembly. The assembly steps are shown in Figure 45.

The shaft, steering flexure and grasping forceps were retrieved from previous work. The COVID-19 situation did not allow printing these parts, which means that an already created design has to be adapted such that only the shaft, flexure and grasping forceps remain. The cable trays in the shaft from the previous work are rotated 45° compared to the design in Figure 44. This results in rotated grasping forceps in the fully assembled prototype, Figure 46.

Figure 42: Exploded view of a 3D drawing of the LapaJoy containing 5 parts in total.

5 Test evaluation

Tests were executed to compare the retrieved data with the requirements to validate the working principle and evaluate the performance of the 3D-printed ergonomic handle in terms of grasping, steerability, locking, forces and assembly.

5.1 Assembly time

The assembly time is an important aspect for the cost-effectiveness of an instrument and was therefore measured. The assembly time was divided into three segments;

1. Cable assembly grasper control.
2. Cable assembly steering control.
3. Part assembly.

The cable assembly of the grasper control took 12 minutes on the first attempt. The assembly of the steering control cables took one hour and three minutes the first attempt, and the second attempt took 37 minutes. The duration of assembly of the grasper and steering control can still be shortened by experience, as there is still room for improvement. However, the holes of the shaft, flexure and grasping forceps were already cleaned since the shaft is from previous work.

5.2 Grasping test

The closing and opening range of the grasping forceps were tested. It is important that the jaws can fully close upon which the jaws can open again to their initial state. The jaws must close fully to grasp thin tissue and open again to the initial state to create unchanging conditions. The test setup of how the instrument was clamped during all executed tests is shown in Figure 46. In this way, the instrument was in place at a constant angle and distance from the camera. The grasping forceps' initial jaw angle in the open state was measured in Adobe Illustrator, upon which the grasping forceps are closed. After closing the grasping forceps by pulling the grasper trigger, the trigger controlled by the index finger was pushed forward to its initial open position. The jaw angle in the open state was again measured. This grasping process was repeated to show the performance of the opening range after multiple grasps.

The initial angle of the grasping forceps was 18.5° 47a. The test showed that it is possible to fully close the grasping forceps 47b. The different jaw angles between each opening and closing cycle were measured and decreased by 2.4°, 0.2°, 0.6°, 0.8°, respectively. After closing the grasping forceps for 5 minutes, the jaw decreased another 1.1° and after 10 minutes, another 0.8°.

5.3 Steering angle test

The manoeuvrability of instruments in MIS is limited and is therefore important to be increased. The steering test was performed to determine the maximum obtained steering angle of the end-effector. First, the end-effector was manipulated from the initial position into the outermost upward direction. The manipulation angle was obtained by measuring the manipulated end-effector relative to the shaft's horizontal axis in Adobe Illustrator. The steering control was brought back in the neutral position upon which the instrument was manipulated in the following position. The device achieves an up, down, right and left steering angle of 21.3°, 21°, 15.6° and 12.3 ° respectively, Figure 48.

5.4 Steering and grasping control locking test

The prototype's designed control systems allow to lock the grasper and steering control at any time and simultaneously. Locking the end-effector and grasping forceps during task execution relieves the surgeon from tiresome postures. The locking tests evaluated the performance of the design. The instrument was again placed in the holder for those tests.

The grasper lock was tested by pulling the grasper and releasing the grasper at each different locking interval to evaluate the grasper's performance. The grasper locked directly upon release in each attainable position. However, the grasper lock was only able to reach four out of eight grasper lock intervals, shown in Figure 49. Fatigue of the grasper flexure occurred after 50 till 60 cycles of opening and closing, Figure 50a, and broke at the bottom part, Figure 50b.

The steering lock test was executed by pressing the joystick inward, moving the joystick into position and releasing the joystick. This process was executed for five outermost steering positions and five positions between the initial and outermost angles to determine if the joystick design can withstand the end-effector flexure's counteracting force.

The results showed that the steering control could lock the end-effector in the ten different positions. It can be concluded that the end-effector can be locked in all positions for the conceivable angles. Four of the outermost locked positions (up, down, right and left) of the end-effector are shown in Figure 51.

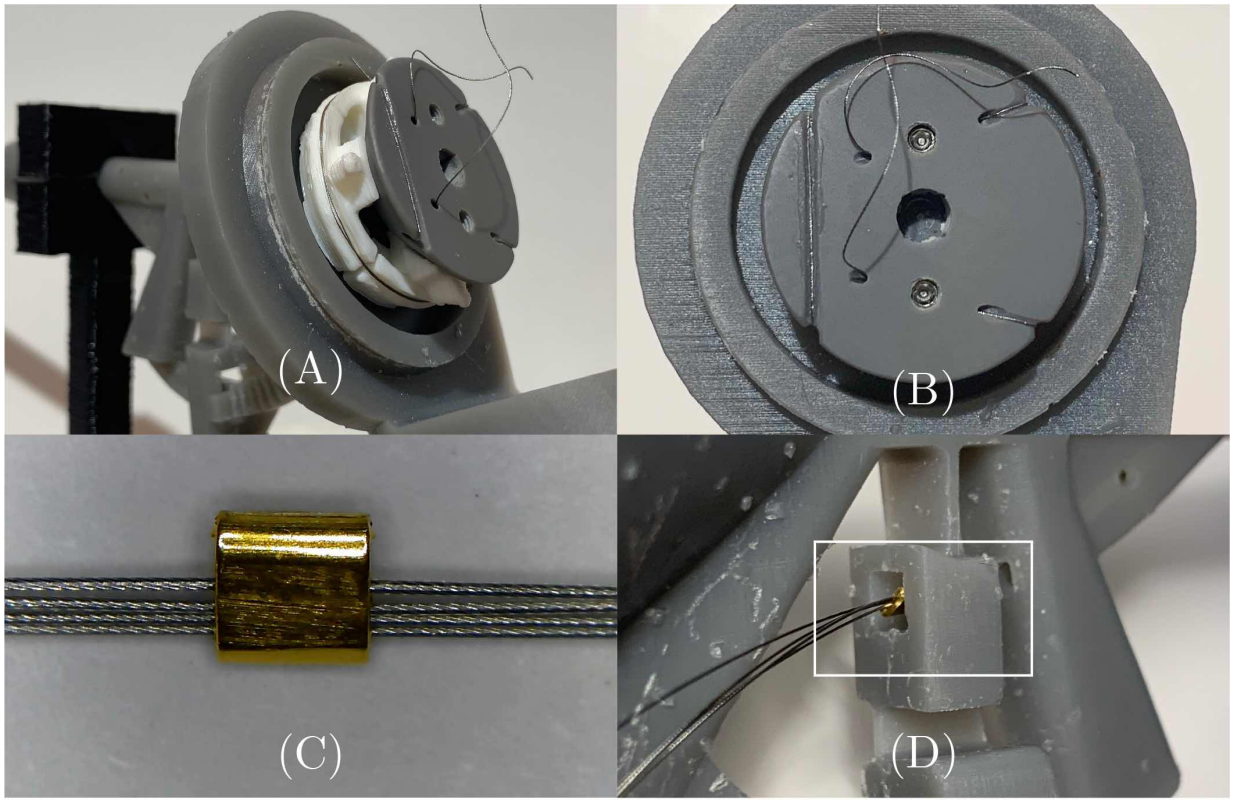

Figure 43: Cable attachments of the bridge and grasper. A) A supportive removable part to simplify the positioning in the neutral position, part is shown in white. B) Cable control attachment with set screws onto the bridge for steering segment. C) Microscope image of cable clamp principle. D) Cable attached to the grasper.

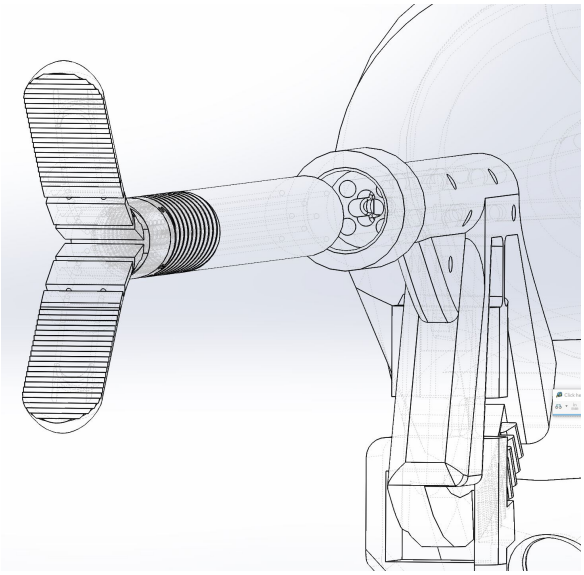

Figure 44: Correct cable tray alignment within the 3D design.

5.5 Bending force test

Another interesting incidental of the instrument is the unwanted bending of the flexure that occurs when a force is applied to the end-effector. The test showed the bending result of the steering segment flexure by a vertically applied force on the grasping forceps. The weights were added per ten grams in the middle of the jaws, and the end-effector was locked in place. The total amount of 90 grams resulted in a bending angle of 35°. The joystick in this configuration did not move. However, severe tension within the flexure occurred, and no extra weight was added. The results are shown in Figure 52. The bending angle of the flexure was plotted against the applied moment onto the flexure and shown in Figure 53.

Furthermore, the test showed that the end-effector slowly moves back towards the initial state after the release of the applied weight. However, 0.9 Newton force applied in the middle of the grasping forceps results in an end-effector deformation of almost ten degrees.

6 Discussion

6.1 Tests

6.1.1 Result discussion

Tests were conducted to validate the working principle and evaluate the 3D-printed ergonomic handle's performance in grasping, steerability, locking, forces and assembly. The assembly is easily accessible and was completed within a reasonable amount of time of 50 minutes. During the assembly, it was necessary to constantly pull the single cable through the design little by little while the shaft had to be moved simultaneously towards the handle's shaft holder. However, when the shaft would have been directly connected to the instrument, the assembly would have been simpler and less time-consuming.

The grasping test determined the repetitive opening

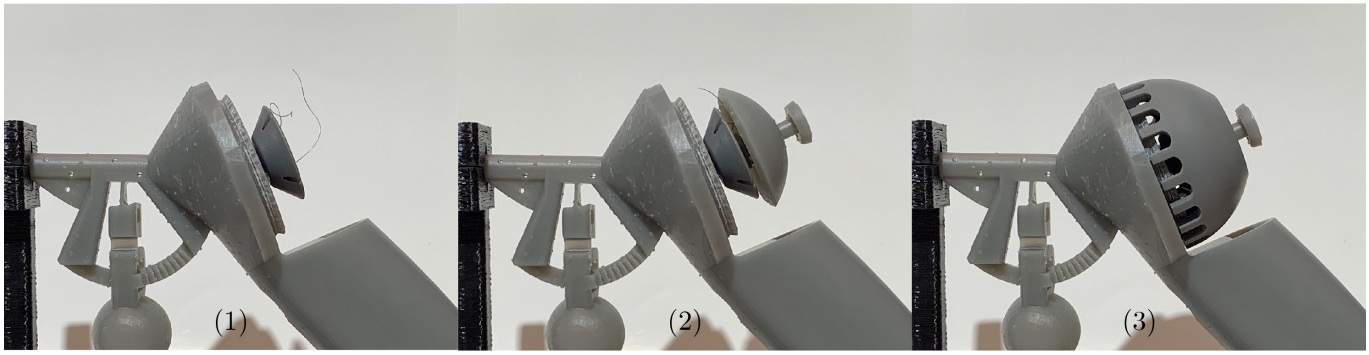

Figure 45: The steps shown for part assembly.

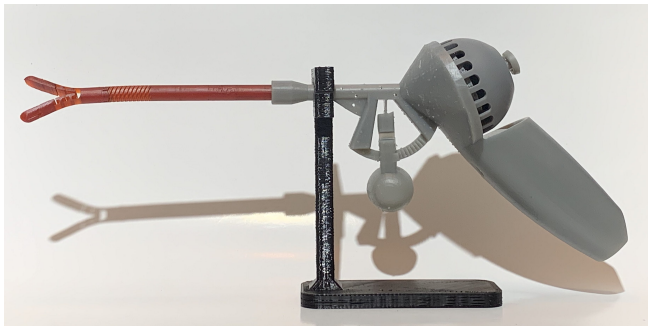

Figure 46: Fully assembled instrument.

and closing range of the grasping forceps. The test showed that the grasping forceps' angle in the open state reduced after each cycle by 4.6% on average. The angle reduced an additional 7.6% and 6% after locking the grasping forceps for five and ten minutes, respectively. It can be concluded that plastic deformation of the material occurs after each cycle. The improvement of thicker bending flexures can increase the jaws' springback but involves a greater applied grasping force as a downside. A better solution may be found in other material properties to increase the springback and reduce the grasping forceps' plastic deformation.

As described in the requirements, the end-effector's steering angle should achieve 60° in 2 DoF. However, the design cannot meet the requirement by 40°. A design flaw was found wherein a maximum theoretical cable elongation occurs of 1.7 mm, which results in a maximum bending angle of 28°, calculated in Matlab, Appendix F.4 and F.5. The holes within the current handle design have a diameter of 1.8 mm, resulting in sideways cable displacement. The cable elongation must also compensate for the sideways cable displacement. A cable elongation of 3.7 mm results in a theoretical end-effector manipulation of 60°. The average practical bending angle compared to the theoretical efficiency of the LapaJoy is 0.63, meaning that the carried out cable elongation of the joystick in practice must be 5.9 mm. If smaller cable trays can be achieved within the handle design, less cable play occurs. Less cable play increases the steering control's efficiency, which increases the maximum attainable manipulation angle of the end-effector.

Another discussion point is that different steering directions resulted in different bending angles of the end-effector, visually explained by Figure 54. Figure 54b shows that a joystick motion aligned with the virtual square diagonals results in the greatest cable deflection possible. In the configuration of Figure 54c, where the joystick motion is perpendicular to the lines of the virtual square, it results in the smallest deflection of the end-effector possible. A solution for this phenomena can be found in limiting the joystick deflection in specific directions. A dome configuration as such ensures that each outermost steering direction of the joystick ends in an end-effector manipulation of the same magnitude, Figure 55a. However, with a solution as such, only the smallest possible deflection can be achieved. Another solution can be found in adding extra cables to the system, which makes use of the greatest angle possible, Figure 55b.

With the conducted test of the steering control lock and grasping control lock, the grasper lock can be discussed. The grasping forceps used for the LapaJoy prototype was from a previous design and did not have an initial jaw angle of 45°. The grasper lock range, however, was calculated for the 45° jaw angle. Therefore, the current design cannot lock the grasper over its entire locking range due to the grasping forceps' initial jaw angle. Furthermore, there is to criticise that only eight locking positions can be obtained within this design. More locking positions should be achieved by improving the design of the grasper lock system.

The point of discussion that emerged from the bending test is the extensive play within the design that occurred due to material properties and cable play. The plastic deformation of the bending angle of almost ten degrees after applying a force of 0.9 Newton resulted in a reduced manipulation angle of the end-effector in the opposite direction of the applied force. The yield strength of the used plastic is responsible for the plastic deformation of the material. Deformation occurs when the yield strength limit is exceeded by external forces, such as tensile forces, bending forces or compressive forces. Therefore, research has to be done on different material properties with a higher modulus of elasticity and higher yield strength. The more suitable material properties can increase the flexure's springback and reduce the plastic deformation while applying a force.

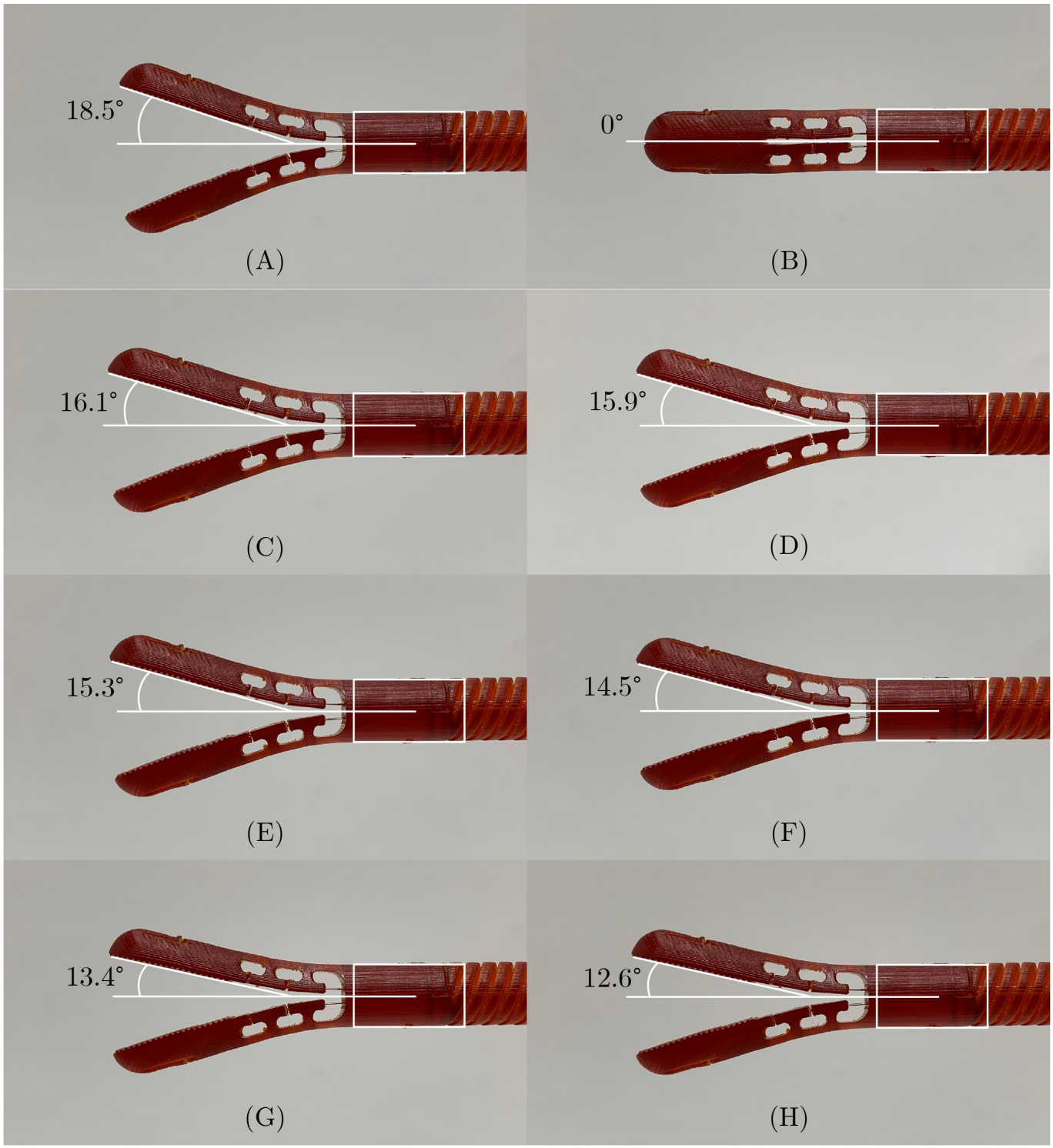

Figure 47: Grasping test. A) Initial state. B) Closed grasping forceps state, repetition between every measurement. C-F) Grasping repetition in sequence. G) Grasping forceps after 5 minutes of locking. H) Grasping forceps after 10 minutes of locking.

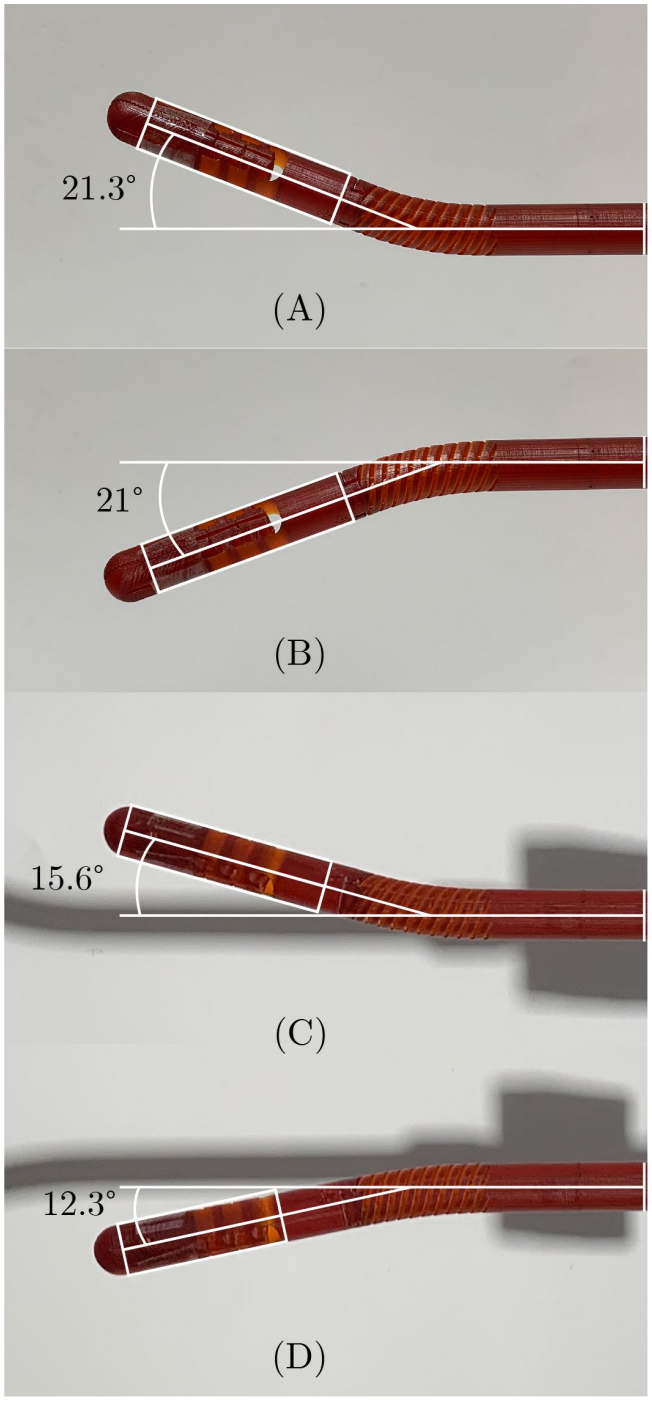

Figure 48: Steering test. A-B) Side view of grasping test setup. C-D) Top view of grasping test setup.

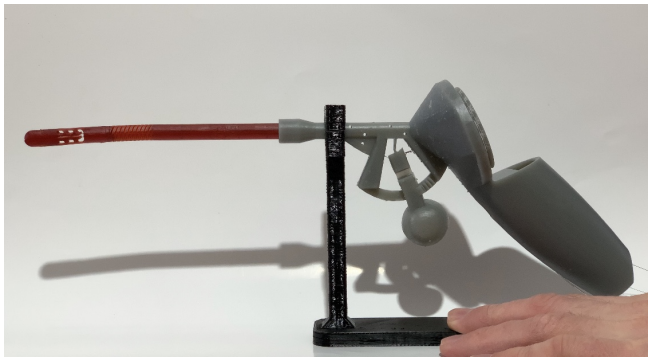

Figure 49: Grasper lock in outermost position upon full closure of the grasping forceps.

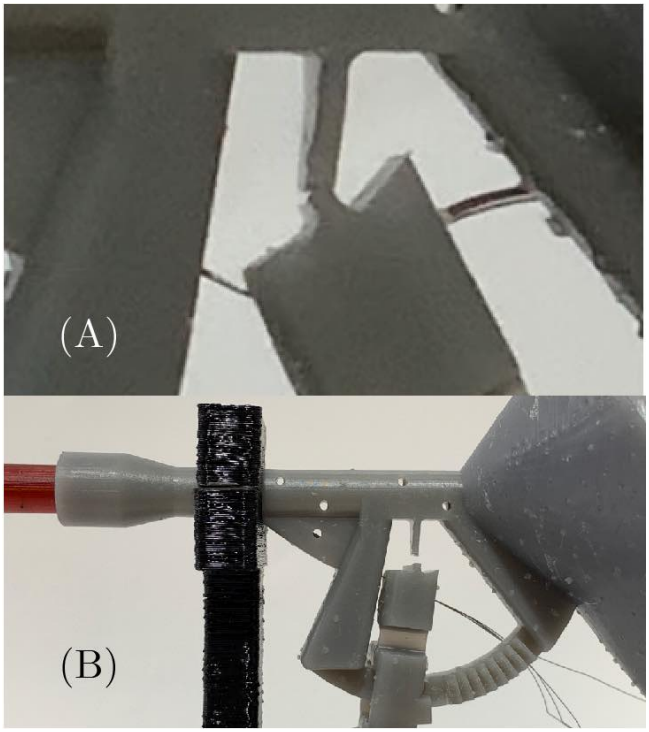

Figure 50: Defects during the grasping tests. A) Fatigue occurs. Screenshot taken from video. B) Failure of the flexure after approximately 60 grasping cycles.

6.1.2 Limitations

The steering and grasping test results were based upon visual angles. No pressure force or grasping gain was measured. According to Böhrs, a pressure applied greater than 3 kg/cm^2 causes pressure areas in the surgeon's finger and applied pressure of more than 5 kg/cm^2 causes pain [29]. Furthermore, the blood flow and nerves will be obstructed with high applied pressure forces. Less blood flow and obstruction of the nerves leads to numbness of the fingers [15, 27, 28]. If the pressure force is indeed too high, it could lead to less precise control during surgery. However, no conclusion can be drawn about the applied pressure that affects the ergonomics of the joystick control or grasper trigger since no pressure forces were measured.

6.1.3 Improvements based upon test results

Multiple improvements can be immediately implemented within the design, namely;

1. Shaft directly printed onto the handle.
2. Increase the number of locking positions of the grasper.
3. Fatigue of grasper flexure.
4. No angular difference of maximum end-effector bending.
5. Amplification of the conceivable steering angle.

The jaw angle of the current design is only 18.5°, which does not show the grasping system's full potential. A newly printed shaft with an increased jaw angle

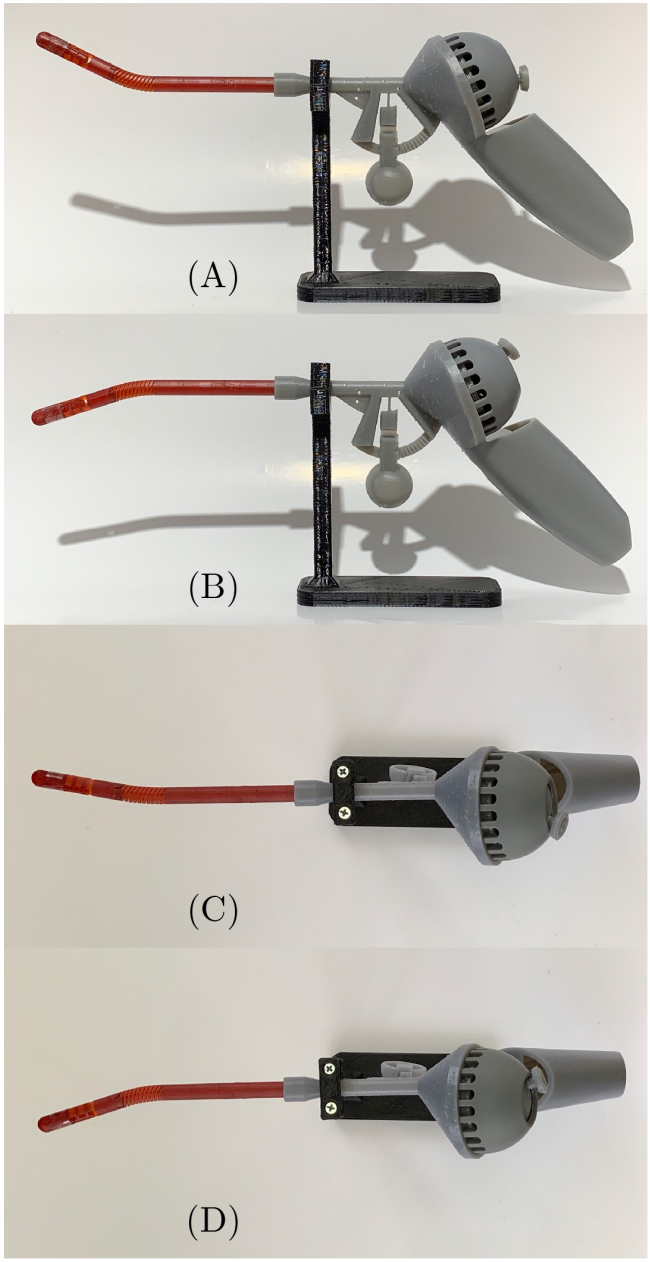

Figure 51: Four out of the ten steering lock positions during the test. A-B) Side view of locking test. C-D) Top view of locking test.

would directly solve this problem. On top of that, if the build volume of the printer is larger than the build volume of the Formlabs Form 3B and can print with a hole resolution of 50 μm, it is possible to print the shaft directly onto the handle itself. The newly printed instrument then also directly solves the previously addressed shaft assembly problem.

Furthermore, experiments showed that the jaws were not yet fully closed by the third locking interval of the grasper. Using the fourth locking interval, a pressure between the jaws was present. Additional intervals must be added by designing smaller locking teeth. Moving the locking system further away from the centre of rotation results in an increase in the circular path length that also allows for more locking intervals.

A simple solution for the fatigue is thickening the flexure where the highest stress occurs, Figure 56. In this case, the bending stress of the flexure will be distributed more evenly. However, a better solution to this problem could be a change in material properties that can withstand the forces and has superior bending properties. The different material properties must first be researched.

The difference in the end-effector's bending angle results from different cable deflection of the joystick in different steering directions of the joystick, explained by Figure 54. To minimise the difference, not only the solution of Figure 55b must be implemented. Extra cable trays, fixation modules in the shaft, and bridge attachments must be created within the design to solve the problem of the different bending angles.

The last improvement that could be directly implemented into the design is the amplification of the steering angle. Based on the current design dimensions and Matlab calculations (Appendix F.5), a maximum theoretical angle of 76.3° can be achieved by placing the cable trays centre 13 mm from the joystick's centre of rotation. Figure 57 shows the change of cable trays placements towards a better design. A maximum bending angle of 48° can be achieved in practice due to the 0.63 efficiency of the current design.

6.2 Design

6.2.1 Prototype evaluation

The goal of this study was to design a 3D-printed ergonomic control handle for an existing end-effector. The ergonomic control handle was based on anthropology data, using 3D-printing as a manufacturing technique to minimise part assembly and components. The majority of laparoscopic instruments consist of many components because of the different assembled control features. The LapaJoy combines multiple functions with an ergonomic design while benefiting from minimised part assembly over other instruments.

The prototype meets all ergonomic dimension requirements. However, the instrument's intuitiveness, meaning easy in use and logically ordered control system layout, was not tested and validated by surgeons. The not validated intuitiveness of the instrument is a shortcoming for the design evaluation and should be investigated. Furthermore, the movement of the grasper trigger must be reconsidered to conclude the ergonomics of the grasper. The index finger, in a closing hand movement, moves towards the palm in wrapping motion. However, the current trigger design moves along the shaft's longitudinal axis, which does not mimic the closing hand movement. Also, the trigger cup does not allow for a different index finger grip during the grasping movements. If the trigger cup allows for different finger grips during grasping, it could contribute to a more ergonomic movement. Additionally, the grasper control must be placed off centre to the left for right-handed use to provide a better ergonomic posture and vice versa for left-handed control.

The joystick configuration allows the instrument to be controlled by a single hand and avoids external

Figure 52: Bending force test by applying weights. A) Initial state. B-J) 10 grams of weight added for each step with the new bending angle. K) Directly after removing weights. L) After 25 minutes of removing the weights.

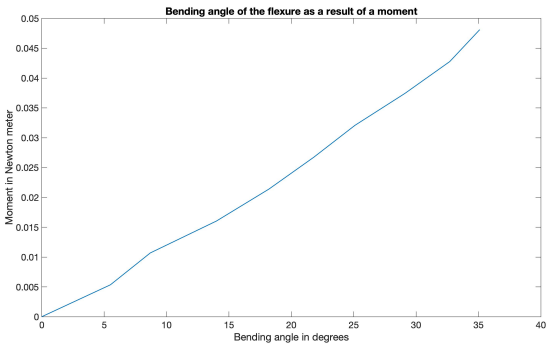

Figure 53: Bending angle of the flexure as a result of an applied moment onto the flexure.

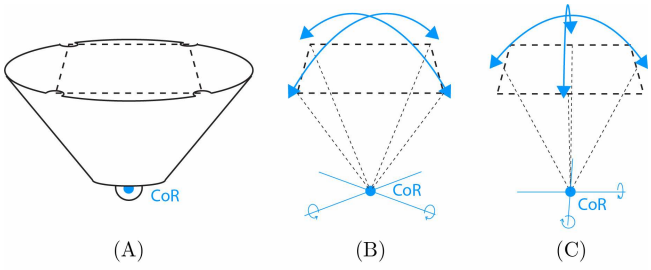

Figure 54: Visualisation of the varying maximum cable elongations through the different steering directions. A) Virtual square between cable attachments points. B) Joystick movements with greatest distance from centre of rotation leading to greatest end-effector manipulation. C) Joystick movements with smallest distance from centre of rotation leading to smallest end-effector manipulation.

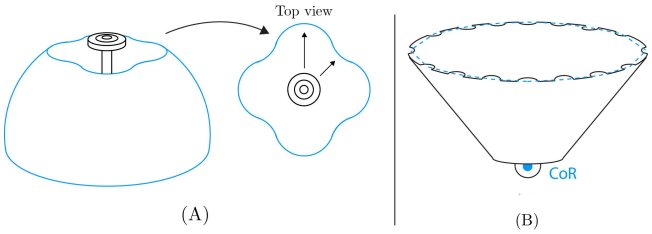

Figure 55: Solutions to compensate for the varying cable elongations. A) Dome design for limited joystick movements. B) Multiple cable design which results in less difference between smallest and greatest end-effector deflections.

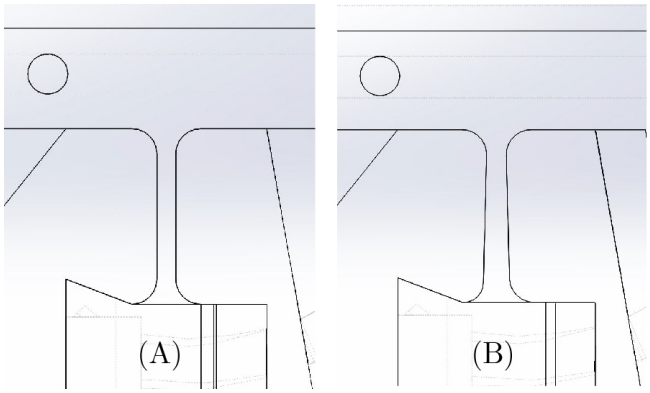

Figure 56: Improvements to reduce fatigue of the grasper flexure. A) Thin configuration of the grasper flexure. B) Flexure thickness adjusted for stress gradient.

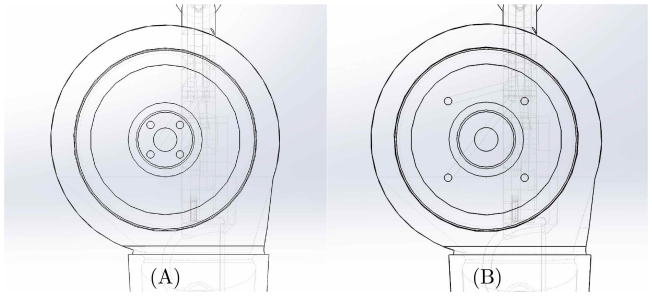

Figure 57: Improvement to increase the amplification of the steering angle. A) Old cable tray configuration. B) New cable tray configuration.

forces onto the surroundings while performing tasks. The most appointed fingers control the different control functions. The thumb controls the end-effector in 2 DoF, and the end-effector locks upon release of the instrument. The index finger controls the grasping forceps, and the grasping forceps locks in place upon releasing the grasper trigger. The innovative two-finger control system sets the LapaJoy apart from current laparoscopic instrument designs.

Instruments such as the DragonFlex and Maestro can rotate the end-effector around its axis by rotating the handle itself. This principle was also applied to the LapaJoy to realise shaft rotation without adding extra parts to the design. However, the absence of a control feature to rotate the shaft without rotation of the handle itself results in a worse ergonomic posture. Ten out of the sixteen different instruments can rotate the shaft or end-effector around its axis within the found literature. Therefore, product advancement can be achieved by adding a rotating shaft or end-effector to the LapaJoy. By rotating the shaft, the steering control and grasping control must be connected such that it allows for rotation. By only rotating the grasping forceps, the steering control can remain unaffected. It is therefore strongly suggested to research the different end-effector rotation possibilities.

The vulnerability of the design was visible in use. After multiple cycles of closing and opening the dome, the 3D-printed spring within the joystick design broke. Different spring designs can be investigated, such as wave springs which will lead to better spring properties. The grasper's flexure also showed signs of fatigue, and the flexure broke off after approximately 50 to 60 cycles. The material properties play an essential role in the fatigue of the spring and grasper flexure. Materials with different modulus, springback and elongation properties must be investigated to achieve an even better and more reliable product.

Furthermore, the bridge should contain an extra set screw hole such that glueing the cable can be avoided. The set screw makes sure that the cable can be clamped by a better, easier and more reliable method. Figure 43b shows the glued cable onto the groove located on the left side of the bridge.

The number of parts for the laparoscopic instrument was minimised to five. In perspective, the DragonFlex consists of eleven parts, and the joystick control of the Duoflex consists of thirteen parts, Figure 58. The LapaJoy is a promising instrument in terms of ergonomics, ease of use and assembly time compared to current laparoscopic instruments.

Figure 58: Part assembly of laparoscopic instruments. A) Dragonflex consisting of eleven parts. B) Joystick control of the DuoFlex, which consists of thirteen parts. Taken from [7,37].

6.2.2 Parametric designing

In total, 95% of the Dutch population can reach and control all functional elements. It can be beneficial to have an instrument that the majority of the people can use. However, creating a handle that most people can use is essentially one that is not a perfect fit for the vast majority of the population. Therefore, the parametric ratio between the handle dimensions and the surgeon's hand size based on anthropometric measurements will be the continuation of a better product.

The advantage of a parametric design is that the relevant interdependent dimensions can be directly adjusted to the correct scale. The most critical aspects for a parametric design are defining the parametric design problems based on: an initial problem-solving plan, the parameters, the design variables, and problem definition parameters [68]. A parametric design is a scientific study on its own and therefore out of this research scope. However, recommendations based on knowledge and discoveries for parametric designing can be given to start with.

It is crucial to determine which hand measurements are related to the handle's size and which dimensions can be adjusted without compromising the functionality. A characteristic dimension has to be determined to define the parametric scaling factor for the ergonomic handle grip's different parameters. Based on personal insights, the handle design's characteristic dimension should be the base of the hand to the metacarpal head of the middle finger, which is responsible for the characteristic diameter of the handle design. The parametric relation between the hand width and the characteristic dimension will result in the handle length. The additional 12° angle along the grip can be seen as a constant value for all hands and should not be scaled parametrically to the characteristic dimension.

The grasper trigger placement was located along the index finger axis, at a certain distance from the index finger's metacarpophalangeal joint. The grasper trigger parameter should be scaled to the design's characteristic dimension along the index finger line. The joystick placement was based on the thumb's length from root to tip and compensates for its flexion. It furthermore compensates for the distance from the thumb's tip to the middle part of the thumb's phalanges that controls the joystick. Furthermore, the joystick was placed to the left from the central line of the shaft axis for right-hand use to realise the resting hand posture. The left placement was based on half the thumb thickness and should be defined by a parametric ratio in the parametric design.

A parametric model can be realised if all constants relate to the ergonomic handle's characteristic dimension. However, some difficulties regarding the scalable parametric model will have to be considered. The fingers' thickness and length cannot be defined as parametric ratios since these values are not constant throughout individuals. The design performance must be predicted by experimental and analytical methods, where an evaluation must be made on the best result of each design proposal. The best design proposal must be further researched until the most promising parametric scalable design is developed.

6.2.3 Minimal assembly design

The easily accessible and minimised assembly design requirement of less than or equal to five parts was achieved. The wish for non-assembly design, meaning no assembly, was not. However, an ongoing question is whether it is feasible and more convenient to have a minimal assembly design than a minimised assembly design. This section discusses various print techniques and approaches that could potentially fulfil the wish of a non-assembly design. Conceptual working principles will be discussed. However, the different given conceptual designs should still be investigated and tested before a proof of concept can be shown.

With the advent of 3D-printing, it is possible to manufacture complex structures with reduced or entirely excluded post-processing steps [69]. Printability is the key challenge in developing non-assembly designs. Different printing techniques can be deployed for non-assembly designs. Each printing technique has its pros and cons, resulting in different properties, possibilities, strategies, and solutions. The design aspects that must be investigated to go from a minimised towards a non-assembly design are summed up below:

- Combined ball and socket joint design.
- Pre-tension within the design.
- Combined bridge and joystick design.

The ball and socket joint design must be printed with supports. The support material, printed with the current printing technique, has to be removed by cutting away the support. Support materials as such complicate the realisation for non-assembly designs. Another printing technique, fused deposition modelling (FDM), could allow for a non-assembly design of a ball and socket joint if extensive mechanical play is added to the design [69]. However, mechanical play is not desirable. In the paper of Calì et al., a ball and socket joint was printed with selective laser sintering (SLS) technique without mechanical play by an innovative way as shown in Figure 59 [70].

The advantage of selective laser sintering is that the unsintered powder material forms the support. The unsintered powder allows for complex design structures to be easily created, bearing in mind that the support material must be removed afterwards. However, the clearance needed for features printed with the SLS technique is in millimetres, wherein the clearance needed for the LapaJoy design is in micrometres.

PolyJet is another 3D-printing technique that can achieve the desired resolution for this design [71]. A great advantage of the PolyJet 3D-printing technique is printing multiple materials within the same print. Printing different materials can change the properties of different system parts, where material selection is based upon its intended purpose. PolyJet printers can also create soluble support material that can thrive the complexity of structures since hard to reach support

material can now be dissolved [72]. PolyJet is a promising technique for non-assembly design.

Using the PolyJet printing technique, a ball and socket joint can be printed with support material that can be dissolved. Clearance is important for removing support material from the ball and socket joint connection and must have a minimum clearance of 0.4 mm [71]. Furthermore, pre-tension must be present within the steering control to build up pressure between the joystick and dome to ensure friction within the system. Since it is not possible to print pre-tension, different solutions must be found to include pre-tension within a non-assembly design. To ensure pre-tension, either the joystick's disc must be pressed onto the dome, or the dome must be pressed onto the disc of the joystick to lock the end-effector in place. On top of the travel distance necessary to create pre-tension, the distance must also compensate for the gap of the removed support material from the ball and socket joint. Therefore, additional clearance must be taken into account.

Different systems can build up the pre-tension of either the joystick or dome by displacement of the parts. The pre-tension can, for example, be achieved by a bistable, screw-on, or push through system. A bistable system is a system where two steady states are defined. Between the two steady states, multiple unstable modes are present. The two steady states can be defined as active discontinuous friction control. Both the dome or joystick can potentially be brought in the second steady-state, where a single structure compliant mechanism can achieve the bistable system. The generated force input brings the bistable systems into a second steady state. Since the dome is a static object, it is recommended to focus on a conceptual bistable dome design system. Figure 60 shows conceptual designs of bistable systems whereupon the dome can be attached.

Another proposal is the screw-on design. The dome will be printed with large mechanical play and soluble supports. When tightening the dome, large mechanical play will be removed by the threads that have a closer fit, Figure 61a. The same print approach can be used for a push through design, Figure 61b. Again, the dome will be printed with large mechanical play and soluble support. However, the dome is now pushed instead of twisted to create pre-tension within the design, Figure 61b.

In addition to the previous discussed non-assembly designs, the bridge and joystick must also become non-assembly designs. The ball of the ball and socket joint will be directly implemented into the bridge. A different design can combine the bridge and joystick while keeping all functionalities. The cables will be attached to the bridge, and the joystick can be pressed to get free from the dome. PolyJet can print multiple materials, including elastic materials for spring designs. The bridge, joystick and spring are combined to a conceptual non-assembly design, as shown in Figure 62. However, the conceptual non-assembly design has, as a downside, the reachability of the cable attachments. A cableless design might be the solution, but an entirely new design must then be created.

Compared to the current minimised part assembly design of the LapaJoy, it does not save time since the click on design of the LapaJoy is assembled within seconds and very similar to the steps taken within the non-assembly design.

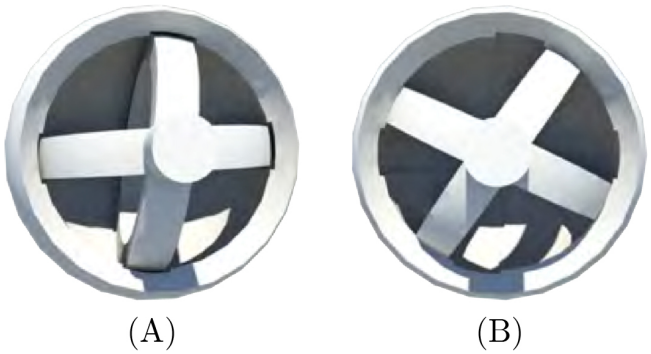

Figure 59: Non-assembly ball and socket joint. A) Print configuration. B) Twisted in operating configuration. Taken from [70].

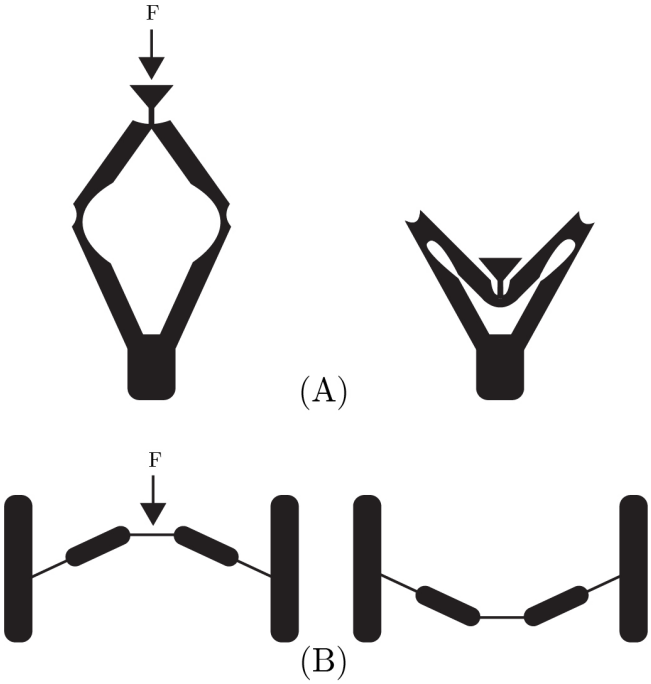

Figure 60: Two different dome attachment solutions for a bistable compliant mechanism design. Force is used to deflect the mechanism into another steady state.

6.3 Recommendations

Based on the outcome of this research, recommendations were addressed. A critical performance aspect is a qualitative analysis that reveals the clear correlation between tissue trauma and increased grasp pressure, which has been left out. According to Chandler et al., trauma most likely occurs at or above the threshold of 150 kPa (0.15 N/mm^2) [73]. The jaws' applied pressure should not surpass this threshold, and inconsistent friction that can damage tissue should not occur. An interesting test to acquire insight into the grasping pressure would be to determine the grasper system's

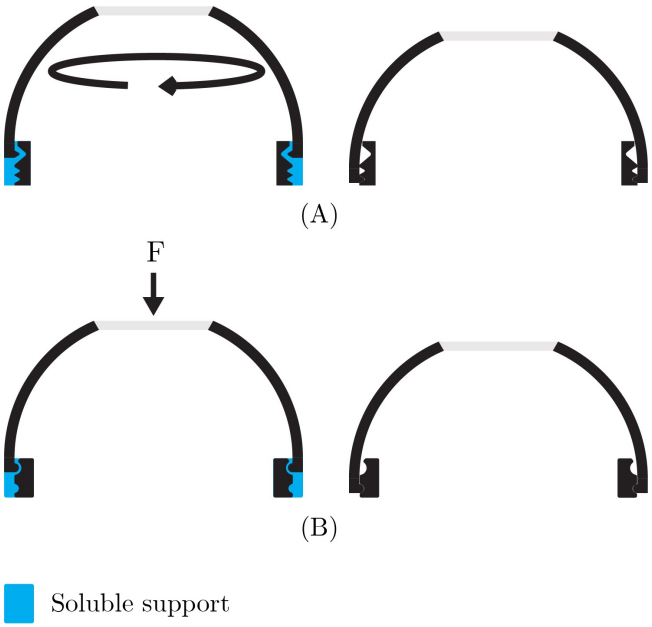

Figure 61: Non-assembly dome design. A) Dome with screw on design. B) Push through design of the dome.

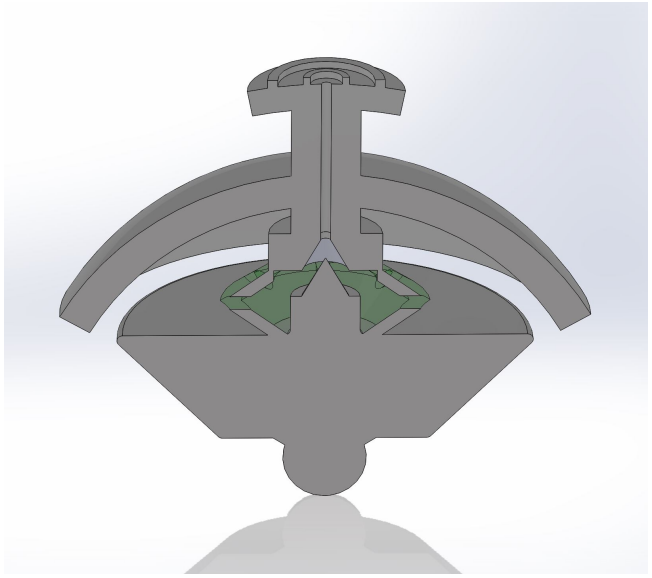

Figure 62: Section view of the non-assembly design. The spring, indicated by transparent green, is made from elastic material.

gain. Here, the applied grasp force of the index finger will be compared to the jaws' output force. Not only the pressure of grasping forceps will then be determined, but also the gain of the system will be known. The gain can then be linked to the feedback of the grasping system.

Furthermore, it is recommended to carry out tests to ensure that compressive forces are less than 3 kg/cm^2 to avoid complications. On top of that, surgeons' intuitiveness must be elaborated to make a correct statement about the instrument's ease of use and ergonomics.

Additional scientific research can be conducted on parametric designing, design optimisation and material properties. Improvement in ergonomics will arise when the design becomes parametric scalable. Optimisation of the flexures and joystick spring dimensions will create a more reliable design. By ensuring smaller cable tray diameters within the handle, less cable play will occur. Using better-suited materials for the intended purpose will lead to better flexural springback, less fatigue, and less plastic deformation.

A recommendation is made to examine the discussed design improvements in Section 6.1.3. It is also recommended to explore the possibility of locking the grasping forceps in any desired position by a continuous locking system. Furthermore, it is recommended to perform research on the possibility of shaft rotation and whether minimal assembly is better than minimised assembly.

The last recommendation for future research is the maximum attainable steering angle. The maximum attainable steering angle in practice of 45° is not comparable to state-of-the-art steerable laparoscopic instruments that stretch within 60°. Therefore, it is recommended to determine and develop the required joystick's cable deflection to achieve a 60° bending angle of the end-effector while maintaining an ergonomic design.

7 Conclusion

In this research, the design process of a fully 3D-printed ergonomic handle for a steerable laparoscopic instrument with minimised part assembly has been described. By going systematically through the design steps of the design analysis and the design processes, a prototype arose; The LapaJoy.

This research demonstrates the potential of 3D-printing as a manufacturing technique to create an ergonomic handle that integrates multiple control functions. The entire laparoscopic instrument consists of five parts and four parts potentially. The single hand-held instrument can steer the end-effector in 2 degrees of freedom, grasp tissue, and lock the end-effector and grasping forceps in place. All functions can be controlled simultaneously using only the index finger and thumb.

The LapaJoy is a promising design. However, the instrument cannot be deployed as it is in its current state. Although the LapaJoy was based on anthropometric data, scientific tests and extensive testing in the real world will determine the performance and ergonomic value of the 3D-printed LapaJoy. Future research should also investigate and find solutions to increase the maximum attainable bending angle of the end-effector, reduce fatigue of the flexures, reduce plastic deformation, and improve material properties.

To conclude, the LapaJoy with minimised part assembly has great potential as an inexpensive disposable laparoscopic instrument. Further development of the LapaJoy will lead to a reliable product that can soon be incorporated in minimally invasive surgery.

References

[1] P. L. Anderson, R. A. Lathrop, and R. J. Webster, "Robot-like dexterity without computers and motors: a review of hand-held laparoscopic instruments with wrist-like tip articulation," *Expert Review of Medical Devices*, vol. 13, no. 7, pp. 661–672, 2016.

[2] X. Wang, S. Wang, J. Li, G. Zhang, and Z. Wu, "Conceptual design of a novel multi-DoF manual instrument for laparoscopic surgery," *The International Journal of Medical Robotics and Computer Assisted Surgery*, vol. 9, pp. 75–82, 3 2013.

[3] A. G. Gallagher, N. McClure, J. McGuigan, K. Ritchie, and N. P. Sheehy, "An Ergonomic Analysis of the Fulcrum Effect in the Acquisition of Endoscopic Skills," *Endoscopy*, vol. 30, pp. 617–620, 9 1998.

[4] A. R. Lanfranco, A. E. Castellanos, J. P. Desai, and W. C. Meyers, "Robotic Surgery: A Current Perspective," *Annals of Surgery*, vol. 239, no. 1, pp. 14–21, 2004.

[5] H. Schreuder and R. Verheijen, "Robotic surgery," *BJOG: An International Journal of Obstetrics & Gynaecology*, vol. 116, pp. 198–213, 1 2009.

[6] A. Khajuria, "Robotics and surgery: A sustainable relationship?," *World Journal of Clinical Cases*, vol. 3, no. 3, p. 265, 2015.

[7] F. Jelínek, R. Pessers, and P. Breedveld, "DragonFlex Smart Steerable Laparoscopic Instrument," *Journal of Medical Devices*, vol. 8, pp. 1–9, 3 2014.

[8] Alphatron Medical Systems B.V., "Alphatron Medical." https://www.alphatronmedical.com/-nieuws/nieuwflexdex.html, last accessed 7/4/20, 2020.

[9] DEAM, "LaproFlex steerable laparoscopic instrument." https://www.deam.com/product-details/laproflex/, last accessed on 9/3/2020., 2020.

[10] F. Jelínek, "Steering and Harvesting Technology for Minimally Invasive Biopsy," *Surgery*, vol. 121, no. 4, pp. 472–479, 2015.

[11] G. Bazuin, *MonoFlex: A 3D-Printed Non-Assembly Steerable Instrument*. PhD thesis, Delft University of Technology, 2019.

[12] L. Santos-Carreras, M. Hagen, R. Gassert, and H. Bleuler, "Survey on surgical instrument handle design: Ergonomics and acceptance," *Surgical Innovation*, vol. 19, no. 1, pp. 50–59, 2012.

[13] F. M. Sánchez-Margallo and J. A. Sánchez-Margallo, "Ergonomics in Laparoscopic Surgery," in *Laparoscopic Surgery*, no. March, InTech, 2 2017.

[14] U. Matern and P. Waller, "Instruments for minimally invasive surgery," *Surgical Endoscopy*, vol. 13, no. 2, pp. 174–182, 1999.

[15] M. A. Van Veelen, D. W. Meijer, R. H. Goossens, and C. J. Snijders, "New ergonomic design criteria for handles of laparoscopic dissection forceps," *Journal of Laparoendoscopic and Advanced Surgical Techniques - Part A*, vol. 11, no. 1, pp. 17–26, 2001.

[16] S. Chowdhary, *Pediatric endourology*, vol. 19. 2014.

[17] K. D. Tung, R. M. Shorti, E. C. Downey, D. S. Bloswick, and A. S. Merryweather, "The effect of ergonomic laparoscopic tool handle design on performance and efficiency," *Surgical Endoscopy*, vol. 29, no. 9, pp. 2500–2505, 2015.

[18] U. De, "View Ergonomics and laparoscopy," no. June, pp. 2–5, 2014.

[19] S. D. Choi, "A review of the ergonomic issues in the laparoscopic operating room," *Journal of Healthcare Engineering*, vol. 3, no. 4, pp. 587–603, 2012.

[20] C. Fan, D. Dodou, and P. Breedveld, "Review of manual control methods for handheld maneuverable instruments," *Minimally Invasive Therapy and Allied Technologies*, vol. 22, no. 3, pp. 127–135, 2013.

[21] L. M. Okken, M. K. Chmarra, E. Hiemstra, F. W. Jansen, and J. Dankelman, "Assessment of joystick and wrist control in hand-held articulated laparoscopic prototypes," *Surgical Endoscopy*, vol. 26, no. 7, pp. 1977–1985, 2012.

[22] A. Olieman, "Engineering models of product design." http://wikid.io.tudelft.nl/WikID-/index.php/Engineering_models_of_product_design, last accessed on 10/4/2020., 2011.

[23] M. Patkin, "A Check-List for Handle Design," *Ergonomics Australia On-Line*, vol. 15, p. 22, 2001.

[24] J. M. Landsmeer, "Power grip and precision handling.," *Annals of the rheumatic diseases*, vol. 21, pp. 164–170, 1962.

[25] M. A. Van Veelen and D. W. Meijer, "Ergonomics and design of laparoscopic instruments: Results of a survey among laparoscopic surgeons," *Journal of Laparoendoscopic and Advanced Surgical Techniques - Part A*, vol. 9, no. 6, pp. 481–489, 1999.

[26] R. Berguer, S. Gerber, G. Kilpatrick, and D. Beckley, "An ergonomic comparison of in-line vs pistol-grip handle configuration in a laparoscopic grasper," *Surgical Endoscopy*, vol. 12, no. 6, pp. 805–808, 1998.

[27] N. T. Nguyen, H. S. Ho, W. D. Smith, C. Philipps, C. Lewis, R. M. De Vera, and R. Berguer, "An ergonomic evaluation of surgeons' axial skeletal and upper extremity movements during laparoscopic and open surgery," *The American Journal of Surgery*, vol. 182, pp. 720–724, 12 2001.

[28] R. E. Lawther, G. R. Kirk, and M. C. Regan, "Laparoscopic procedures are associated with a significant risk of digital nerve injury for general surgeons," *Annals of the Royal College of Surgeons of England*, vol. 84, no. 6, p. 443, 2002.

[29] H. Böhrs, *Arbeitsstudien in der Betriebswirtschaft*. Wiesbaden: Gabler Verlag, 1967.

[30] A. K. Hemal, M. Srinivas, and A. R. Charles, "Ergonomic problems associated with laparoscopy," *Journal of Endourology*, vol. 15, no. 5, pp. 499–503, 2001.

[31] M. L. Uhrich, R. A. Underwood, J. W. Standeven, N. J. Soper, and J. R. Engsberg, "Assesment of fatigue, monitor placement, and surgical experience

during simulated laparoscopic surgery," *Surgical Endoscopy and Other Interventional Techniques*, vol. 16, no. 4, pp. 635–639, 2002.

[32] H. J. Bullinger, *Ergonomie*. Technologiemanagement Wettbewerbsfähige Technologieentwicklung und Arbeitsgestaltung, Wiesbaden: Vieweg+Teubner Verlag, 1994.

[33] S. a. Nephew, "Smith & Nephew. SERPENT articulating instruments." https://www.smith-nephew.com/global/assets/pdf/products/surgical-/sportsmedicine/serpent%20brochure%2052268c-%20oct.2015.pdf, last accessed on 3/9/2020.

[34] S. Yoshida, I. Yoshino, Y. Moriya, H. Hoshino, T. Okamoto, M. Suzuki, and K. Shibuya, "Video-assisted thoracoscopic surgery extended thymectomy for myasthenia gravis using manual manipulators: The Radius Surgical System," *Annals of Thoracic Surgery*, vol. 92, no. 6, pp. 2246–2248, 2011.

[35] N. Yoshiki, "Single-incision laparoscopic myomectomy: A review of the literature and available evidence," *Gynecology and Minimally Invasive Therapy*, vol. 5, no. 2, pp. 54–63, 2016.

[36] IndiaMART InterMESH Ltd., "SILS Clinch Graspers." https://www.indiamart.com/-proddetail/sils-clinch-graspers-9052593955.html, last accessed on 9/3/2020., 2020.

[37] M. Vosse, "DuoFlex : Development of a New Multi-Steerable Laparoscopic Instrument," 2010.

[38] A. Sakes, K. Hovland, G. Smit, J. Geraedts, and P. Breedveld, "Design of a Novel Three-Dimensional-Printed Two Degrees-of-Freedom Steerable Electrosurgical Grasper for Minimally Invasive Surgery," *Journal of Medical Devices*, vol. 12, 3 2018.

[39] P. L. Anderson, R. A. Lathrop, S. D. Herrell, and R. J. Webster, "Comparing a Mechanical Analogue with the da Vinci User Interface: Suturing at Challenging Angles," *IEEE Robotics and Automation Letters*, vol. 1, no. 2, pp. 1060–1065, 2016.

[40] I. Medgadget, "Hands-On With The Revolutionary FlexDex Laparascopic Instrument Platform." https://www.medgadget.com/2016/06/flexdex-minimally-invasive-tool-control-system.html, last accessed on 9/3/2020., 2020.

[41] Indes., "DEAM – Laparoscopisch instrument." https://indes.eu/portfolio/deam-laparoscopisch-instrument/, last accessed on 9/3/2020, 2020.

[42] P. Breedveld, "I-Flex - Steering Towards Miniaturization Limits." https://www.bitegroup.nl/category/maneuverable-devices/i-flex/, last accessed on 9/3/2020., 2012.

[43] Unemed, "The Intuitool ™ : An Ergonomic Laparoscopic Grasper A harsh learning curve : laparoscopic surgery,"

[44] S. F. Hardon, F. Schilder, J. Bonjer, J. Dankelman, and T. Horeman, "A new modular mechanism that allows full detachability and cleaning of steerable laparoscopic instruments," *Surgical Endoscopy*, vol. 33, no. 10, pp. 3484–3493, 2019.

[45] N. Di Lorenzo, I. Camperchioli, and A. L. Gaspari, "Radius surgical system and conventional laparoscopic instruments in abdominal surgery: Application, learning curve and ergonomy," *Surgical Oncology*, vol. 16, pp. 69–72, 2007.

[46] F. M. Sánchez-Margallo, J. A. Sánchez-Margallo, and A. Szold, "Handheld Devices for Laparoscopic Surgery," in *New Horizons in Laparoscopic Surgery*, vol. i, p. 13, InTech, 9 2018.

[47] A. M. Polyukhov, "'Hand clasping' and 'arm folding'. Population, hereditary and neurophysiological aspects," *Genetika*, vol. 16, no. 7, pp. 1294–1300, 1980.

[48] F. Jelínek, E. A. Arkenbout, P. W. Henselmans, R. Pessers, and P. Breedveld, "Classification of joints used in steerable instruments for minimally invasive surgery: A review of the state of the art," *Journal of Medical Devices, Transactions of the ASME*, vol. 9, no. 1, 2015.

[49] M. S. Sanders and E. J. McCormick, *Human Factors In Engineering and Design*. McGraw-Hill Education, 7th ed., 1993.

[50] C. Fan, F. Jelínek, D. Dodou, and P. Breedveld, "Control devices and steering strategies in pathway surgery," *Journal of Surgical Research*, vol. 193, pp. 543–553, 2 2015.

[51] C. Fan, H. Clogenson, P. Breedveld, J. J. van den Dobbelsteen, and J. Dankelman, "Comparison of two control methods for minimally invasive surgical instruments," *Journal of Medical Devices, Transactions of the ASME*, vol. 6, no. 2, pp. 3–8, 2012.

[52] A. H. Zahraee, J. K. Paik, J. Szewczyk, and G. Morel, "Toward the development of a hand-held surgical robot for laparoscopy," *IEEE/ASME Transactions on Mechatronics*, vol. 15, no. 6, pp. 853–861, 2010.

[53] K. Doné, S. Takahashi, A. Nickel, X. Ding, and S. Hallbeck, "How should Trackball Directional Movement Intuitively Relate to an End Effector?," *Proceedings of the Human Factors and Ergonomics Society Annual Meeting*, vol. 47, pp. 1122–1125, 10 2003.

[54] C. L. Taylor and R. J. Schwarz, "The anatomy and mechanics of the human hand.," *Artificial limbs*, vol. 2, pp. 22–35, 5 1955.

[55] A. G. González, D. R. Salgado, L. G. Moruno, and A. S. Ríos, "An ergonomic customized-tool handle design for precision tools using additive manufacturing: A case study," *Applied Sciences (Switzerland)*, vol. 8, no. 7, 2018.

[56] R. Brouet, R. Blanch, and M.-P. Cani, "Understanding Hand Degrees of Freedom and Natural Gestures for 3D Interaction on Tabletop," in *Lecture Notes in Computer Science (including subseries Lecture Notes in Artificial Intelligence and Lecture Notes in Bioinformatics)*, vol. 8117 LNCS, pp. 297–314, 2013.

[57] J. R. Martin, V. M. Zatsiorsky, and M. L. Latash, "Multi-finger interaction during involuntary and voluntary single finger force changes,"

Experimental Brain Research, vol. 208, pp. 423–435, 2 2011.

[58] J. Dirken, *Productergonomie: Ontwerpen voor gebruikers*. Delft: Delft Academic Press / VSSD, 1997.

[59] N. J. Seo and T. J. Armstrong, "Investigation of grip force, normal force, contact area, hand size, and handle size for cylindrical handles," *Human Factors*, vol. 50, no. 5, pp. 734–744, 2008.

[60] J. Molenbroek, "DINED anthropometric database." https://dined.nl/en/database/tool, last accessed on 3/8/2020., 2020.

[61] S. Manasnayakorn, A. Cuschieri, and G. B. Hanna, "Ideal manipulation angle and instrument length in hand-assisted laparoscopic surgery," *Surgical Endoscopy and Other Interventional Techniques*, vol. 22, no. 4, pp. 924–929, 2008.

[62] A. Fingerhut, G. B. Hanna, N. Veyrie, G. Ferzli, B. Millat, N. Alexakis, and E. Leandros, "Optimal trocar placement for ergonomic intracorporeal sewing and knotting in laparoscopic hiatal surgery," *American Journal of Surgery*, vol. 200, no. 4, pp. 519–528, 2010.

[63] D. H. Tilley, A. R., "The measure of man and woman: Human factors in design," ch. Manual Con, pp. 74–75, New York: John Wiley & Sons, 1994.

[64] B. Bhushan and M. Caspers, "An overview of additive manufacturing (3D printing) for microfabrication," *Microsystem Technologies*, vol. 23, no. 4, pp. 1117–1124, 2017.

[65] K. S. Lee and M. C. Jung, "Ergonomic evaluation of biomechanical hand function," *Safety and Health at Work*, vol. 6, no. 1, pp. 9–17, 2015.

[66] A. G. González, J. G. Sanz-Calcedo, O. López, D. R. Salgado, I. Cambero, and J. M. Herrera, "Guide Design of Precision tool Handle Based on Ergonomics Criteria Using Parametric CAD Software," *Procedia Engineering*, vol. 132, pp. 1014–1020, 2015.

[67] C. Culmone, P. W. J. Henselmans, R. I. B. van Starkenburg, and P. Breedveld, "Exploring non-assembly 3D printing for novel compliant surgical devices," *Plos One*, vol. 15, no. 5, p. e0232952, 2020.

[68] F. Fu, *Design and Analysis of Tall and Complex Structures*. 2018.

[69] J. S. Cuellar, G. Smit, A. A. Zadpoor, and P. Breedveld, "Ten guidelines for the design of non-assembly mechanisms: The case of 3D-printed prosthetic hands," *Proceedings of the Institution of Mechanical Engineers, Part H: Journal of Engineering in Medicine*, vol. 232, no. 9, pp. 962–971, 2018.

[70] J. Calì, D. A. Calian, C. Amati, R. Kleinberger, A. Steed, J. Kautz, and T. Weyrich, "3D-printing of non-assembly, articulated models," *ACM Transactions on Graphics*, vol. 31, no. 6, 2012.

[71] Proto3000, "PolyJet 3D Printing Design Guidelines." https://proto3000.com/service/3d-printing-services/materials/overview/design-guidelines/polyjet-3d-printing-design-guidelines/#fso-1397424134-4, last accessed on 15/01/2021., 2021.

[72] A. Pugalendhi, R. Ranganathan, and M. Chandrasekaran, "Effect of process parameters on mechanical properties of VeroBlue material and their optimal selection in PolyJet technology," *International Journal of Advanced Manufacturing Technology*, vol. 108, no. 4, pp. 1049–1059, 2020.

[73] J. H. Chandler, F. Mushtaq, B. Moxley-Wyles, N. P. West, G. W. Taylor, and P. R. Culmer, "Real-Time Assessment of Mechanical Tissue Trauma in Surgery," *IEEE Transactions on Biomedical Engineering*, vol. 64, no. 10, pp. 2384–2393, 2017.

A Appendix: Monoflex

A.1 Analysis of the Monoflex

Since the handle might be implemented in the design of the Monoflex. The analysis of the Monoflex is crucial for understanding the kinematics of the system. The system was divided into three segments, each having an application to fulfil the desired task. Figure 63 shows the three divided segments by the dashed vertical lines and Figure 64 visualises the movements of the Monoflex by a schematic cans in series drawing.

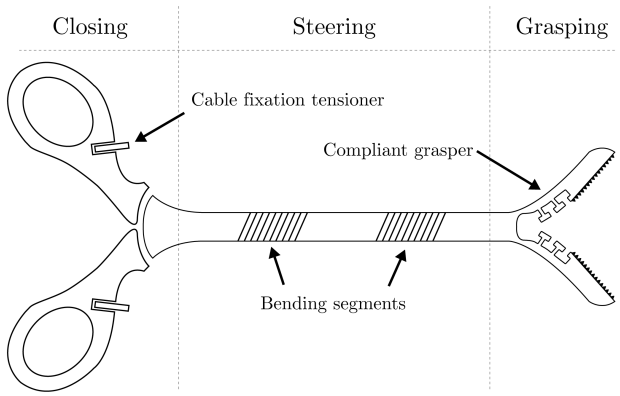

Figure 63: Simplified schematic drawing of the Monoflex.

A.1.1 Closing

The left segment closing of the laparoscopic instrument in 63 shows the inline scissor grip. The inline scissor grip serves as the articulation handle for steering control. It also controls the cable tension for the closing mechanism of the gripper. The two scissor handles can move up and down independently from each other. Closing depends on the constant length of the cables, where Figure 65 shows the cables as dashed lines. Figure 65b shows the simplified cable tension principle. The dashed line in the open situation has a smaller arc length than the solid line. In the closed situation, the arc length of both lines, the solid line and dashed line, are the same. Arc length extension concludes that cable tension occurs in the system by closing the scissor. Calculation of the length ratio between the two arcs is important. If the closing mechanism has to make a large movement to close the jaw, the mechanism can potentially be outside the ergonomic reach zone of the surgeon's hand, leading to fatigue or other discomforts. By the ratio between the two arc lengths, design choices can be made. Translating the arc length elongation to the same curvature ratio principle in the grasping section can realise a zero angle between the two jaws with minimal input effort when closing. Figure 65c shows a single segment of the simplified visualisation of the cable tension principle indicated by symbols. The ratio between the inner and outer arcs were related by κ (the curvature). The following steps show the ratio between the arc length of the inner cable compared to the constant arc length for a given curvature (κ) and height (h).

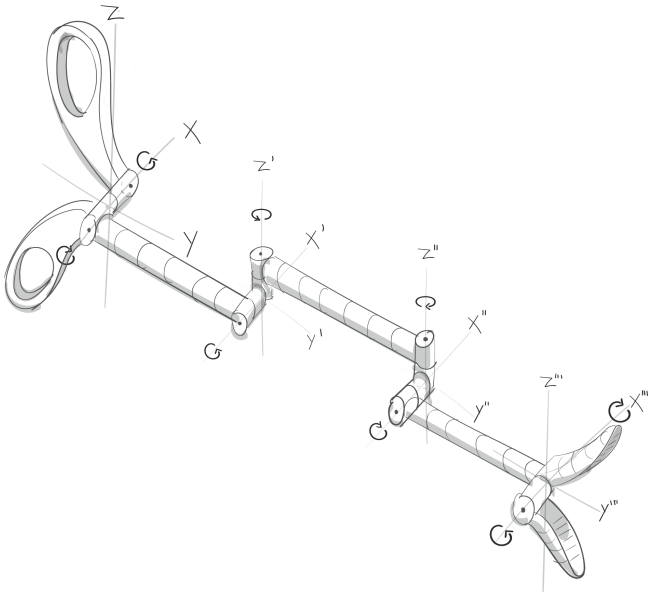

Figure 64: Schematic drawing of cans in series regarding the Monoflex.

1. The arc length of b:

$$a_b = \frac{1}{\kappa} \cdot \theta \tag{1}$$

2. The arc length of c:

$$a_c = (\frac{1}{\kappa} - h) \cdot \theta \tag{2}$$

3. The ratio of arc length c compared to arc length b:

$$\frac{a_c}{a_b} = \frac{(\frac{1}{\kappa} - h) \cdot \theta}{\frac{1}{\kappa} \cdot \theta} = \kappa \cdot (\frac{1}{\kappa} - h) = 1 - \kappa h \tag{3}$$

4. The parametric arc length of c with respect to the curvature of the base:

$$a_c(\kappa) = a_b(1 - \kappa h) \tag{4}$$

A.1.2 Steering

The steering analysis was based on the cable behaviour inside the steering segment that is actuated by the hand articulation of the inline scissor grip. Inside the Monoflex, four cables enable the movement of the end-effector. These cables are all running through an individual cable guiding tray inside the shaft of the steering segment. Figure 66 and 67 show the steering situations that can be provided by the system actuated by the hand articulation. As seen in Figure 66a, the top right and the bottom right cable are under tension resulting in a movement of the end-effector to the right. Figure 66b shows the inverse movement. Steering left, and right (yaw motion) adds one degree of freedom to the system. When moving the handle control into a downward position, as shown in Figure 67a, it leads to tension in the top cable couple in the top. The movement has the effect that the end-effector moves upward. Figure 67b shows the inverse movement.

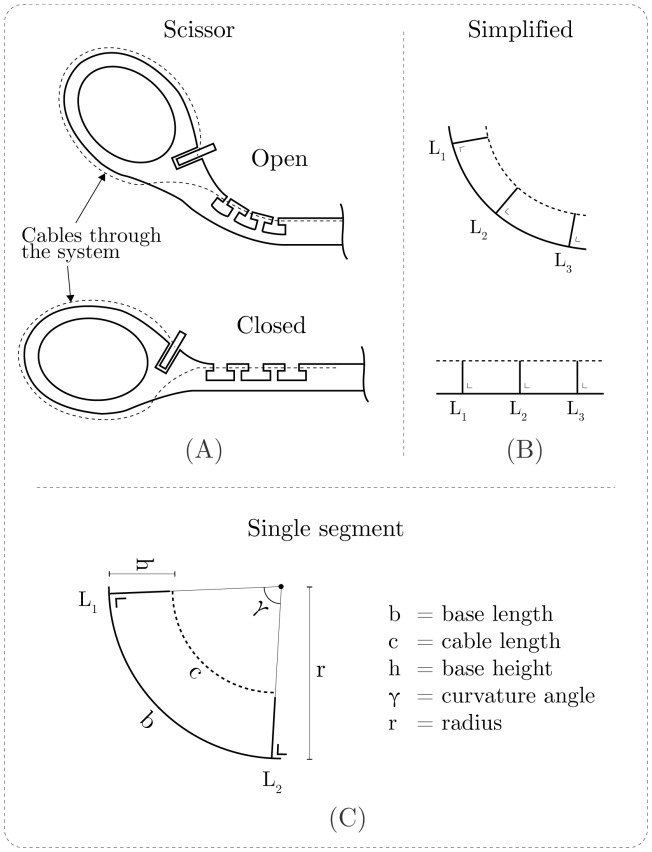

Figure 65: Grasping principle of the Monoflex. A) Schematic drawing of the Monoflex's closing principle. B) Simplified segment drawing of the cable curvature and constant arc length. C) A single segment of the simplified closing mechanism.

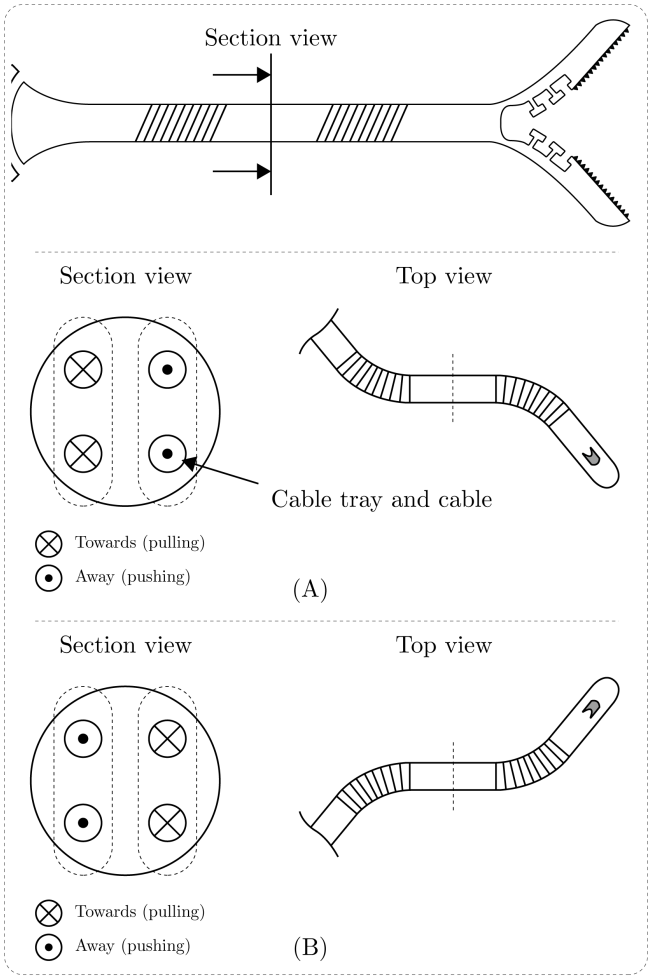

Figure 66: Schematic motion analysis. A) Right half cables under tension, steering to the right of end-effector. B) Left half cables under tension, steering to the left of end-effector.

Moving up and down (pitch motion) adds one degree of freedom to the system. There is no amplification inside the steering system, which means that the magnitude of the input motion results in a one to one inversed output ratio.

A.1.3 Grasping

The cables connected from the two scissor handles to the two jaws, are divided by the upper jaw and lower jaw. The upper cables connect the upper scissor handle to the upper jaw, and the lower cables connect the lower scissor handle to the lower jaw. Closing the upper scissor handle leads to tension in the cable that results in closing the upper jaw. The same holds for the bottom scissor handle and the lower jaw. The system of the two independent compliant springs in the jaw, as seen in Figure 68, results in the opening of the jaw when no cable tension is present. The two cable sets combined with the two compliant springs add two extra DoF to the system. These two scissors are independent from each other, as seen in Figure 68. However, closing of the jaws is based on the same principle as closing the scissor. The alignment of the cable bridges limits the closing angle showed in Figure 68. The alignment means that grasping takes place at the centre line of the shaft and was therefore considered a 1 DoF system.

A.1.4 Conclusion of the Monoflex analysis

The Monoflex has achieved a total of three degrees of freedom, of which two degrees of freedom are committed to the steering direction. Figure 64 shows the kinematic system by a cans in series schematic drawing to visualise the possible movements of the Monoflex. The input motion of the handle articulation is parallel to the yaw or pitch motion of the end-effector. However, looking at the parallel motion of the in- and output motion, it is less intuitive than reversed motion when the input moves up that the end-effector moves in an upward direction [52]. Same holds for left-left and right-right in- and output motion. Looking at the handle design of the Monoflex in its current state, it can result in wrist overloads during tasks due to its scissor handle and should be improved.

B Appendix: Joint type configurations

Joint mechanisms that enable rotational movements in 1 DoF and 2 DoF that are given in the paper of Jelinek et al.. The mechanisms in Figure 69 highlight different joint configurations that are categorised by several joint types [48].

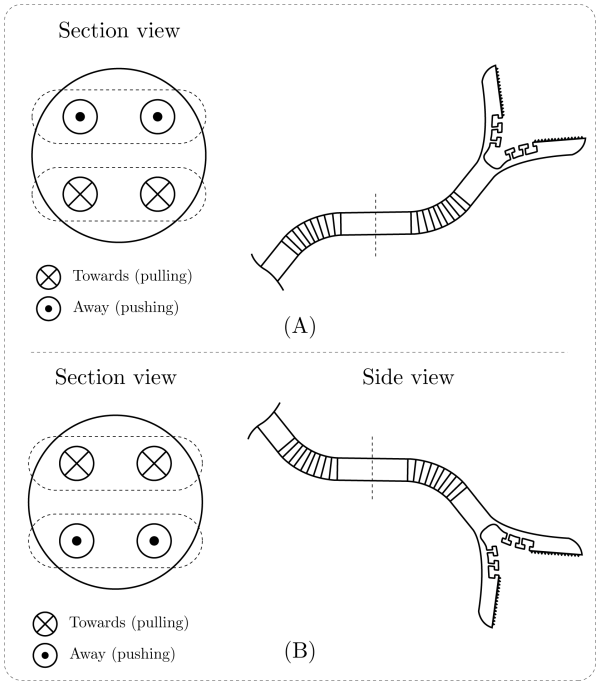

Figure 67: Schematic motion analysis. Same section view as Figure 66. A) Top half cable couple under tension, upwards movement end-effector. B) Bottom half cable couple under tension, downwards movement end-effector.

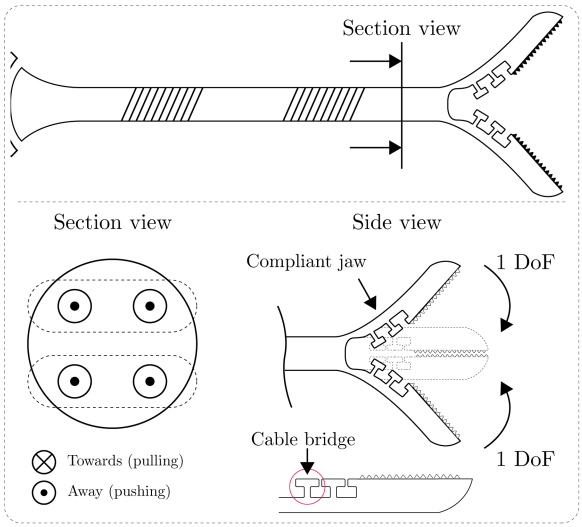

Figure 68: Cable analysis inside the grasping segment, resulting in closing by cable tension and opening by the compliant spring when no cable tension is present.

C Appendix: Grasper design

The study by L. Bazuin did research on bending flexure joint geometries to create a 3D-printed non-assembly steering instrument [11]. Based on the research of L. Bazuin, the best proven bending flexure joint principle was adjusted and applied with the same bending flexure joint thickness to the ergonomic handle design in this study. The grasper that is connected by cables to the jaws of the end-effector, controls the tension of the cable. The working principle is explained in section A.1.1 where the difference in arc length between the inner and outer joint bending sections results in tension of the cable.

The described interlocking system in the conceptual design shows design problems in its early working principle. An interlocking system as such cannot be locked without covering the full range of motion. Besides, the system must be able to exceed the maximum allowable grasping force, if necessary, which is not possible with an interlocking design. Although a system as such is a continuous locking system, the system does not suffice on closer inspection. The schematic drawing in Figure 70 shows the new conceptual design where friction occurs between the bending flexure joint and the walls. With this new design actively locking of the grasper is achievable.

Furthermore, the locking feature of steering and grasping is still open to design choices. The desired locking mechanism is a continuous mechanism. The disadvantage of continuous locking is that the locking mechanism is based on friction, which has a limited friction force. However, a continuous locking system has no interval positions and can take any desired locked position. In the preliminary design of the ergonomic handle, a deliberate choice is made between the two locking kinematics towards the realisation of minimal part assembly and design possibilities.

First, the bending flexure joint design is tested for its working principle, where Figure 71 shows the 3D drawing. The bending flexure joint slides between the two friction plates and locks the grasper in place by the generated friction within the system. However, the design in Figure 71 does not suffice to evenly increase the bending flexure joint curvature since the friction appears to be higher at specific places. Therefore, a new design must be created that does not hinders the movement of the bending flexure joint by friction.

Grasping, which results in increase the curvature of the bending flexure joint-segment. Points on the bending joint-segment now follow a path. A visualisation is made by the blue dashed curved line in Figure 70A which describes the path of the bending joint's endpoint. The described path is calculated in Matlab, where the curvature radius and the central angle are parameters. The Matlab script can be found in Appendix F.1. The described path with different grasping intervals is shown in Figure 73 in Appendix D.1. The data in Table 4 in Appendix D.1, which is calculated in the Matlab script, is used to draw the specific path in SolidWorks. This path does not interfere with the bending flexure joint-segment, and therefore only the non bending segment of the grasper. The end-point of the bending joint flexure is used to generate the friction and the grasper joint-segments are now free to move while grasping. The 3D drawing of the improved bending flexure joint friction design is shown in Figure 72.

However, by testing the new grasper configuration, it is concluded that the motion is not defined by single motion. The grasper manipulation now results in, besides the increase of bending joint's curvature, also in translation in the X and Y plane of the entire grasping control. The translation is unwanted since the motion of the end-point of the bending joint flexure cannot be

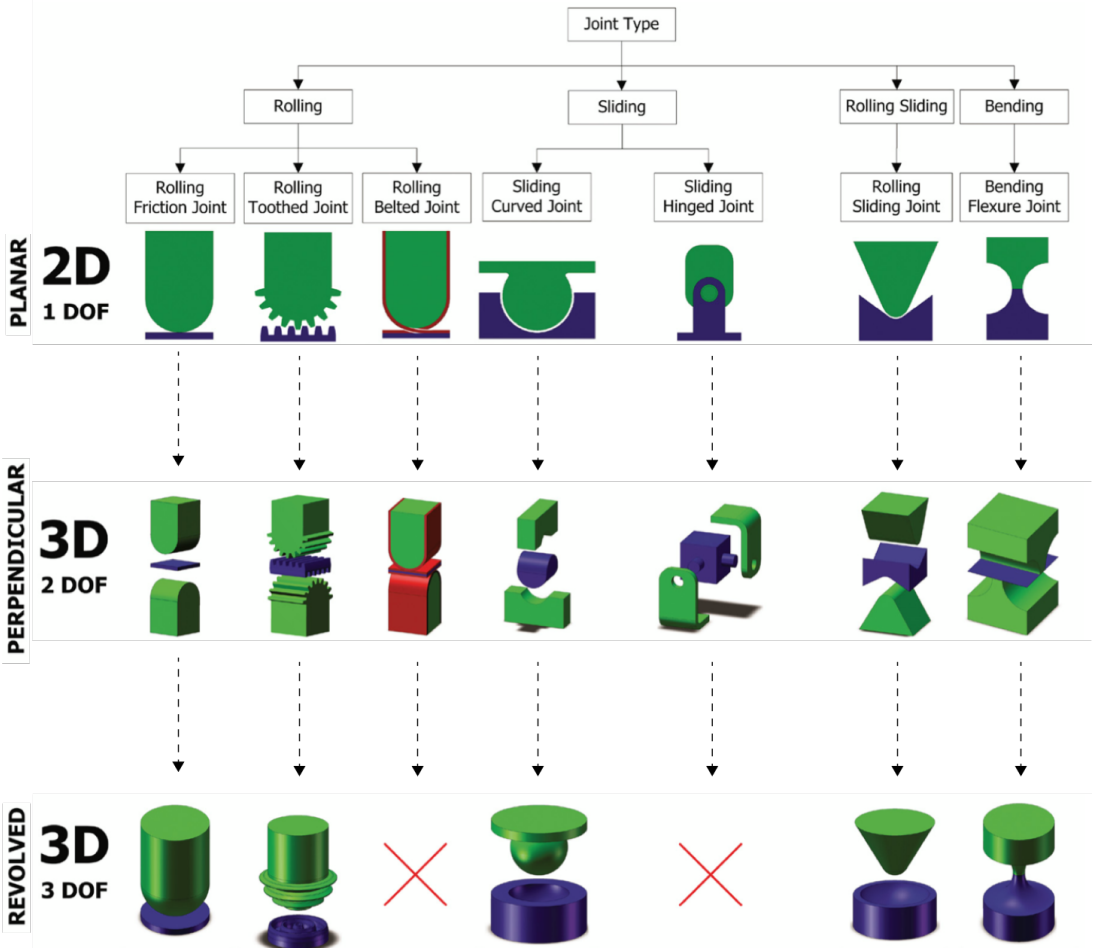

Figure 69: Joint type classifications categorised by several joint types. Taken from [48].

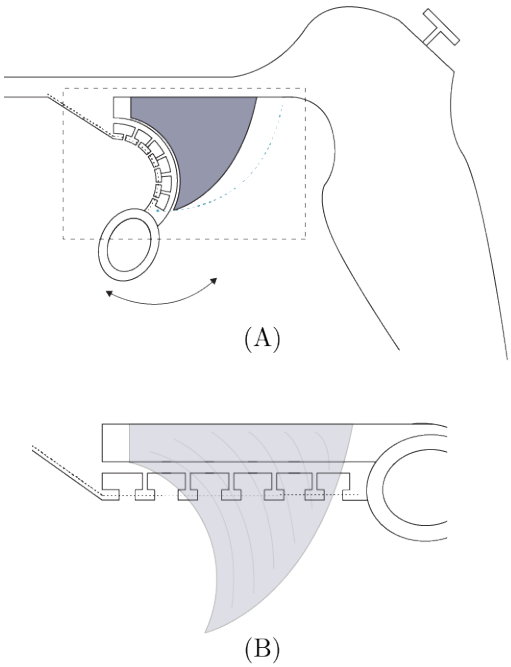

Figure 70: Visualisation of a conceptual grasper locking principle by friction. A) Schematic drawing of grasper in open state. B) Section zoom of schematic drawing of the grasper in locked state.

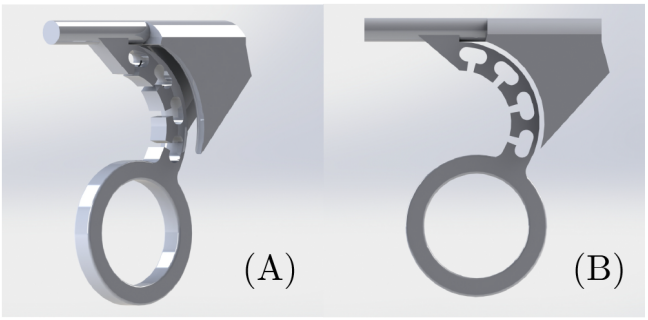

Figure 71: 3D drawing of the initial conceptual grasper principle. A) 3D view of the SolidWorks drawing. B) Side view of the SolidWorks drawing.

defined by the prescribed path.

D Appendix: Bending joint flexure

D.1 Bending joint flexure path

First, the initial position of the bending flexure joint is determined and is shown as the curved line with the smallest radius in Figure 73. The initial state is determined by the degrees of the central angle and radius. From there on multiple intersection were

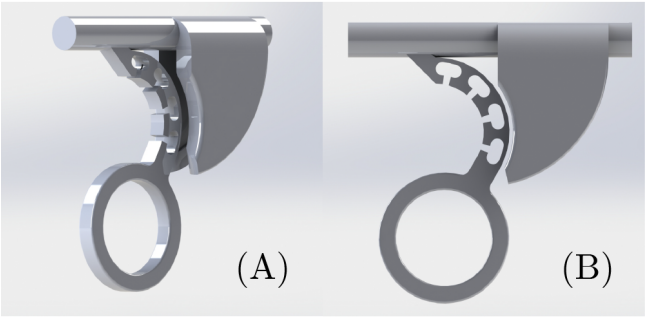

Figure 72: 3D drawing of the improved conceptual grasper principle. Friction does not intere with the bending flexure joint-segment. A) 3D view of the SolidWorks drawing. B) Side view of the SolidWorks drawing.

calculated having a different radius with a constant arc length. Those iterations are shown as the following curvatures. No interruption in the flexure takes place while changing the grasper's curvature if the imposed friction follows traveled path of rigid part of the bending flexure joint. The rigid part is at the end point of bending flexure joint that does not have bending segments. The traveled path of the end point is now calculated and visualised in Figure 73 with the dashed line that runs through the coordinates. The length between the base (coordinate (0,0)) and the coordinates of the end point can be calculated by trigonometry. The distance and angle direction with the horizontal plane are shown in Table 4 and were used for the SolidWorks drawing to determine the path of the friction plates. The Matlab code is shown in Appendix F.1.

Line Length [mm]	Angle [deg]
29.4449	-60.0000
30.3831	-55.0000
31.2546	-50.0000
32.0555	-45.0000
32.7822	-40.0000
33.4313	-35.0000
34.0000	-30.0000
34.4857	-25.0000
34.8861	-20.0000
35.1994	-15.0000
35.4242	-10.0000
35.5595	-5.0000
35.6047	0

Table 4: Calculated line specifications for Solidworks drawing to follow the bending flexure joint end point.

D.2 Arc length conversion

The different radius of the bending joint flexure segment of the cable tray radius and the most outer radius results in an increase of the cable tray arc length by changing the radius. The arc length change can on its turn be used for cable tension as explained previously in section A.1.1. The arc length increase must be calculated to create a system that is comfortable in use and fulfil the goal of closing the jaws. Therefore a Matlab script was created to calculate the exact arc length change in millimeters of the cable tray and shown in Table 5. The Matlab code is shown in Appendix F.2. The arc length change of the bending joint flexure must be related to the change of the jaws' bending joint to calculate the desired change in arc length and therefore the radius.

Line Length [mm]	Angle [deg]
0	120.0000
0.6981	110.0000
1.3963	100.0000
2.0944	90.0000
2.7925	80.0000
3.4907	70.0000
4.1888	60.0000
4.8869	50.0000
5.5851	40.0000
6.2832	30.0000
6.9813	20.0000
7.6794	10.0000

Table 5: Calculated arc length increase in mm with the given central / curvature angle.

E Appendix: Control cable elongation

The grasping forceps close due to a difference in cable length. To create a length difference that allows for closing the grasping forceps, an arc length difference must be present within the flexure, which is the case in the grasping forceps as shown by the radii of the circles in Figure 74. The arc length that remains constant during flexing of the bending joint segment has a smaller radius, compared to the variable arc length of the bending joint segment. By shortening the arc length of the variable arc length, the grasping forceps closes. The cable elongation that is needed to close the grasper, with the compensation taken into account for friction, cable slack, twist of the flexure, and extra grasping force if needed, is 3.8 mm calculated in Matlab and shown in Appendix F.3. The grasper must allow for a cable elongation of 3.8 mm in total over the maximised angle allowance of 37°. An arc length that allows for a cable elongation over an angle of 37° can be calculated which was also done by the Matlab script given in Appendix F.3.

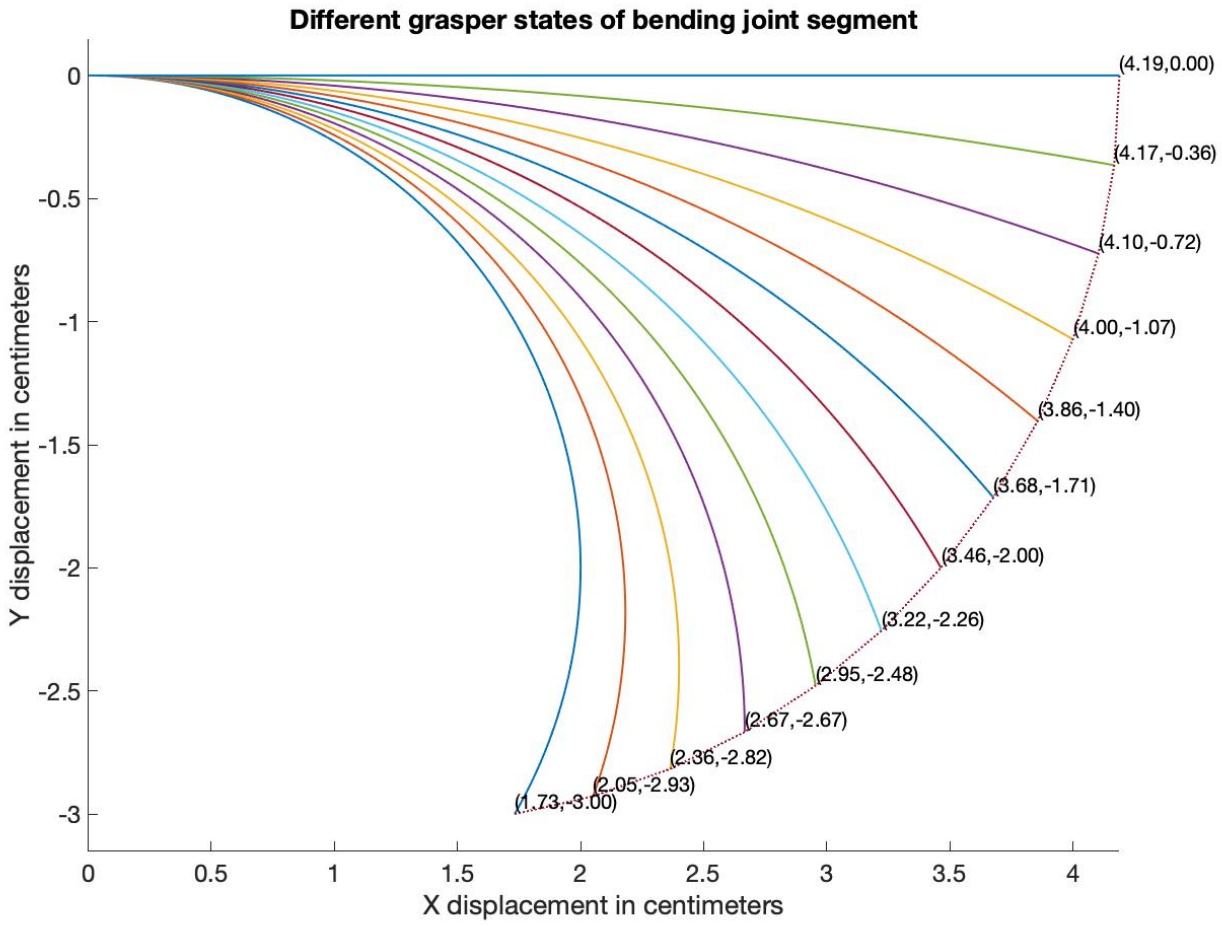

Figure 73: Matlab plot of the end point of the bending flexure joint's path while grasping.

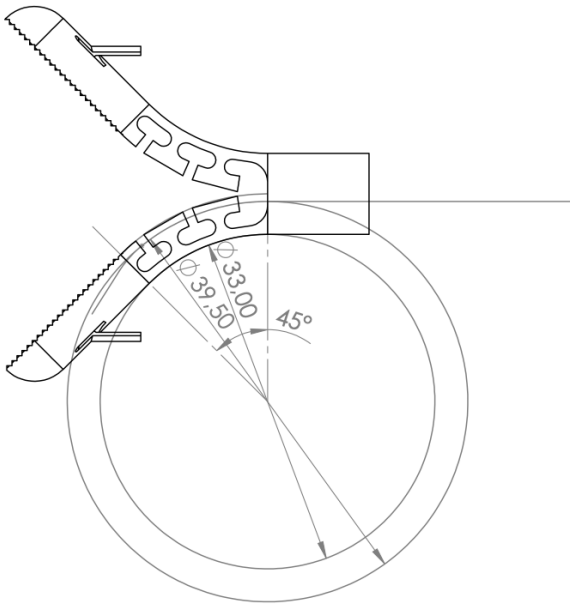

Figure 74: Different Radii given by specific bending locations for cable elongation calculation.

F Appendix: Matlab scripts

F.1 Bending joint flexure path

```
close all;
clear all;
clc
tic

Start = 120;                                % Degrees of bending joint in initial state
Startradius = 2;                            % Radius of circle of the bending joint

%%
ArcLength = (Start*Startradius)/180*pi;     % Arclength in centimeters
degrees = [Start : -10: 0];                 % Degrees of points of intersection base at
Degrees = degrees';                         % Transpose matrix Row into Column

a = 1;
r = zeros(length(Degrees),1);
for deg = Start:-10:0;
    r(a) = ArcLength/(pi/180*deg);          % Radius of the different closing grasper angles
    a = a + 1;
end
infLocations = isinf(r);
r(infLocations) = r(length(Degrees)-1,1)    % Vertical line becomes inf degrees

M = [r Degrees]                             % Radius of curvature by the different grasper degrees

b = 1;
y = zeros(length(Degrees),1);
for b = 1:length(M)
    y(b) = -M(b,1);                         % Radius into minus y direction from 0,0 point
    b = b + 1;
end

c = 1;
x1 = zeros(length(Degrees),1);
for c = 1:length(M)
    if Degrees(c)>90;
        x1(c)= cosd(Degrees(c,1)-90);       % Angle between radius line and below horizontal
        c = c + 1;                          % line for x coordinate calculations
    else Degrees(c)<=90;
        x1(c)=cosd(90-Degrees(c,1));        % Angle between radius line and above horizontal
        c = c + 1;                          % line for x coordinate calculations
    end
end

d = 1;
X = zeros(length(Degrees),1);
for d = 1:length(M)
    X(d) = x1(d,1)*M(d,1);                  % X coordinate of opening grasper en point
d = d+1;
end
X(~X) = ArcLength;                          % Zero creates inf. create the arc length when line is
                                            % vertical
e = 1;
y1 = zeros(length(Degrees),1);
for e = 1:length(M)
    if Degrees(e)>90;
        y1(e)= -sind(Degrees(e,1)-90);      % Angle between radius line and below horizontal
        e = e + 1;                          % line for y coordinate calculations
    else Degrees(e)<=90;
        y1(e)=sind(90-Degrees(e,1));        % Angle between radius line and above horizontal
        e = e + 1;                          % line for y coordinate calculations
    end
end

f = 1;
Y1 = zeros(length(Degrees),1);
for f = 1:length(M)
    Y1(f) = y1(f,1)*M(f,1);                     % X coordinate of opening grasper en point
f = f+1;
end
infLocations = isinf(Y1);
Y1(infLocations) = r(length(Degrees)-1,1);
Y = y+Y1;                                       % Y coordinate compared to base 0,0
```

```
73
74 XY = [X Y];                                          %Coordinates
75
76
77 g = 1;
78 angle_2 = zeros(length(M),120);
79 for g = 1:length(M)
80 angle_2(g,:) = linspace(pi,pi-M(g,2)/180*pi,120);       % Linspace iteration points for circulair
81 g = g + 1;                                             % bending joint
82 end
83
84 h = 1;
85 x_2 = zeros(length(M),120);
86 y_2 = zeros(length(M),120);
87 for h = 1:length(M)
88 x_2(h,:) = M(h,1)*cos(angle_2(h,:)-pi/2);               % X and Y coordinates on circulair
89 y_2(h,:) = M(h,1)*sin(angle_2(h,:)-pi/2)-(M(h,1)-2);    % bending joint per grasper opening state
90 h = h + 1;
91 end
92
93 x_3 = linspace(0,ArcLength,100);                       % Create line for infinite radius x
       coordinate
94 y_3 = zeros(1,100);                                    % Create line for infinite radius y
       coordinate
95
96 figure
97 hold on
98 for i = 1:length(M)
99     plot(x_2(i,:),y_2(i,:)-2,'LineWidth',2)            % Plot different grasping states bending
           joint
100 end
101 axis equal
102 plot (X,Y,':','LineWidth',2);                         % Plot coordinates en point grasper joint
103 newstr = strtrim(cellstr(num2str([X(:) Y(:)]...
104     ,'(%.2f,%.2f)')));                                 % Remove white space
105 text(X,Y,newstr,'VerticalAlignment','bottom',...
106     'FontSize',20,'LineWidth',0.5);
107 plot (x_3,y_3,'LineWidth',2)                          % Plot infinite radius
108 title    ('Different grasper states of bending joint segment');
109 xlabel   ('X displacement in centimeters');
110 ylabel   ('Y displacement in centimeters');
111 set      (gca,'FontSize', 24,'LineWidth',1)
112 hold off
113
114 i = 1;
115 LengthLine = zeros(length(XY),1);
116 DegreesLine = zeros(length(XY),1);
117 for i = 1:length(XY)
118     LengthLine(i)= sqrt(XY(i,1)^2+XY(i,2)^2);          % Length of line and degrees of line
119     DegreesLine(i)= atand(XY(i,2)/XY(i,1));            % from point 0,0 for SolidWorks drawing
120     i = i + 1;
121 end
122 Data = [LengthLine DegreesLine]
```

F.2 Cable extension by bending joint flexure

```
1
2 % Run GrasperCircle.m first for all variables. No function is used so use
3 % the workspace values
4
5 %%
6 arc_b = ArcLength;                                    % Arc length base in mm
7 height = 4;                                           % Base height in mm
8
9
10 k = 1;
11 arc_c = zeros(length(r),1);                          % Last value of radius is infinite.
12 cable = zeros(length(r),1);
13
14 for k = 1:length(r)
15     arc_c(k) = arc_b*(1-(1/r(k,1))*height);          % Cable length in mm (Arc length c in figure)
16     cable(k) = abs(arc_c(1)-arc_c(k,1));             % Cable extension length in mm
17     k = k + 1;
18 end
```

```

Extension = [cable Degrees]                    % Cable extension from difference in curvature
```

F.3 Required cable elongation grasper

```
close all;
clear all;
clc
tic

%% Parameters
Start = 45;                                % Degrees of bending joint in initial state
Start2 = 37;
Startradius = 33/2;                        % Radius of fixated length
Startradius1 = 39.5/2;                     % Radius of bending joint to straight

%% Calculation
ArcLength = (Start*Startradius)/180*pi;    % Arclength fixated length in mm

ArcLength1 = (Start*Startradius1)/180*pi;  % Arclength of beding joint in mm

Cable_Elongation = ArcLength1 - ArcLength; % Total theoretic cable elongation

Cable_Elongation1 = Cable_Elongation*1.5;  % Compensation factor

ArcLength2 = Cable_Elongation1;            % Change of parameter

Startradius2 = ArcLength2/(Start2)*180/pi  % Distance cable connection CoR.
```

F.4 Current theoretical cable elongation of joystick design

```
close all;
clear all;
clc

%% Current cable elongation of joystick design

Initial_Length = 2.5;                              % Length in zero angle state
A_b            = 21;                               % Arc length hard line in mm
h              = 7.05/2;                           % Radial distance [mm] of cable tray towards
    centre of shaft


New_extra_height = sind(20)*5;                     % New extra z position
New_x_point      = cosd(20)*5;                     % New x position
New_x_result     = 5-New_x_point;                  % X length difference new state vs initial state
New_Total_Cable_length = sqrt((Initial_Length...
    +New_extra_height)^2+New_x_result^2);          % New total cable length (initial plus
        elongation)
Cable_elongation_current_design = ...
    New_Total_Cable_length - Initial_Length        % Theoretical cable elongation of current design


A_c = 21-Cable_elongation_current_design;          % Arc length of cable within flexure

Curvature = (1-A_c/A_b)/h;                         % Curvature of flexure in outermost position
Angle     = A_b*Curvature*180/pi                   % Theoretical manipulation angle end-effector
```

F.5 Required cable elongation of joystick design and new theoretical cable elongation

```
close all;
clear all;
clc
tic

%% Required and theoretical cable elongation of joystick design

Start = 60;                                        % Maximum bending angle of flexure in Degrees
Flexure_length = 21;                               % Length of the flexure in mm
Arc_length = Flexure_length;                       % Arc length same as centre of flexure length while
    bending
Shaft_Radius = 7.05/2;                             % Radial distance [mm] of cable tray towards centre
    of shaft

Startradius1 = Arc_length/(2*pi*(Start/360));      % Radius [mm] of the centre of the bending joint
Startradius2 = Startradius1 - Shaft_Radius;        % Radius [mm] of the right edge of the bending joint
```

```
% Theoretical required CableElongation:
Required_CableElongation = Arc_length-(2*pi*Startradius2*(60/360))

% New method of cable elongation
Distance = cosd(20)*13.8;                          % Distance of cable groove hole from centre
Distance2 = sqrt(14^2+14^2)/2 ;                    % Distance of smallest part
ExtraHeight = sind(20)*13.8 ;                      % New extra height outermost
ExtraHeightLow= sind(20)*((sqrt(14^2+14^2))/2) ;   % New extra height least
Neutral = sqrt((13.8-Distance)^2+13.5^2) ;         % Cable length in neutral position
NewLength = 13.5 + ExtraHeight ;                   % New cable length
ElongationGreat = NewLength - Neutral              % Theoretical elongation

New_x = Distance - Distance2;                      % Smallest rotation point towards cable groove
NewLengthSmall = sqrt((13.5+ExtraHeightLow)^2+New_x^2);
ElongationSmall = NewLengthSmall - Neutral         % Theoretical elongation of smallest rotation point

% Theoretical angles
Arc_length1 = 21 - ElongationGreat;                % Greatest achieved Arc length change
Arc_length2 = 21 - ElongationSmall;                % Smallest achieved Arc length change
k1 = (1-(Arc_length1/Arc_length))/Shaft_Radius;
k2 = (1-(Arc_length2/Arc_length))/Shaft_Radius;
Theta_Greatest = ((Arc_length*k1)/pi)*180          % Greatest achieved end effector angle
Theta_Smallest = ((Arc_length*k2)/pi)*180          % Smallest achieved end effector angle
toc
```

G Appendix: Technical drawings

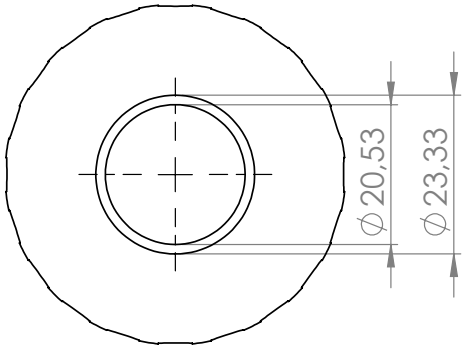

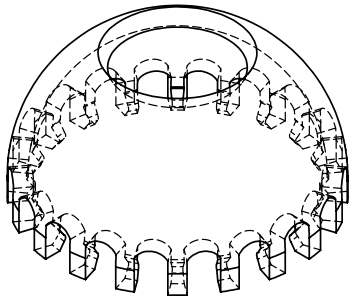

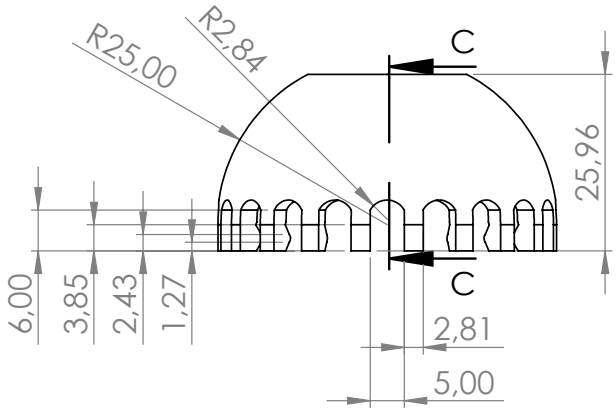

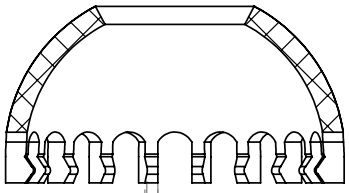

SECTION C-C

1,63

1,91

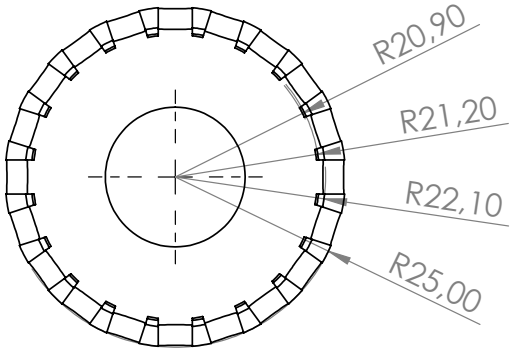

UNLESS OTHERWISE SPECIFIED: DIMENSIONS ARE IN MILLIMETERS SURFACE FINISH: TOLERANCES: LINEAR: ANGULAR:	FINISH:	DEBURR AND BREAK SHARP EDGES	DO NOT SCALE DRAWING / REVISION

	NAME	SIGNATURE	DATE
DRAWN			
CHK'D			
APPV'D			
MFG			
Q.A			

TITLE:

MATERIAL:

DWG NO. Dome_Final

A4

WEIGHT:

SCALE:1:1

SHEET 1 OF 1

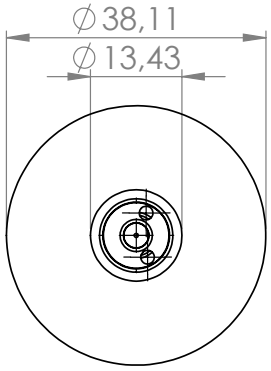

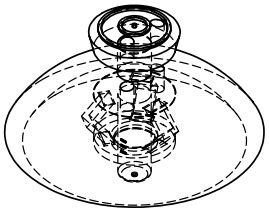

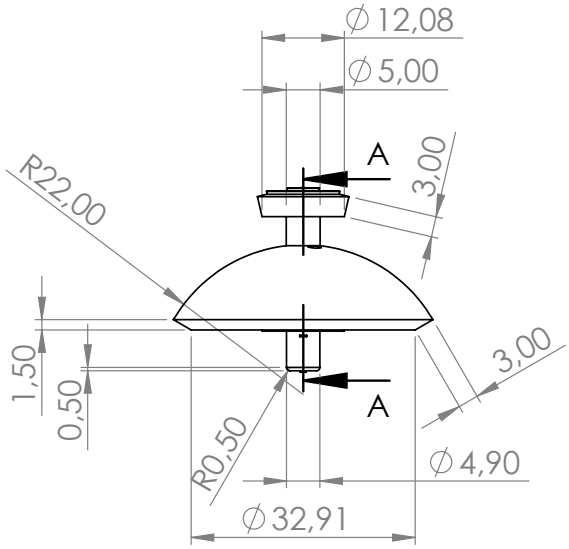

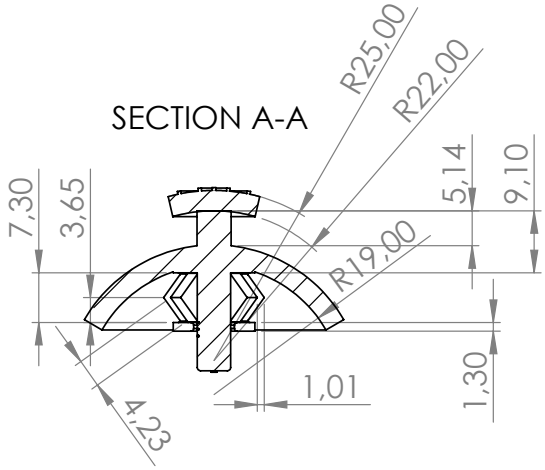

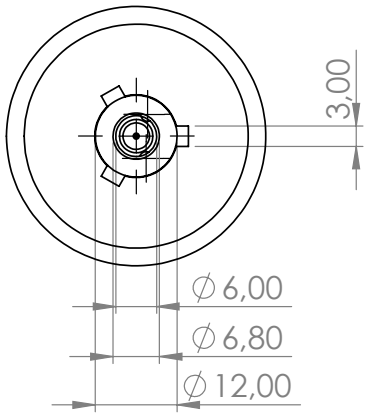

UNLESS OTHERWISE SPECIFIED: DIMENSIONS ARE IN MILLIMETERS SURFACE FINISH: TOLERANCES: LINEAR: ANGULAR:		FINISH:		DEBURR AND BREAK SHARP EDGES		DO NOT SCALE DRAWING	REVISION
	NAME	SIGNATURE	DATE			TITLE:	
DRAWN							
CHK'D							
APPV'D							
MFG							
Q.A				MATERIAL:		DWG NO. Joystick_Final	A4
				WEIGHT:		SCALE:1:1	SHEET 1 OF 1

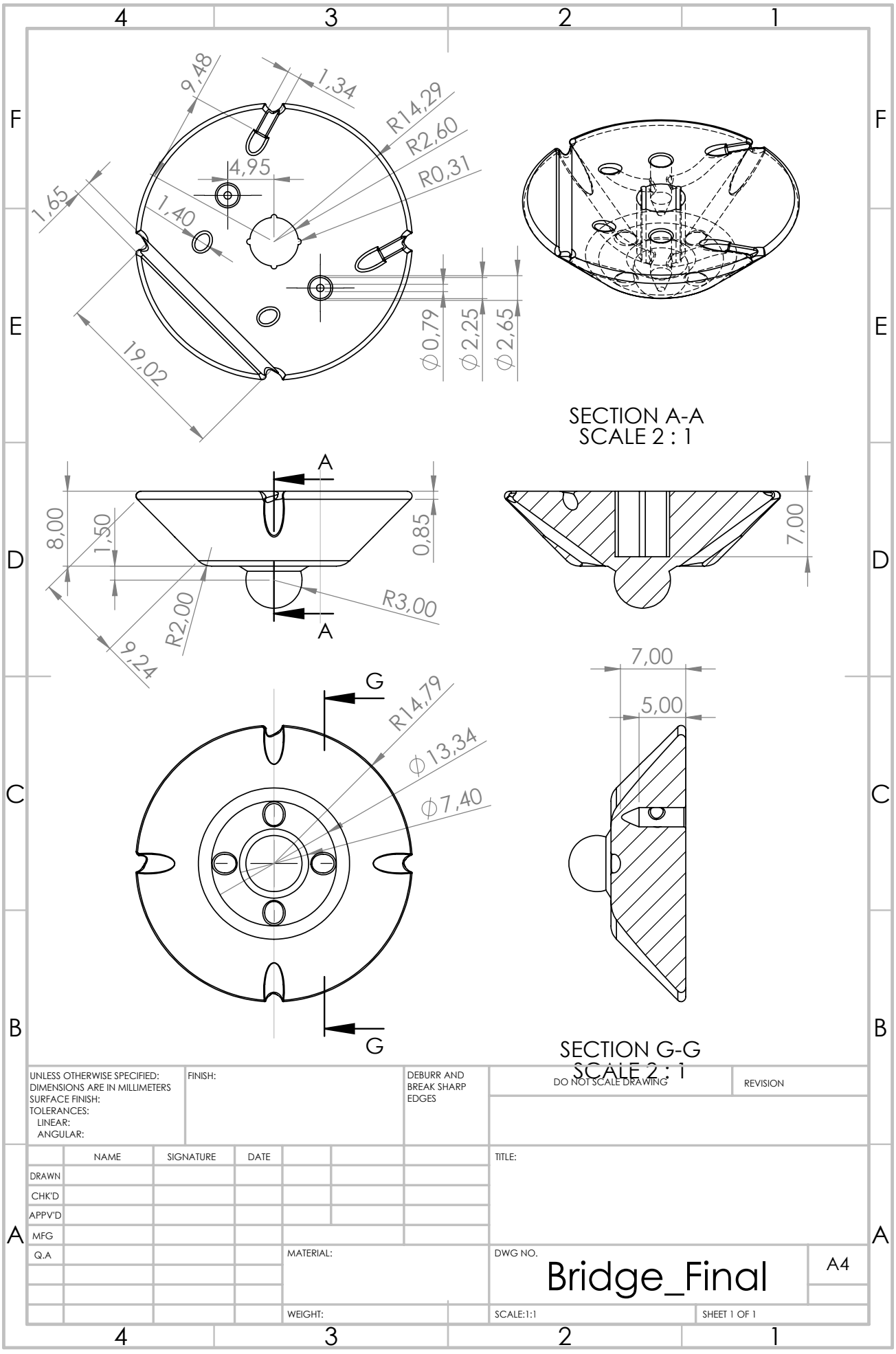
9,48
1,34
R14,29
R2,60
R0,31
4,95
1,65
1,40
19,02
⌀0,79
⌀2,25
⌀2,65
SECTION A-A
SCALE 2 : 1
A
8,00
1,50
0,85
R3,00
R2,00
9,24
A
7,00
G
R14,79
⌀13,34
⌀7,40
G
7,00
5,00
SECTION G-G
SCALE 2 : 1
UNLESS OTHERWISE SPECIFIED:
DIMENSIONS ARE IN MILLIMETERS
SURFACE FINISH:
TOLERANCES:
LINEAR:
ANGULAR:
FINISH:
DEBURR AND BREAK SHARP EDGES
DO NOT SCALE DRAWING
REVISION
NAME
SIGNATURE
DATE
DRAWN
CHK'D
APPV'D
MFG
Q.A
TITLE:
MATERIAL:
DWG NO.
Bridge_Final
A4
WEIGHT:
SCALE:1:1
SHEET 1 OF 1

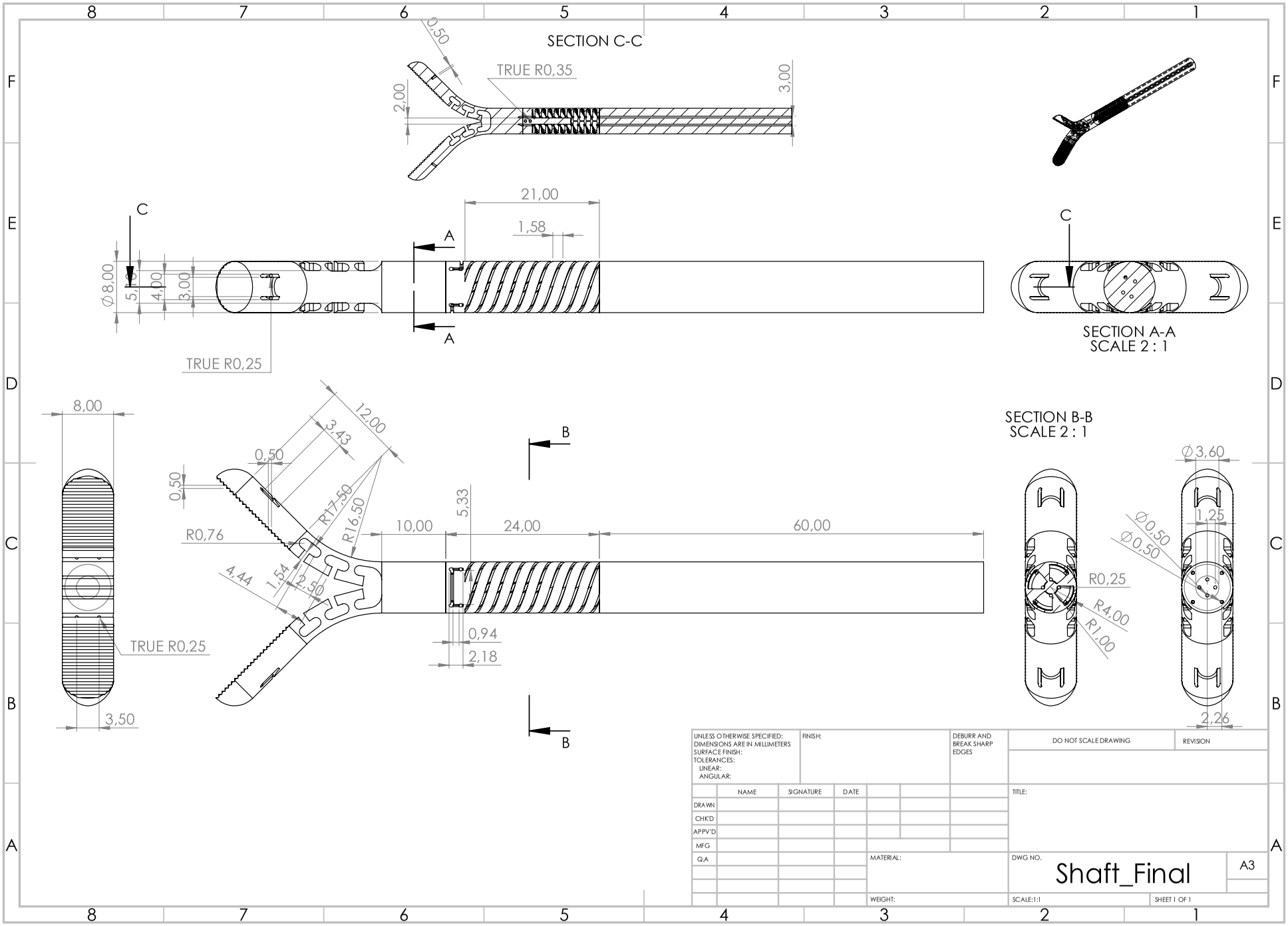
SECTION C-C
0,50
TRUE R0,35
2,00
3,00
21,00
1,58
C
A
A
Ø8,00
5,00
4,00
3,00
TRUE R0,25
C
SECTION A-A
SCALE 2 : 1
8,00
12,00
3,43
0,50
0,50
R17,50
R16,50
R0,76
B
B
10,00
5,33
24,00
60,00
4,44
1,54
2,50
0,94
2,18
TRUE R0,25
3,50
SECTION B-B
SCALE 2 : 1
Ø3,60
1,25
Ø0,50
Ø0,50
R0,25
R4,00
R1,00
2,26
UNLESS OTHERWISE SPECIFIED:
DIMENSIONS ARE IN MILLIMETERS
SURFACE FINISH:
TOLERANCES:
LINEAR:
ANGULAR:
FINISH:
DEBURR AND BREAK SHARP EDGES
DO NOT SCALE DRAWING
REVISION
NAME
SIGNATURE
DATE
DRAWN
CHK'D
APPV'D
MFG
Q.A
MATERIAL:
WEIGHT:
TITLE:
DWG NO.
Shaft_Final
A3
SCALE:1:1
SHEET 1 OF 1

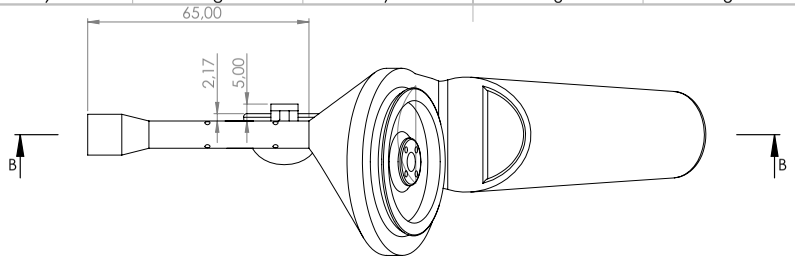

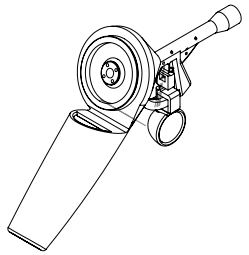

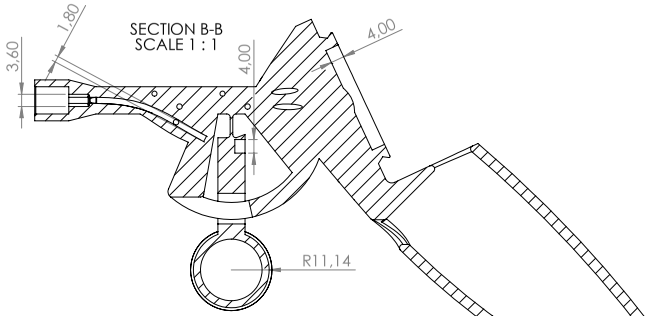

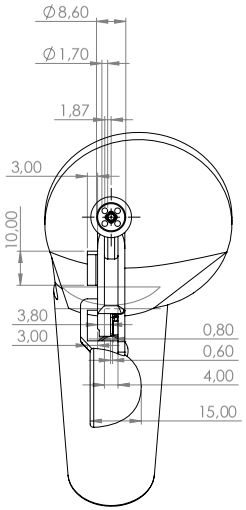

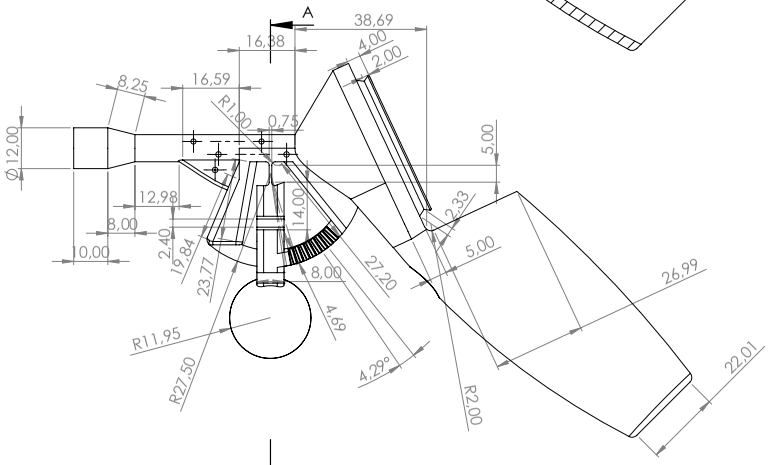

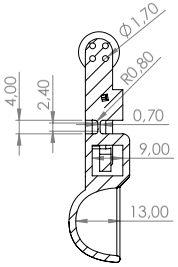

SECTION A-A
SCALE 1 : 1

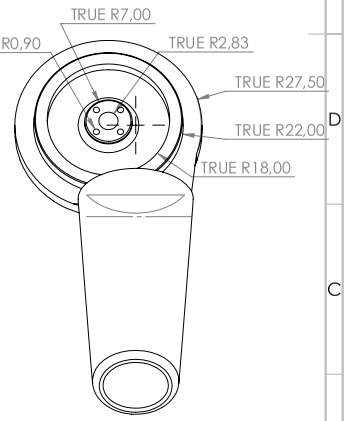

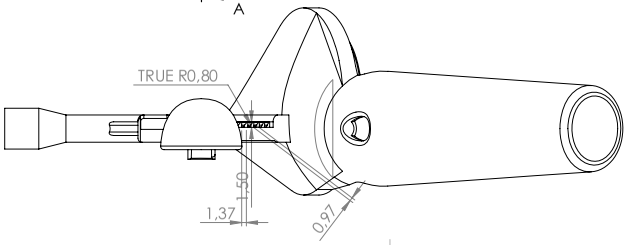

UNLESS OTHERWISE SPECIFIED: DIMENSIONS ARE IN MILLIMETERS SURFACE FINISH: TOLERANCES: LINEAR: ANGULAR:			FINISH:			DEBURR AND BREAK SHARP EDGES	DO NOT SCALE DRAWING / REVISION
	NAME	SIGNATURE	DATE				TITLE:
DRAWN							
CHK'D							
APPV'D							
MFG							
Q.A				MATERIAL:			DWG NO. Handle_Final A2
				WEIGHT:			SCALE:1:2 SHEET 1 OF 1